Universidad
Carlos III de Madrid
www.uc3m.es

Ph. D. Thesis

Design and characterization of new tunable devices based on liquid crystal technology for microwave applications

Author:

Javier Torrecilla Rosell

Supervisors:

Virginia Urruchi del Pozo

José Manuel Sánchez-Pena

DEPARTAMENTO DE TECNOLOGÍA ELECTRÓNICA

Leganés, July 2015

Ph. D. Thesis

DESIGN AND CHARACTERIZATION OF NEW TUNABLE DEVICES BASED ON LIQUID CRYSTAL TECHNOLOGY FOR MICROWAVE APPLICATIONS

Author: **Javier Torrecilla Rosell**

Supervisors: Virginia Urruchi del Pozo
José Manuel Sánchez-Pena

Signature

President:

Vocal:

Secretary:

Mark:

Leganés, 29th July 2015

ACKNOWLEDGEMENTS

En primer lugar, me gustaría agradecer a mis directores de Tesis Virginia Urruchi y José Manuel Sánchez-Pena pues sin su apoyo científico y consejos no hubiera sido posible la realización de este trabajo.

Mi agradecimiento a Carlos Marcos por su inestimable ayuda a la hora de la realización de este trabajo mientras coincidimos en el Grupo de Displays y aplicaciones Fotónicas, como también al resto de componentes del mismo: Carmen Vázquez, Francisco Algorri, Jesús Plinio Pinzón, Ricardo Vergaz, Isabel Pérez, Pedro Contreras, Juan Carlos Torres, Braulio García, David Sánchez, Alberto Tapetado y Vicente Marzal. Gracias por el apoyo prestado en todo momento y por el buen ambiente que siempre tuvimos.

Al Grupo de Fotónica Aplicada de la Escuela Superior de Ingenieros de Telecomunicación (CEMDATIC, Universidad Politécnica de Madrid): José Manuel Otón, Eva Otón, Noureddine Bennis, Amanda García, etc. por su gran ayuda y por el uso de sus instalaciones a la hora de fabricar los dispositivos diseñados en este trabajo.

También me gustaría agradecer a Julia Arias, Ernesto García y María del Mar Sánchez por invitarme a realizar una estancia en el Departamento de Tecnología Electrónica de la Universidad Miguel Hernández de Elche, así como por la buena acogida recibida y su inestimable ayuda a la realización de este trabajo. Por idénticos motivos, me gustaría agradecer a Aníbal Fernández, Lawrence Seddon y Sally Day, del Liquid Crystal Group de University College London.

A la Universidad Militar de Varsovia por su provisión de cristales líquidos experimentales, cuyo uso ha sido clave a la hora de desarrollar este trabajo.

Agradecer igualmente el apoyo financiero del Ministerio de Economía y Competitividad (proyectos TEC2009-13991-C02-01, TEC2014/00354/001) y de la Comunidad de Madrid (proyecto FACTOTEM2 S2009/ESP/1781).

Finalmente, me gustaría agradecer a mi gente más allegada por el apoyo que siempre he tenido, principalmente a Verónica, a mis padres Javier y Margarita y a mi hermana Isabel. Gracias por todo. Y para terminar, mi último recuerdo, por supuesto, para mi tío Juan Carlos, quien siempre me animó a ser doctor y que, desgraciadamente, recientemente nos dejó. Va por ti.

INDEX

FIGURE INDEX

TABLE INDEX

Abstract

The PhD. Thesis work presented in this document has been made in the research group Grupo de Displays y Aplicaciones Fotónicas (GDAF) of Departamento de Tecnología Electrónica from Universidad Carlos III de Madrid.

One of the most traditional GDAF research interest is the study of new devices based on liquid crystals (LC). In this specific research subject, this Thesis work has been focused, including several studies about tunable devices at microwave frequencies based on LC technology. The previous experience of the Group in this field includes the devising of some preliminary approaches related to LC tunable devices, specifically phase retarders. However, no previous systematic study similar to this was made in the scope of this research Group.

The main aim of this Thesis work is, indeed, to contribute to the development of new tunable devices at microwave frequencies based on new and advanced LC mixtures with electrical properties that match the requirements at GHz bands. In particular, this work has focused on the design of passive tunable filters, due to the rich functionality of these devices in telecommunication systems at microwave frequencies.

The document is structured in several parts. It begins with a revision of the different available technologies used in tunable devices at GHz frequencies. Then, the main theoretical fundamentals and concepts of passive filters, notch filters and band-pass filters, are treated. In the third chapter the general processes that are involved in the manufacturing of the devices are presented.

A depth study of LC-based notch filters, using a microstrip spurline structure, is detailed in chapter 4. The different steps with the restrictions that concern the design and the characterization of the manufactured devices are presented. The optimization of the devices configurations and the prediction of the filters frequency response have been made by using commercial electromagnetic software tools. Additionally, the dielectric properties at microwave frequencies of the LC mixtures used in the different devices have been estimated.

Chapter 5 is devoted to tunable LC-based band-pass filters based on microstrip dual-mode technology. In the same way, the optimization of the different filter configurations, as well as the design, simulation and measurement of the frequency response of the filters are described in this chapter.

Finally, in the last chapter, the main conclusions of this Thesis work and the future research lines are presented.

Resumen

El Trabajo de Tesis Doctoral presentado en esta memoria se ha realizado dentro del Grupo de Displays y Aplicaciones Fotónicas del Departamento de Tecnología Electrónica de la Universidad Carlos III de Madrid.

Entre las principales líneas de investigación del GDAF se encuentra el estudio de nuevos dispositivos cuya implementación práctica se basa en el empleo de cristales líquidos (CL). Dentro de esta línea de investigación se han realizado previamente algunos estudios acerca del empleo de CL para el diseño de dispositivos sintonizables a frecuencias de microondas. Así, previamente a la realización de este trabajo, se diseñó y caracterizó experimentalmente un desfasador sintonizable basado en las propiedades de estos materiales. Sin embargo, no se había realizado dentro del grupo un estudio sistemático acerca de dispositivos sintonizables a estas frecuencias similar al presentado en este trabajo de Tésis.

El objetivo de este Trabajo de Tesis Doctoral es contribuir al desarrollo de dispositivos sintonizables a frecuencias de GHz basados en CL. Principalmente, el presente trabajo se ha centrado en el diseño de filtros, dada la importancia que estos dispositivos tienen en sistemas de comunicaciones de la citada banda de frecuencias.

El documento se estructura en varias partes. Comienza con una revisión del estado del arte de los dispositivos sintonizables a frecuencias de microondas, realizando un barrido de las diferentes tecnologías que se vienen utilizando hasta la fecha de hoy, para posteriormente presentar los principales conceptos teóricos y la fabricación de dispositivos. En particular, los filtros pasivos, concretamente filtros notch y paso banda, son el ámbito central de discusión y el núcleo del presente trabajo.

En el cuarto capítulo se presenta un estudio exhaustivo sobre filtros notch con estructura microstrip spurline basados en CL, abordando las distintas fases desde el estudio de las distintas configuraciones y variantes de la tecnología empleada, hasta la implementación de los dispositivos finales. Concretamente, se han diseñado, simulado y caracterizado experimentalmente la respuesta espectral de dos filtros notch basados en CL. La elección de la configuración óptima de cada dispositivo, así como la predicción de la respuesta en frecuencia del mismo, se ha llevado a cabo utilizando herramientas de simulación software comerciales. Por otro lado, la caracterización de las propiedades de los CL a las frecuencias de interés, es otra de las principales aportaciones de este trabajo.

De la misma manera, el quinto capítulo está dedicado al diseño de filtros sintonizables paso-banda con tecnología microstrip dual-mode basados en CL. La optimización de las distintas configuraciones para filtros dual-mode, así como el diseño, implementación, simulación y caracterización experimental de la respuesta espectral de los distintos dispositivos fabricados, son los principales puntos a tratar en dicho capítulo.

Adicionalmente se incluyen, en la parte final de la memoria, las principales conclusiones del presente trabajo, así como las líneas de investigación para el futuro inmediato.

LIST OF ACRONYMS

Acronym	Meaning
AC	Alternating current
BST	Barium Strontium Titanate
BW	Bandwidth
DC	Direct Current
DUT	Device Under Test
GDAF	Grupo de Displays y Aplicaciones Fotónicas
GDV	Group Delay Variation
IL	Insertion Loss
ILV	Insertion Loss Variation
JCR	Journal Citation Reports
LC	Liquid Crystal
LTI	Linear and Time Invariant
MEMS	Microelectromechanics Systems
MW	Microwave
MWP	Microwave Photonics
NGD	Negative Group Delay
NLC	Nematic Liquid Crystal
PROMETEO	Procesado de Materiales y Tecnologías Optoelectrónicas
PTFE	Polytetrafluoroethylene
RF	Radiofrequency
RL	Return Loss
RMS	Root Mean Square
SBS	Stimulated Brillouin Scattering
SMA	Subminiature version A
TE	Transverse Electric mode
TEM	Transverse Electromagnetic mode
TM	Transverse Magnetic mode
UV	Ultraviolet
WLAN	Wireless Local Area Network

CHAPTER 1. INTRODUCTION, MOTIVATIONS AND GOALS

1.1. Introduction

The microwave (MW) band of frequencies (300 MHz – 300 GHz), which is also divided into sub-bands (see Appendix II), is widely used in telecommunications (satellites, radar, mobile communications, etc.) because of its advantages in bandwidth and low interferences.

The advances of the new telecommunication systems at these frequencies during the last 20 years have involved a growing demand of designing flexible devices. The new requirements of the current communications are getting more varying, so it is necessary the development of systems able to be adapted to this new scenario.

This increase of services leads to a necessity of working with different networks, bands of frequencies, etc. or even in different countries, as well as the creation of platforms able to support different technologies and services. For example, the wireless local area networks (WLAN) operate at 2.45 GHz and 5.25 GHz in Europe and at 5.75 GHz in USA. Due to it, the importance of implementing flexible and reconfigurable systems is clear.

In order to achieve a higher flexibility of the systems, the ability of designing tunable devices, whose properties can be changed according to the requirements, is considered a critical issue. Because of this fact, there has been an increasing interest in developing tunable devices at microwave frequencies for satisfying this demand.

Nevertheless, the goal is not only to manage reconfigurable devices at this band of frequencies, but also the design of prototypes with low cost, size and power consumption.

For this purpose, some different technologies have been studied: MEMS, varactor diodes, ferroelectric materials, etc. In section 1.2, the state of art of the tunable devices at microwave frequencies is presented. A promising technology for the design of these devices with some reported examples is the use of liquid crystals (LC). Their anisotropic properties make these materials to be very suitable for implementing tunable devices.

The study of LC for non-optical applications is one of the researching lines of the Group of Displays and Photonics Applications (GDAF) of Universidad Carlos III de Madrid. Due to the growing interest in developing voltage-controlled devices at microwave frequencies, this work, which is part of the researching area of GDAF, is dedicated to the design, fabrication, and characterization of tunable devices at GHz frequencies based on LC.

1.2. Tunable devices at microwave frequencies. State of art

Because of the mentioned interest in the development of tunable devices at microwave frequencies, several research groups have published studies about tunable devices at these frequencies, such as filters, phase shifters or antennas. In this section, some of the most representative prototypes are presented. First, the state of art of the different technologies used for designing tunable devices is revised. Then, some different examples of LC-based tunable devices are described.

1.2.a. Tunable technologies at microwave frequencies

In order to develop tunable devices at microwave frequencies, some different materials and technologies, which permit tuning by applying an electromagnetic field, have been studied. After the comparison of technologies, the research have focused on the reduction of the power consumption, size and cost, as well as the optimization of the performance of the device, concretely, the attenuation and the tuning range.

The most representative tunable devices at microwave frequencies, such as phase shifters, antennas, filters and other devices, and the used technologies, are described next.

i) Tunable phase shifters

The development of tunable phase shifters is very important because these are key devices in the design of antenna arrays, radar sensors or multiband mobile communications. The first tunable phase shifter designs dates of the early nineties and they were based on PIN diodes [1.1].

A widely employed and similar alternative is the use of microelectromecanics systems (MEMS), which use variable capacitors. In 2000, California University developed a MEMS-based tunable phase shifter which obtained a maximum phase shift of 180 degrees at 25 GHz and 270 degrees at 35 GHz [1.2]. Its structure is shown in Figure 1. Later MEMS designs have achieved a total phase control (maximum phase shift of 360 degrees) up to 40 GHz [1.3]. Nevertheless, at that moment, every tunable phase shifter generated discrete phase steps. Then, the interest has been focusing on developing continuous phase shifts. The most using technologies for this purpose have been varactor diodes and ferroelectric films.

The main property of varactor diodes is the fact that their impedance can be varied by applying an external voltage. In 2007, TU Delft University (Netherlands) designed a varactor diodes-based phase shifter achieving a maximum phase shift of 160 degrees at 2 GHz [1.4].

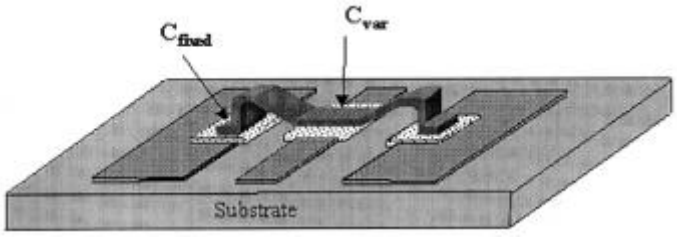

Figure 1.1. MEMS based phase-shifter structure [1.1]

Ferroelectric films for tunable devices have been used since 2000. That year, a tunable phase shifter based on ferroelectric films which obtained a maximum phase shift of 157º at 30 GHz was reported [1.5]. Later studies have achieved higher phase shifts, but applying higher levels of applied voltage. Darmstadt Technology University (Germany) presented in 2003 a ferroelectric films-based tunable phase shifter with a maximum phase shift of 360 degrees at 38 GHz by applying 100 V [1.6]. Recently, in 2012, California University have achieved maximum phase shift of 406.5 degrees with ferroelectric films, but applying a magnetic field [1.7]. In 2014, University of Ottawa (Canada) has developed a phase-shifter which obtained 360º of phase shift in a band of frequencies between 10 GHz and 40 GHz [1.8].

Recently, Microwave Photonics (MWP) techniques and graphene-based technologies have been proposed to design tunable microwave devices. In 2014, University of Sidney (Australia), has developed the first microwave tunable phase shifter based on Stimulated Brillouin Scattering (SBS). A maximum phase shift of 240º was measured in a frequency range from 1 GHz to 15 GHz [1.9]. Finally, last year, Universidad Politécnica de Valencia reported a tunable phase shifter based on silicone graphene waveguide obtaining a full phase shift of 360º at 40 GHz [1.10].

ii) Tunable antennas

The design of tunable antennas is more recent than other reconfigurable devices. Nevertheless, tunable patch antennas have been widely studied. The most used technologies for the design of reconfigurable antennas have been MEMS, ferrite technology and, recently, varactor diodes.

In 2006, the Auburn University (Alabama, USA) presents a frequency tunable microstrip antenna based on MEMS with a circular patch which achieves a tuning range of 1.6% at 16.8 GHz. The problem of this design was the necessity of using very high voltage levels, about 50 V [1.11]. Later, other studies performed by Ankara University of Technology (2007), a slightly improvement of the tuning range at 16 GHz was obtained (2%) with an important reduction of the applied external voltage (12 V) [1.12].

In the same way, from 2007 on, some studies about tunable antennas based on ferrite technology, whose directivity can be controlled by applying a magnetic field, have been reported [1.13].

Recently, from 2013 on, the use of varactor diodes for tunable antennas at low frequencies (365 – 500 MHz) has been proposed [1.14]. In 2014, University of South Florida (USA) has developed tunable antennas based on BST varactors at higher frequencies, obtaining tuning ranges from 2.32 GHz to 2.55 GHz [1.15], whose design is shown in Figure 1.2, and from 2.42 GHz to 2.66 GHz, respectively [1.16].

A new alternative for tunable antennas in GHz and THz which is being studying at present, is the use of graphene, which can be used as a variable resistance. In 2015, a prototype of graphene-based tunable antenna in X band (8 GHz – 12 GHz) has been presented by Politechnica University of Bucharest (Romania) [1.17]. The main problem of this technology is the high voltage levels that are required to get a large tunability.

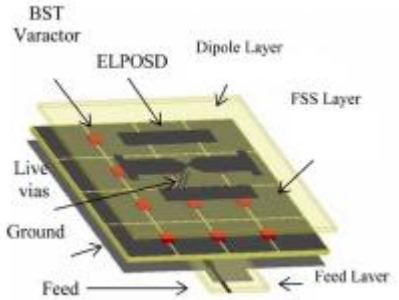

Figure 1.2. Schematic of BST varactor diode antenna [1.15]

iii) Tunable filters

Filters are very important devices in telecommunication systems since they have the ability of selecting or rejecting bands of frequency. The design of tunable devices, whose band of frequency to select or reject can be controlled, is therefore, a very interesting subject of investigation.

In 1999, some bandpass tunable filter designs based on MEMS at Ka band (26 – 40 GHz) were presented. These filters achieved tuning range of 4.2 and 2.5% at 26.6 GHz and 32 GHz, respectively [1.18]. Then, MEMS-based tunable filters have obtained larger tuning ranges, about 6% at 12 GHz and at 18 GHz [1.19]. Next studies (2007) achieved similar tuning ranges, but at higher frequencies, up to 75 GHz [1.20]. In 2015, a MEMS based notch filter presented by Jadavpur University (India) obtained a tuning range near 10% at 35 GHz by using metamaterials [1.21].

MEMS-based tunable filters don't usually achieve high tuning ranges compared to other used technologies. For example, by using varactor diodes, a higher tuning range is obtained,

but at lower frequencies, nearby 1 GHz. Michigan University developed a bandpass filter between 0.7 GHz and 1.33 GHz which obtained a tuning range of 60% [1.22]. In 2013, Southwest Jiaotong University (China) presented filter designs based on varactor diodes at higher frequencies, between 2 GHz and 3 GHz [1.23]. Tuning ranges higher than 60% have been achieved but at lower frequencies, near 1 GHz [1.24].

From 2008 on, high tuning ranges have been achieved at high frequencies by using hexaferrite resonators. For example, Fig. 1.3 shows a filter based on hexaferrite which obtained a tuning range of 70% at 39 GHz. The filter frequency was changed by applying an external magnetic field [1.25].

Microwave Photonics (MWP) techniques have received great attentions during the last two years for the design of tunable microwave filters because of a large tuning range can be reached. In 2014, University of Sidney (Australia), who had developed a tunable phase shifter based on Stimulated Brillouin Scattering (SBS), reported the first SBS tunable notch filter whose reject frequency could be tuned from 2 GHz to 8 GHz [1.26]. In 2015, University of Georgia, designed another notch filter by using a Lyot filter with a tuning range from 1.8 GHz to 10 GHz [1.27].

Figure 1.3. Tunable filter based on hexaferrite resonators [1.21]

iv) Other tunable devices

Other tunable devices which have been reported are tunable capacitors. In 1999, a tunable capacitance between 1.5 pF and 33.2 pF was obtained at 40 GHz by using MEMS [1.28]. Later, ferroelectric materials have been also employed for the design of tunable capacitors [1.29].

On the other hand, piezoelectric transductors, which are materials whose properties change electrically, have been used for the design of tunable oscillators [1.30], [1.31]. Graphene technology has been also used recently for the design of tunable attenuators at 5 GHz [1.32]. However, it is not commercially available nowadays.

v) A promising alternative for the design of tunable devices

The previously described alternatives for designing tunable devices don't usually satisfy simultaneously the specifications of cost, size or consumption, as well as the whole performance is not often the desirable one. For example, the main problem of using MEMS is the requirement of an active frequency control system, lacking repetitiveness in manufacture. Ferrite technology needs a magnetic field for tuning, which leads to a high power consumption and size. On the other hand, varactor diodes need very high voltage for obtaining good tuning ranges at frequencies higher than 1 GHz [1.33]. At the moment, the novel graphene technology also requires high voltages up to 200 V in DC. Table 1.1 shows a comparison showing advantages and disadvantages of the different employed tunable technologies.

Technology	Advantages	Disadvantages
MEMS	- Low cost, size, weight and power consumption.	- Low tuning ranges obtained - Lack of repetitiveness.
Varactor diodes	- Large tuning ranges at low frequencies	- High power consumption at frequencies higher than 1 GHz
Ferrite technology	- Large tuning ranges	- High power consumption and size
Ferroelectric materials	- Large tuning ranges - Possibility of working at high frequencies - Low losses	- Requeriment of using high voltages to manage tunability, which implies high power consumption
Graphene	- Size	- Requeriment of using high voltages to manage tunability. - Technology already in study
Microwave photonics based-techniques	- Very large tuning ranges.	- Technology already in study. - Size.

Table 1.1. Advantages and disadvantages of the different technologies used for tunable devices at microwave frequencies

Hence, some other alternatives have been studied. Concretely, the use of liquid crystals (LC) has aroused the interest for the design of tunable devices, due to its anisotropic properties, which are studied in depth in Chapter 2 of this work. In the next section, the main studied and designed prototypes of LC-based tunable devices at microwave frequencies are presented.

1.2.b. Tunable devices based on liquid crystals

Liquid crystals are, therefore, suitable materials for their employment in tunable applications. Concretely, their molecules ability of being oriented along with an applied external electric field allows LC-based devices to be voltage-controlled. Furthermore, their reduced power consumption compared to other technologies [1.34] has permitted LC to lead the displays market during more than twenty years.

Concerning to optical applications, displays are the major application of LC. However, there is a growing interest in using these materials in non-optical applications. For example, there have been several publications about LC devices at microwave frequencies as described above.

i) Tunable phase shifters based on liquid crystals

The first study about a LC-based phase shifter dates from 1993. The designed phase shifter was manufactured by using a microstrip line with a substrate of alumina ($\varepsilon_r = 9.8$) and a nematic LC whose dielectric anisotropy was $\Delta\varepsilon = 0.2$. A maximum phase shift of 20º at 10.5 GHz was achieved by applying 16 V [1.35].

Later prototypes have obtained higher tuning ranges by using LC of high birefringence, as well as other dielectric substrates. In 2001, NHK laboratories (Tokyo) reported a tunable phase shifter design with a maximum phase shifter of 80º at 20 GHz by applying 70 V (the LC dielectric anisotropy was not mentioned) [1.36].

In the design of LC-based tunable devices, it should be pointed out the research contributions of Technology University of Darmstadt (Germany). This research group has reported several studies about LC devices. In 2003, two phase shifters, with two different used LC's and TMM3 as dielectric substrate ($\varepsilon_r = 2.4$), were presented. The first design, which used a LC whose dielectric anisotropy was $\Delta\varepsilon = 0.3$, achieved maximum phase shifts of 35º and 65º at 10 GHz and 20 GHz, respectively. With a LC of high birefringence (not reported values), 140º and 270º at 10 GHz and 20 GHz, respectively, were obtained [1.6]. Fig. 1.4 shows the detail of the designed device. This structure is common to other devices reported.

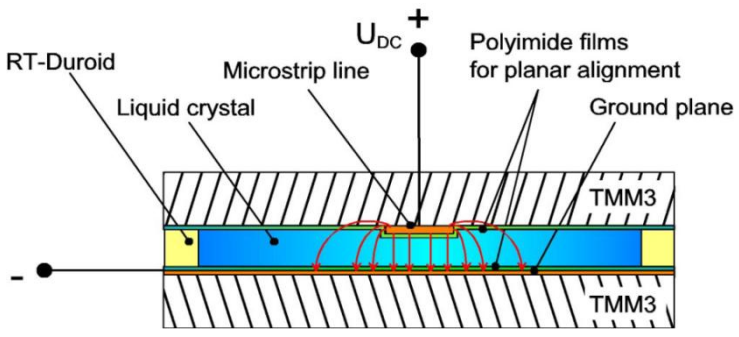

Figure 1.4. LC-based tunable phase shifter developed in [1.6]

More recent designs have focused on phase shifters at higher frequencies, achieving higher tuning ranges. In this way, in 2006 a tunable phase shifter with a maximum phase shift of 200º at 108 GHz using a LC of $\Delta\varepsilon = 0.3$ was developed [1.37]. In this paper, another phase shifter which obtained 400º at the same frequency was also reported, but the LC dielectric anisotropy was not mentioned. Later studies performed by the same university have tried to remove observed non-linear effects in previous designs [1.38]. On the other hand, from 2012 on, some phase shifters at very high frequencies (110 – 220 GHz) have been reported [1.39], achieving, in 2014, a large phase shift of 384º by using LC of high birrefirngence [1.40]. Other studies have used twisted nematic LC [1.41].

ii) Tunable antennas based on liquid crystals

The design of tunable antennas must play a very important role in future telecommunication systems. The earliest LC-based antenna prototype was presented in 2003. It consisted of a patch antenna whose dielectric substrate was a LC of $\Delta\varepsilon = 0.2$, achieving a resonant frequency variation between 4.5 GHz and 4.7 GHz [1.42]. Nowadays, the study of frequency-agile patch antennas based on LC continues. In 2014, University of Nicosia (Cyprus) reported a patch antenna using Merck E7 as LC ($\Delta\varepsilon = 0.35$ [1.43]) obtaining a frequency shift from 5.45 GHz to 5.84 GHz applying 10 V_{rms} [1.44]

Nevertheless, in the last decade, the interest of LC-based tunable antennas has focused on reflectarray antennas. This kind of antennas is a very interesting alternative due to its advantages in cost, size, easy fabrication or low loss. Reflectarray antennas are based on a reflecting surface forming of several periodic cells. Each periodic cell is composed of a perturbation element which generates a phase shift. In a LC-based reflectarray antenna, the perturbation element is the LC, and the phase shift generated can be controlled by applying an external voltage [1.45].

Queen's University of Belfast (Northern Ireland, United Kingdom), in collaboration with Universidad Politécnica de Madrid, has widely contributed to the development of reflectarray antennas. This researching group proposed the first theoretical design of a LC-based reflectarray antenna in 2005 [1.46]. A year later, they presented a design of reflectarray antenna at 10 GHz achieving 200º of maximum phase shift using a single metallic patch in the LC cells and using Merck BL006 as the LC [1.47]. A later design added a second metallic patch in the cell, obtaining a phase shift up to 300º [1.48]. From 2011, LC-based reflectarray antennas at 100 GHz were reported [1.49], [1.50], as well as the characterization of LC cells for reflectarrays [1.51] and studies about the dependence of the LC permittivity as a function of the applied voltage [1.52]

There are other studies about reflectarray antennas reported by Technology University of Darmstadt which works at 35 GHz and achieving a maximum phase shift of 350º by using LC of high birefringence and D/A converters [1.53]. The manufactured reflectarray is shown in Figure 1.5. In 2011 they developed a reflectarray antenna at higher frequency (77 GHz) with a larger phase shift (582º) due to the use of LC of high dielectric anisotropy [1.54].

Figure 1.5. Manufactured reflectarray based on LC [1.53].

Finally, it is also remarkable the contribution of University of New Mexico (USA) to the study of reflectarray antennas. In 2014, they reported a LC reflectarray design which used a passive matrix of control [1.55]

On the other hand, in 2011, a design of LC-based microstrip antenna, with tunable directivity, was reported by National Defense Academy of Japan. [1.56]. Other prototypes have focused on obtaining a continuously tunable polarization [1.57] or working at higher frequencies (60 GHz) [1.58], [1.59].

iii) Tunable filters based on liquid crystals

In spite of the importance of filters in telecommunication systems, there are not many studies about LC-based tunable filters. Nevertheless, some designs of band-pass filters have been reported and, following, are described.

In 2007, Queen´s University of Belfast reported a band-pass filter design at 134 GHz using a high anisotropic LC ($\Delta\varepsilon = 1$) and manufactured on quartz. However, the filter tuning range was low, nearby 3% [1.60].

Later, in 2010, a LC-based 3-pole filter at 20 GHz was presented By Darmstadt University. A higher tuning range, about 10%, was managed. An inverted microstrip line structure, which is typical of LC-base devices, was used, as shown in Fig. 1.4 (a). The manufactured filter is shown in Fig. 1.4 (b). The used LC is not detailed [1.61]. In 2014, University of Essex (United Kingdom) reported a filter at 77 GHz which managed a tuning range a bit larger than 7% using a not specified nematic LC [1.62].

As it was previously mentioned, there are not many LC-based designs and most of reported examples are band-pass filter, not notch filters or low-pass filters Due to it, the design of LC tunable filters supposes a very interesting line of researching.

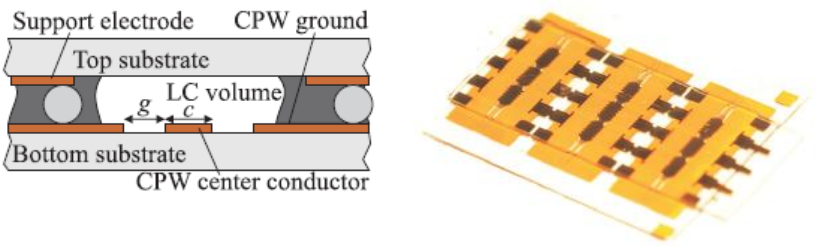

a) Filter structure. **b) Manufactured device**

Figure 1.6. LC-based tunable filter designed in [1.61]. Structure and manufactured device.

iv) Other LC-based tunable devices

Apart from studies about tunable phase shifters, antennas and filters, there are other reported examples of tunable devices at microwave frequencies based on LC.

In 2005, Tsing-Hua University (Taiwan) designed a tunable capacitor at 5 GHz which achieves a capacity variation between 0.85 pF and 1.1 pF, by using a high anisotropic LC [1.63].

There are also studies about LC-based tunable wavelength/frequency selectors, such as the performed by Exeter University (United Kingdom). This device used a LC whose dielectric anisotropy was $\Delta\varepsilon = 0.6$, allowing frequency selections between 26 GHz and 40 GHz by applying up to 7 V [1.64].

1.3. Motivation, goals and methodology

Once the state of art of microwave tunable devices, either based on liquid crystals or on some other technologies, has been revised, the motivations and the main goals of this work are presented in this section.

The Displays and Photonic Applications Group (GDAF) is a research group of the Department of Electronic Technology of Carlos III University, Madrid, whose main lines of researching are the following:

- Development of advanced instrumentation and optical fiber sensors. Integration in WDM networks.
- Design and characterization of photonic devices for optical networks.
- Research and development of prototypes of assistance technologies.

- Electro-optical devices and applications with special focus on liquid crystals and electrochromic materials

Concerning LC materials, there has been an increasing and recent interest in the study of these materials in non-optical applications. Some LC-based devices have been developed in the frequency range of kHz and MHz, such as a VCO with a liquid crystal cell of tunable capacity, resonators or oscillators. This work expects to continue the research about LC non-optical applications by studying LC devices at higher frequencies, for instance, the microwave band of frequencies.

In this way, previously to this work, the first prototype of LC-based tunable device developed by GDAF was a tunable phase-shifter. This device was designed, simulated and measured, obtaining a maximum phase shift of 45º at 10 GHz [1.65]. The next step of this line of research is the development of other tunable structures.

Taking these points into account, the aims of this Thesis work can be defined as follows:

- The main goal of this work is, therefore, the design, and fabrication of new LC-based tunable devices and applications at microwave frequencies as well as the experimental characterization of these devices. The tuning range or the designed tunable devices has been considered as one of the most important parameters of merit.

- Specifically, as there are not many reported examples of tunable LC-based filters, which it was shown in the previous section, it has been considered an interesting subject for research. In fact, this Thesis work is mainly focused on the design of tunable LC filters. In that sense, some notch and band-pass filters structures have been studied.

- Nevertheless, the design of tunable LC filters is not the only aim of this Thesis work. Additionally, another goal is the proposal and simulation of new and innovative for other tunable devices based on LC, such as phase shifters, antennas, etc.

- Other important aim of this Thesis work is to study the possibility of using experimental liquid crystals of high dielectric anisotropy in order to achieve a higher tuning range of the devices. These experimental LC, which have been developed by Military University of Warsaw (Poland) have been employed in some of the designed devices.

- Usually, as the use of LC in MW is relatively recent, the LC dielectric properties (permittivity and loss tangent) are unknown at these frequencies. Therefore, it is necessary to carry out an estimation of such LC parameters. In this work, the estimations of the permittivity and loss tangent of some of the used LC in the different designed devices are described.

In order to reach these goals, the methodology used is as follows:

- Theoretical study and proposal of tunable devices.
- Detailed definition of specifications
- Simulation of the structures
- Device manufacturing
- Experimental characterization
- Proposals of improvement based on theoretical study and new simulations

1.4. Organization of the work

This section presents the organization of this Thesis work. In this first chapter of the work the state of art of tunable devices at microwave frequencies has been studied, as well as the motivation and main goals of the Thesis work.

In chapter 2, some theoretical considerations for the design of tunable devices at microwave frequencies based on LC, specifically tunable microwave filters, are given. First, the main properties of liquid crystals are described. Then microwave filters are studied, as well as the microstrip technology, used for the design of these devices, is widely explained. Concretely, the inverted-microstrip line structure, which is used in LC-based designs, is described in depth.

Chapter 3 is dedicated to the general considerations in the manufacturing process of tunable devices based on LC. The fabrication of the different substrates of the structure and the process of filling a device with LC are the main points of this chapter.

Chapter 4 is focused on tunable notch filters based in LC. Concretely, two tunable notch filters have been designed, simulated and experimentally characterized, and the permittivity of the used LC has been estimated as well. Two variants of the microstrip spurline structure have been used to implement both notch filters: the conventional structure and the spiral structure, respectively.

Chapter 5 deals with tunable band-pass filter based on LC. A dual-mode structure is employed to design the microstrip filter in order to reduce the size of the device. The dual-mode band-pass LC filter is designed and measured. Then, in order to improve the performance of this device, some modifications in the filter structure have been carried out. The new improved device has been also manufactured and characterized.

Finally, chapter 6 presents the main conclusions of the work, as well as the future lines of research.

1.5. References

[1.1] C. Marcos, "Contribución al desarrollo de sensores y sistemas sintonizables eléctricamente basados en cristal líquido para aplicaciones en la industria aeroespacial". Tesis doctoral, Universidad Carlos III, Leganés, 2011.

[1.2] A. Borgioli, Yu Liu, Amit S. Nagra, Robert A. York, "Low-Loss Distributed MEMS Phase Shifter", IEEE Microwave and Guided Wave Letters, Vol. 10, No. 1, p. 439-442, Jan. 2000.

[1.3] M. Kim et al. "A DC-to-40 GHz Four-Bit RF MEMS True-Time Delay Network", IEEE Microwave and Wireless Components Letters, Vol. 11, No. 2, p. 56-58, Feb. 2001.

[1.4] J. H. Qureshi et al., "A Low-Loss Compact Linear Varactor Based Phase-Shifter", IEEE Radio Frequency Integrated Circuits Symposium, 2007.

[1.5] E. Erker et al., "A Monolithic Ka-Band Phase Shifter Using Voltage Tunable $BaSrTiO_3$ Parallel Plate Capacitors", IEEE Microwave and Guided Wave Letters, Vol. 10, No. 1, p. 10-11, 2000.

[1.6] C. Weil, S. Müller, P. Scheele, Y. Kryvoshapka, G. Lüssem, P. Best, R. Jakoby, "Ferroelectric- and Liquid Crystal- Tunable Microwave Phase Shifters", 33rd European Microwave Conference, p. 1431-1434, Munich, Germany, 2003.

[1.7] Y. Zhu, G. Qiu, C. S. Tsai, "A magnetically- and electrically-tunable microwave phase shifter using yttrium iron garnet/gadolinium gallium garnet thin film", Journal of Applied Physics, Vol 111, No 7, p. 170-171, 2006.

[1.8] W.Liu, J. Yao, "Ultra-wideband microwave photonic phase shifter with a 360° tunable phase shift based on an erbium-ytterbium co-doped linearly chirped FBG", Optical Letters, Vol. 39, p. 922-924, 2014.

[1.9] M. Pagani, D. Marpaung, D. Choi, S. Madden, B. Luther-Davies, B. J. Eggleton, "Silicon Tunable wideband microwave photonic phase shifter using on-chip stimulated Brillouin scattering", Optics Express, Vol. 22, No 23, p. 28810-28818, 2014.

[1.10] J. Capmany, D. Domenech, P. Muñoz, "Silicon graphene waveguide tunable broadband microwave photonics phase shifter", Optics Express, Vol. 22, No 7, p. 8094-8100, 2014.

[1.11] R. Jackson, R. Ramadoss, "A MEMS-based electrostatically tunable circular microstrip patch antenna", Journal of Micromechanics and Microengineering, Vol 17, No 10, p. 07A502 - 07A502-3, 2012.

[1.12] E. Erdil et al. "Frequency Tunable Microstrip Patch Antenna Using RF MEMS Technology", IEEE Transactions on Antennas and Propagation, Vol. 55, No. 4, p. 1193-1196, 2007.

[1.13] N. Sun et al. "Electronically tunable magnetic patch antennas with metal magnetic films", Electronic Letters, Vol. 43, No. 8, p. 434-436, 2007.

[1.14] S. Zhu, D.G. Holtby, K. L. Ford, K.L., A. Tennant, R.J. Langley, "Compact low frequency varactor loaded Tunable SRR antenna", IEEE Transactions on Antennas and Propagation, Vol. 61, No. 4, p. 2301-2304, 2013.

[1.15] D.Cure, T. M. Weller, T. Price, F. A. Miranda, F. W. Van Keuls "Low-Profile Tunable Dipole Antenna Using Barium Strontium Titanate Varactors", IEEE Transactions on Antennas and Propagation, Vol. 62, No. 3, p. 1185-1193, 2014.

[1.16] D.Cure, T. M. Weller, T. Price, F. A. Miranda, "Study of a Flexible Low Profile Tunable Dipole Antenna Using Barium Strontium Titanate Varactors", Proceedings of the 8th European Conference on Antennas and Propagation, p. 31-35, La Hague, 2014.

[1.17] N. Dragoman, D. Neculoiu, A. Bunea, G. Deligeorgis, M. Aldrigo, D. Vasilache, A. Dinescu, G. Konstantinidis, D. Mencarelli, L. Pierantoni, M. Modreanu, "A tunable microwave slot antenna based on graphene", Applied Physics Letters, Vol. 106, p. 153101-1 - 153101-5, 2015.

[1.18] H. Kim, J. Park, Y. Kim, Y. Kwon "Milimiter-wave michromachined tunable filters", IEEE MTT-S Digest, p. 1235–1238, (1999).

[1.19] K. Entersari, G. Rebeiz "A 12–18-GHz Three-Pole RF MEMS Tunable Filter", IEEE Transactions on Microwave Theory and Techniques, Vol. 53, No. 8, p. 2566-2571, 2005.

[1.20] K. Entersari et al., "A 25–75-GHz RF MEMS Tunable Filter", IEEE Transactions on Microwave Theory and Techniques, Vol. 55, No. 11, p. 2339-2345, Nov. 2007.

[1.21] B. Pradhan, P. Gupta, "RF MEMS Tunable Band Reject Filter using Metamaterials", 2014 International Conference on , p. 1-4, Kolkata, 2014.

[1.22] A. Brown, G. Rebeiz, "A varactor tuned RF filter", IEEE Transactions on Microwave Theory and Techniques, Vol. 48, No. 7, p.1157-1160, Jul. 2000.

[1.23] Q. Xiang, Q. Feng, X. Huang, D. Jia, "Electrical tunable microstrip LC bandpass filters with constant bandwidth“, IEEE Transactions on Microwave Theory and Techniques, Vol. 61, No. 3, p.1124-1130, 2013.

[1.24] J. Mao, W. Che, W. Choi, K. Tam, Q. Xue, "Fully tunable filter design using tunable transformers and multiple mode resonators“, IEEE International Wireless Symposium (IWS), p. 1-3, Beijing (China), 2013.

[1.25] Michael Sterns, Robert Rehner, Dirk Schneiderbanger, Siegfried Martius, Lorenz-Peter Schmidt, “Novel Tunable Hexaferrite Bandpass Filter Based on Open-Ended Finlines”, Microwave Symposium Digest, 2008 IEEE MTT-S International, 2008.

[1.26] B. Morrison, D. Marpaung, R. Pant, E. Li, D. Choi, S. Madden, B. Luther-Davies, B. J. Eggleton, “Tunable microwave photonic notch filter using on-chip stimulated Brillouin scattering”, Optics Communications, Vol. 313, p. 85-89, 2014.

[1.27] J. Ge, H. Feng, G. Scott, M. P. Fok, “High-speed tunable microwave photonic notch filter based on phase modulator incorporated Lyot filter”, Optics Letters, Vol. 40, No 1, p. 809448 - 51, 2015.

[1.28] C. L. Goldsmith, A. Malczewski, Z. J. Yao, S. Chen, J. Ehmke, D. H. Hinzel “A RF MEMs Variable Capacitors for Tunable Filters”, John Wiley & Sons, Inc., p. 362-374, 1999.

[1.29] A. Tombak et al., “Voltage-Controlled RF Filters Employing Thin-Film Barium–Strontium–Titanate Tunable Capacitors”, IEEE Electron Device Letters, Vol. 26, No. 7, p. 462-467, Jul. 2005.

[1.30] T. Yun, K. Chang, “Piezoelectric-Transducer-Controlled Tunable Microwave Circuits”, IEEE Transactions on Microwave Theory and Techniques, Vol. 50, No. 5, May 2002.

[1.31] B. Yang, X. Jin, Y. Chen, J. Zhou, X. Zhang, S. Zheng, H. Chi, “A tunable optoelectronic oscillator based on a dispersion-induced microwave photonic filter”, IEEE Photonics Technology Letters, Vol. 25, no. 10, 2013.

[1.32] L. Pierantoni, D. Mencarelli M. Bozzi, R. Moro, S. Bellucci, “Graphene-based Electronically Tunable Microstrip Attenuator”, 2014 IEEE MTT-S International Microwave Symposium (IMS) , p. 1 - 3, Tampa, 2014.

[1.33] B. A. Belyaev A. A. Leksikov A. M. Serzhantov, V. F. Shabanov, “Physical principles of the design of electrically controllable microstrip devices”, Russian Physics Journal, Vol. 51, No. 9, p. 919-929 2008.

[1.34] P.J. Collings, M. Hird, "Introduction to liquid crystals chemistry and physics", Taylor & Francis, p. 505-538, 1997.

[1.35] D. Dolfi, M. Labeyrie, P. Joffre, J. P. Huignard. “Liquid crystal microwave phase shifter”, Electronics Letters, Vol. 29 No. 10, p. 926-928, 1993.

[1.36] H. Fujikake, T. Kuki, T. Nomoto, Y. Tsuchiya, Y. Utsumi, “Thick polymer-stabilized liquid crystal films for microwave phase control”, Journal of Applied Physics, Vol. 89, No. 10, p. 5295-5299, 2001.

[1.37] S. Mueller, F. Goelden, P. Scheele, M. Wittek, C. Hock, R. Jakoby, “Passive Phase Shifter for W-Band Applications using Liquid Crystals”, Proceedings of the 36th European Microwave Conference, Manchester, p. 306-309, 2006.

[1.38] F. Goelden, S. Mueller, P. Scheele, M. Wittek, R. Jakoby “IP3 Measurements of Liquid Crystals at Microwave Frequencies”, Proceedings of the 36th European Microwave Conference, Manchester, p. 971-974, 2006.

[1.39] Y. Garbovskyi, P. Krivosik, J. Lovejoy, “Liquid crystal phase shifters at millimeter wave frequencies”, Journal of Applied Physics, Vol. 111, No. 5, p. 054504 - 054504-4, 2012.

[1.40] M. Jost, C. Weickhmann, S. Strunck, A. Gaebler, W. Hu, T. Franke, A. E. Prasetiadi, O. H. Karabey, R. Jakoby, “Electrically biased W-band phase shifter based on liquid crystal”, 39th International Conference on Infrared, Millimeter, and Terahertz waves (IRMMW-THz), p. 1-2, Tucson (USA), 2014.

[1.41] C. M. Karwin and K. L. Livesey, “Liquid crystal phase shifters with a twist C.”, Applied Physics Letters, Vol. 103, p. 063508-1 - 063508-3, 2013.

[1.42] C. Person, P. Gelin, F. Huret, “Patch antenna adjustable in frequency using liquid crystal”. 33rd European Microwave, p. 699-702 Munich 2003.

[1.43 F. Yang, J. R. Sambles, “Determination of the permittivity of nematic liquid crystals in the microwave region,” Liquid Crystals, Vol. 30, No. 5, pp. 599–602, 2003.

[1.44] A. C. Polycarpou, M. A. Christou, M. C. Papanicolau “Tunable Patch Antenna Printed on a Biased Nematic Liquid Crystal Cell”, IEEE Transactions on Antennas and Propagation, Vol. 62, No 10, p. 4980-4987, 2014.

[1.45] E. Carrasco-Yepez, M. Arrebola-Baena, J. A. Encinar. “Desarrollo, análisis y diseño de antenas tipo reflectarray”, Universidad Politécnica de Madrid. Ingeniería e investigación Vol. 4, No 4, p. 236-239, 2005.

[1.46] M.Y. Ismail, R. Cahill, "Beam Steering Reflectarrays Using Liquid Crystal Substrate", Tenth IEEE High Frequency Postgr-aduiate Stuident Colloqulium 5 & 6, Leeds September 2005.

[1.47] W. Hu, R. Cahill, V. F. Fusco, H. S. Gamble, D. Linton, R. Dickie, S. P. Rea, N. Grant "Phase control of reflectarray patches using liquid crystal substrate", First European Conference on Antennas and Propagation, p. 6–10, 2006.

[1.48] R. Cahill, V. F. Fusco, H. S. Gamble, D. Linton, R. Dickie, S. P. Rea,N. Grant, "Phase agile Reflectarray cells based on liquid crystals", IET Microwave Antenna Propagation, Vol. 1, No 4, p. 809-814, 2007.

[1.49] G. Pérez-Palomino, P. Baine, R. Dickie, M. Bain, J.A. Encinar, M. Barba, G. Toso, "Design and experimental validation of liquid crystal-based reconfigurable reflectarray elements with improved bandwidth in F-band", IEEE Transactions on Antennas and Propagation, Vol. 61, No 4, p. 1704-1713, 2013.

[1.50] R. Cahill, J. A. Encinar, M. Arrebola, R. Simms, R. Dickie, V. F. Fusco, N. Mitchell, "Recent progress in electronically tunable reflectarray technology using liquid crystals", Journal of Applied Physics, Vol 111, No 7, p. 170-171, 2006.

[1.51] G. Perez-Palomino, J. A. Encinar, M. Barba, "Accurate Electromagnetic Modeling of Liquid Crystal Cells for Reconfigurable Reflectarrays", Proceedings of the 5th European Conference on Antennas and Propagation p. 997 - 1001, 2012.

[1.52] G. Perez-Palomino, R. Florencio, J. A. Encinar. M. Barba, R. Dickie, R. Cahill, P. Baine, M. Bain, and R. R. Boix. "Accurate and Efficient Modeling to Calculate the Voltage Dependence of Liquid Crystal-Based Reflectarray Cells", IEEE transactions on antennas and propagation, vol. 62, no. 5, 2014.

[1.53] R. Marin, A. Mössinger, J. Freese, A. Manabe, and R. Jakoby. "Realization of 35 GHz Steerable Reflectarray Using Highly Anisotropic Liquid Crystal", IEEE Antennas and Propagation Society International Symposium, p. 4307-4310, 2006.

[1.54] S. Bildik, S. Dieter, C. Fritzsch, M. Frei, C. Fischer, W. Menzel, R. Jakoby "Reconfigurable Liquid Crystal Reflectarray with Extended Tunable Phase Range", Proceedings of the 8th European Radar Conference, p. 404-407, 2011.

[1.55] D. T. Doyle, C. D. Woehrle, C. G. Christodoulou, "Development of Liquid Crystal Reflectarrays Utilizing a Passive Matrix Control Scheme", Antennas and Propagation Society International Symposium (APSURSI), p. 1031 – 1032, 2014.

[1.56] T. Kamei, M. Yokota, R. Ozaki, H. Moritake, N. Onodera, "Microstrip Array Antenna with Liquid Crystals Loaded Phase Shifter" Molecular Crystals and Liquid Crystals, Vol. 542, p.167-175, 2011.

[1.57] O. H. Karabey, S. Bildik, S. Strunck, A. Gaebler, R. Jakoby "Continuously polarization reconfigurable antenna element by using liquid crystal based tunable coupled line" Journal of Engineering and Technology Research Vol. 4 No 3, p. 57-64, Feb. 2012.

[1.58] P. Deo, D. Mirshekar-Syahkal, L. Seddon, S. E. Day, F. Aníbal Fernández, "Liquid crystal based patch antenna array for 60 GHz applications" IEEE Radio and Wireless Symposium, p. 127-129, 2013.

[1.59] L. Seddon, P. Deo, D. Mirshekar-Syahkal, S. E. Day, F. Aníbal Fernández, "Accurate modeling of liquid crystal-tuned meander-line phase-shifter", Microwave Symposium Digest (IMS), Seattle, p. 1-3, 2013.

[1.60] R. Dickie, R. Cahill, H. Gamble, Y. Ismail, V. Fusco, D. Linton, N. Grant, S. Rea, "Liquid Crystal Tunable mm Wave Frequency Selective Surface", IEEE Microwave and Wireless Components Letters, Vol. 17, No. 9, p. 3717-3719, 2007.

[1.61] F. Goelden, A. Gaebler, O. Karabey, M. Goebel, A. Manabe, R. Jakoby, "Tunable Band-Pass Filter Based on Liquid Crystal", German Microwave Conference, p. 979-982, Berlin, 2010.

[1.62] M. Yazdanpanahi, P. Deo, D. Mirshekar-Syahkal, "Tunable liquid-crystal millimeter-wave bandpass filter using periodical structure", IEEE Radio and Wireless Symposium (RWS), New Port Beach (USA), 2014.

[1.63] J. Yeh, C. Chang, C. Cheng, J. Huang, and S. S. H. Hsu, "Microwave Characteristics of Liquid-Crystal Tunable Capacitors", IEEE Electron Device Letters, Vol. 26, No. 7, p. 451-453, 2005.

[1.64] C. Weil, S. Müller, P. Scheele, Y. Kryvoshapka, G. Lüssem, P. Best, R. Jakoby, "Ferroelectric- and Liquid Crystal- Tunable Microwave Phase Shifters", 33rd European Microwave Conference, p. 1431-1434, Munich, Germany, 2003.

[1.65] C. Marcos, J. Torrecilla, V. Urruchi, J. M. Sánchez-Pena, "Dispositivo de fase sintonizable para microondas basado en cristal líquido", XXVI Simposiun Nacional Unión Científica Internacional de Radio (URSI), 2011

CHAPTER 2. DESIGN OF TUNABLE FILTERS BASED ON LIQUID CRYSTAL TECHNOLOGY. THEORETICAL CONSIDERATIONS

In this chapter, the main theoretical considerations for the design of tunable microwave devices, specifically filters, based on LC technology are described.

To explore the ability of tuning the liquid crystals (LC) features is the first concern. Regarding added value and innovation of this work of thesis, going into detail about physical theory of motion of the molecular director of the LC molecules (The Continuum Theory) has not been considered an essential requisite, thus this theory is not included in the document. A quick analysis of the behavior involved in the LC switching is summarized. The main contribution is rather focused on testing the tuning capacity power as a whole and estimating a working range. In this sense, devices designed are voltage-controlled for inducing anisotropy changes of the LC molecules.

As explained in the first chapter, the core of the work is specifically focuses on the design of LC-based microwave tunable filters. Following sections of this chapter put in context with a rough background description, stated definitions and parameters well-known for telecommunication filters. In addition, some general considerations for their design are mentioned.

Final section is devoted to explain the filter structure. Microwave filters are mainly designed by using transmission lines such as waveguides or microstrip lines. A special configuration is required for the case of LC-based devices; the inverted microstrip line structure. The implementation of this configuration is mandatory for simple designs of LC filters. It is conditioned by the need to accommodate the dielectric liquid crystal. However, it brings some design constraints in terms of the number of layers and connections of the stack or the dimension size that will be considered.

2.1. Liquid crystal tunability

Liquid crystal tunability gives meaning the devising of filters with spectral response that can be tuned across a range. As it is well-known, the modulation of the LC response derives from an intrinsic quality of some of their properties: the anisotropy. The origin of the anisotropy comes from the shape of the LC molecules.

Liquid crystals are materials composed of organic molecules which present some intermediate physical phases, called mesophases, between the solid state and the liquid state. In this work, liquid crystals in the nematic mesophase are used; this is the most employed phase in LC applications for telecommunications. There are two kinds of LC molecules: discotic molecules (disc shape) and calamitic molecules (elongated shape). Nematic liquid crystals have calamitic molecules. Just, this lack of symmetry according to the considered axis of reference, confers the property of anisotropy to their molecules. And correspondently, LC physical properties depend on the molecule orientation [2.1]. In this work, only two anisotropies of the typical ones for liquid crystals are considered: the anisotropy of the dielectric permittivity (Ɛ) and the anisotropy of the refractive index ($n = \sqrt{\varepsilon_r}$).

Because of LC anisotropy, LC permittivity is expressed as the tensor Ɛ, defined as:

$$\begin{pmatrix} D_x \\ D_y \\ D_z \end{pmatrix} = \begin{pmatrix} \varepsilon_{xx} & \varepsilon_{xy} & \varepsilon_{xz} \\ \varepsilon_{yx} & \varepsilon_{yy} & \varepsilon_{yz} \\ \varepsilon_{zx} & \varepsilon_{zy} & \varepsilon_{zz} \end{pmatrix} \begin{pmatrix} E_x \\ E_y \\ E_z \end{pmatrix} \tag{2.1}$$

where **E** is the electric field and **D** the electric displacement field, defined as **D** = Ɛ**E.**

LC molecules are considered to be uniaxial for the different physical properties [2.1].That is, two different components are defined for the LC permittivity: the component parallel to the long axis, $\varepsilon_{||}$, and the perpendicular component to the long axis, $\varepsilon_{\perp}$ [2.2], as shown in Fig. 2.1.

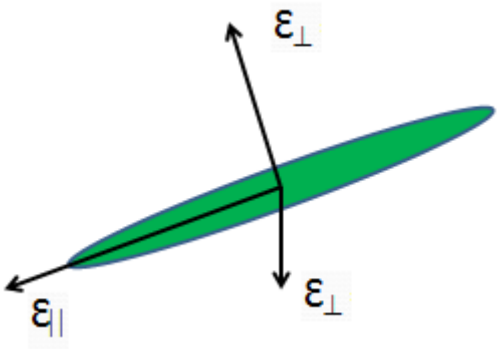

Figure 2.1. Permittivity components of an uniaxial liquid crystal molecule

Thus, tensor Ɛ becomes as follows:

$$\bar{\bar{\varepsilon}} = \begin{pmatrix} \varepsilon_{\perp} & 0 & 0 \\ 0 & \varepsilon_{\perp} & 0 \\ 0 & 0 & \varepsilon_{\parallel} \end{pmatrix} \tag{2.2}$$

The optical anisotropy, Δn, also called birefringence, is defined as:

$$\Delta n = n_{\parallel} - n_{\perp} \tag{2.3}$$

And, the dielectric anisotropy, Δε, is defined, in the same way, as:

$$\Delta\varepsilon = \varepsilon_{\parallel} - \varepsilon_{\perp} \tag{2.4}$$

The dielectric anisotropy may be positive or negative, as a function of the sign of Δε. In this work, only LC materials with positive anisotropy are considered due to their better performance at microwave frequencies.

Furthermore, LC molecules are polar, which means that they are oriented parallel to the direction of an applied electric field (if positive dielectric anisotropy) or perpendicular to the direction of the electric field (if negative dielectric anisotropy). Therefore, and for LC materials with Δε positive, when no voltage is applied, LC molecules are oriented approximately perpendicular to the electric field and LC permittivity is $\varepsilon_{\perp}$. When some voltage is applied, LC molecules rotate and, as the saturation voltage is reached (Figure 2.2), molecules place parallel to the applied electric field and the LC permittivity becomes $\varepsilon_{\parallel}$.

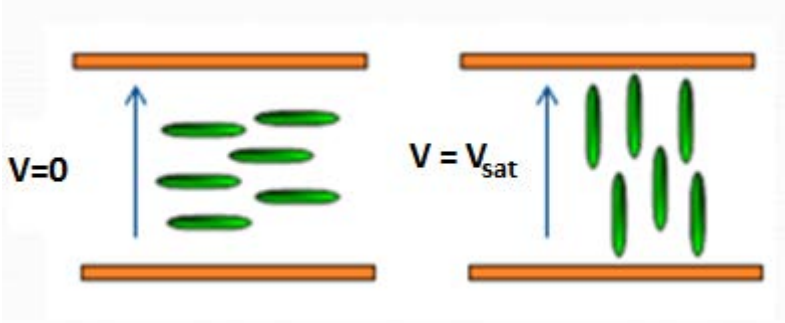

Figure 2.2. LC molecules orientation when no voltage is applied (left) and when applied voltage reaches the saturation value (right).

Thus, LC permittivity can be changed between two extreme values, $\varepsilon_{\perp}$ and $\varepsilon_{\parallel}$, by applying an external electric field. Although Figure 2.2 illustrates a simplified scheme of the working principle, it is clear enough to define the operation. The initial position of molecules, parallel to the glasses on both substrates, is determined by a careful alignment process that will be introduced in the next chapter. It does not include the effect of the manufacturing protocol on the molecules position. Finally, the frequency tuning range for microwave devices will depend partially on the LC dielectric anisotropy, $\Delta\varepsilon$. The largest value of LC dielectric anisotropy; the highest tuning range can be reached.

2.2. Filters at microwave frequencies

In this section, the fundamental concepts of filtering are described from the definition of basic parameters. Also, a brief description of different types of filters, the value of scattering parameters typical for those configurations and several guidelines for the design issues are reported.

2.2.a. Fundamental concepts of filtering

Filters are devices which are able to select or reject signals as a function of any characteristic of the signal. The level of selection or rejection of the signal is determined by the power at the input and at the output of the filter. Fig. 2.3 shows the basic parameters related to the power of signals involved in a filter. P_1 is the available power at the filter input, P_2 is the transmitted power, while P_r represents the reflected power at the filter input. If the filter is considered to be lossless, then $P_1 = P_2 + P_r$.

Figure 2.3. Basic schematic of a filter in terms of powers involved in their ports.

In telecommunications, the frequency is the main characteristic which determines the selection or rejection of a signal. Therefore, linear and time-invariant (LTI) systems, whose response to a sinusoidal signal is another sinusoidal signal of the same frequency, are suitable for the design of filters [2.3]. Assuming a filter as a LTI system, it is defined by its impulse

response *h(t)*. And, in the complex domain, it is defined by the transfer function *H(jω)*, which is the Fourier Transform of *h(t)*. Following these definitions, the discrimination of frequencies will be treated working in the complex frequency domain in this work of Thesis.

The square of the modulus of the transfer function, $|H(j\omega)|$, can be expressed as the ratio of the transmitted power, P_2, to the available power at the input of the filter, P_1:

$$|H(j\omega)|^2 = \frac{P_2(j\omega)}{P_1(j\omega)} \tag{2.5}$$

The square of the modulus of the reflection coefficient, $|\rho(j\omega)|$, is defined as the ratio of the reflected power, P_r, to the available power at the input of the filter, P_1:

$$|\rho(j\omega)|^2 = \frac{P_r(j\omega)}{P_1(j\omega)} \tag{2.6}$$

And additionally, the filter characteristic function, $|K(j\omega)|$, is defined as:

$$|K(j\omega)|^2 = \frac{P_r(j\omega)}{P_2(j\omega)} \tag{2.7}$$

Depending on the frequency response of the filter, the following types of filter can be distinguished:

- **Low-pass filters**. These devices pass the low frequencies and attenuate the high frequencies.

- **High-pass filters**. They are the opposite of the low-pass filters. They pass the high frequencies and reject the low frequencies.

- **Band-pass filters**. They pass a band of frequencies, which is called filter passband, while reject the rest of frequencies.

- **Band-stop filters**. They are also called band-rejection filters. They attenuate a certain band of frequencies, called stop-band or rejection frequency, while allows the rest of frequencies to pass. If the stop-band is very narrow, the device is called a *notch* filter.

- **All-pass filters:** They are a kind of filter where no frequency band is attenuated.

2.2.b. Microwave filters

As stated above, a filter is an electromagnetic device which selects or rejects signals as a function of its carrier frequency. Specifically, passive microwave filters consist of coupled resonators where Maxwell equations can be simplified so that the filter can be modeled by using only resistors, capacitors and inductors [2.4]. Filters configured in that way can be also modeled as a passive two-port network as that shown in Fig. 2.3 [2.5]. The number of resonant frequencies determines the filter order. The matrix that relates the incident, reflected and transmitted powers of the passive two-port network is the scattering matrix or S-parameters matrix [S], which is defined as:

$$[S] = \begin{bmatrix} S_{11} & S_{12} \\ S_{21} & S_{22} \end{bmatrix} \tag{2.8}$$

And taking the previous definitions, the S-parameters can relate with the filter functions as follows:

$$H(j\omega) = S_{21}(j\omega) \tag{2.9}$$

$$\rho(j\omega) = S_{11}(j\omega) \tag{2.10}$$

$$K(j\omega) = \frac{S_{11}(j\omega)}{S_{21}(j\omega)} \tag{2.11}$$

For the particular research of this work of thesis, there are two significant parameters of the filter: the insertion loss (IL) and the return loss (RL) that can be derived from S-parameters.

i) Insertion loss (IL)

IL is the decibel (dB) expression of the ratio of the microwave power received at the end of the filter, P2, to the power transmitted at the filter input, P1. Insertion loss can result from some factors: The loss due to the impedance mismatch at the filter input and output or the dissipative loss associated with each reactive element within the filter if any.

The expression for insertion loss is,

$$IL(dB) = 20\log S_{21} = 10\log\frac{P_2}{P_1} \tag{2.12}$$

It is commonly expressed in positive dB's.

Since the S21 parameter is a measurement of the transmitted power of the device, the value of the filter insertion loss should be very low (in absolute value) in the bands of frequency to pass and very high in the bands of frequency to reject. So, in a *notch filter*, insertion loss is greater than a specified value. For example, a notch filter can be characterized by the frequency range where the insertion loss is greater than 20 dB in the stop-band. The higher the insertion loss, the sharper or narrower the bandwidth. In a *band-pass filter*, insertion loss is less than a specified value. For example, a band-pass filter can be specified to have a maximum insertion loss value of 1 dB within the passband.

ii) Return loss (RL)

The return loss is the decibel (dB) expression of the ratio of the reflected power, P_r, to the available power, P_1, both at the filter input. Again, the return loss is caused due to impedance mismatch between components that, at microwave frequencies, is determined by the material properties and the dimensions of the de structures.

Return loss can be calculated using the following equation,

$$RL(dB) = 20\log S_{11} = 10\log\frac{P_r}{P_1} \tag{2.13}$$

It is commonly expressed in positive dB's.

In the same way, as the S_{11} parameter is related with the reflected power of the filter, the return loss should be low in the selected frequencies and high in the attenuated frequencies. In a notch filter, return loss is not a typical parameter to evaluate the quality of the devices. In a band-pass filter, the larger the value, the better quality of the device under test.

For example, Fig. 2.4 shows a typical frequency response of a band-pass filter. The insertion loss value is minimum (close to 0 dB) in the pass-band, while the return loss is very high.

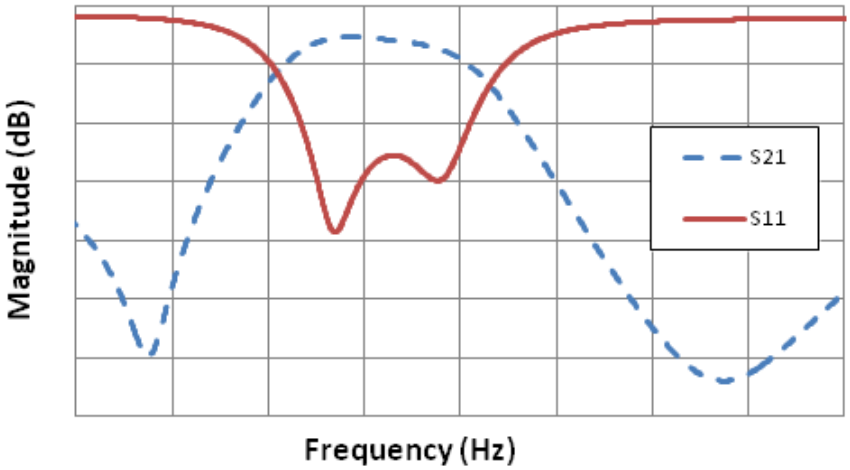

Figure 2.4. S-parameters of a typical band-pass filter.

A very important parameter for the design of filters is the filter selectivity. The selectivity is defined as the attenuation of the rejected frequencies compared to the passed frequencies. The quality factor (Q), which is defined as the ratio between the central frequency of the filter and the 3 dB filter bandwidth ($Q = f_0/BW$) for a single resonator; it is a filter parameter closely related to the filter selectivity. As Q is higher, the filter presents a more selective response. Therefore, in order to obtain a selective filter, it is necessary to implement the device by using a technology that manages a high quality factor [2.6].

At microwave frequencies, filters directly designed with lumped elements (resistors, capacitors and inductors) present very low quality factors. Therefore, these devices are designed with distributed elements or transmission lines, which achieve better performance and can be modeled by using an equivalent RLC circuit [2.7]. Some examples of transmission lines are waveguides, coaxial lines or microstrip lines. The latter technology is studied in depth in the next section.

2.3. Microstrip technology

Microstrip technology is one of the most used transmission lines for the design of microwave devices due to its good performance and easy design. There are many reported designs of microstrip technology for microwave devices. Some examples are patch antennas [2.8], [2.9] or microwave couplers [2.10], [2.11]. However, this technology is also widely employed for the design of microwave filters [2.12], [2.13].

A microstrip line structure is manufactured by using a printed circuit board (PCB). Fig. 2.5 a) shows the geometry of a typical microstrip line. It consists of a conductor of width *w* printed on a grounded dielectric substrate of thickness *d*, whose relative permittivity is ε_r and a ground plane of conductor material. Fig. 2.5 b) shows the distribution of the electric and magnetic field lines in the microstrip line.

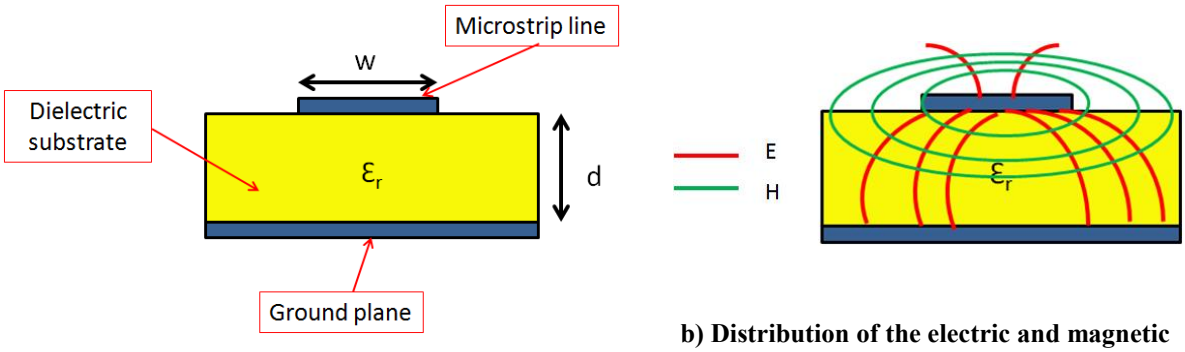

a) Geometry of the layers.

b) Distribution of the electric and magnetic fields.

Figure 2.5. Microstrip line structure.

Due to the presence of the dielectric, which means some field lines propagate in the dielectric region and some field lines in the air region, the electromagnetic analysis of the microstrip line is not easy. The phase velocity in the dielectric region would be $c/\sqrt{\varepsilon_r}$, while it would be *c* in the air region. Thus, a pure TEM wave can´t be supported in a microstrip line, so there is not a static solution [2.14].

For this reason, the fields of a microstrip line are considered to be a hybrid TM-TE electromagnetic mode. Nevertheless, if the dielectric substrate is thin enough (d << λ), the electromagnetic field can be modeled as a quasi-TEM wave, which simplifies the analysis of the microstrip line. A quasi-static solution can be obtained and, the phase velocity (v_p) and the propagation constant (β), can be approximated as follows:

$$v_p = c/\sqrt{\varepsilon_{eff}} \tag{2.14}$$

$$\beta = k_0\sqrt{\varepsilon_{eff}} \tag{2.15}$$

where k_0 is the vacuum wave number $k_0 = 2\pi/\lambda$.

ε_{eff} is the effective permittivity of the microstrip line that is considered as the dielectric constant of a single homogeneous medium instead of the constant of two media: the dielectric and the air regions. Due to the fact that some of the field lines are in the dielectric region and other lines are in the air region, the value of ε_{eff} ranges between the permittivity of the air ($\varepsilon_r = 1$) and the permittivity of the dielectric material (ε_r). ε_{eff} also depends on the microstrip line dimensions and it is calculated as follows:

$$\varepsilon_{eff} = \frac{\varepsilon_r + 1}{2} + \frac{\varepsilon_r - 1}{2} \frac{1}{\sqrt{1 + 12d/w}} \tag{2.16}$$

A key parameter of the microstrip line is its characteristic impedance (Z_0). It depends on the geometry of the microstrip line and its effective permittivity. It is expressed as:

$$Z_0 = \begin{cases} \frac{60}{\sqrt{\varepsilon_{eff}}} \ln\left(\frac{8d}{w} + \frac{w}{4d}\right) & if \ \frac{w}{d} \leq 1 \\ \frac{120\pi}{\sqrt{\varepsilon_{eff}\left[\frac{w}{d} + 1.393 + 0.667 \ln\left(\frac{w}{d} + 1.444\right)\right]}} & if \ \frac{w}{d} > 1 \end{cases} \tag{2.17}$$

In the design of a microstrip line, a strategic aspect to manage is the impedance matching between the characteristic impedance of the microstrip line and the input impedance of the circuit. For example, if the input of the microstrip circuit is a coaxial SMA connector ($Z = 50\ \Omega$), the characteristic impedance of the microstrip line must be designed as $Z_0 = 50\ \Omega$.

As stated in equation (2.17), the characteristic impedance depends on the microstrip line dimensions (*w* and *d*). Therefore, these dimensions have to be optimized in order to obtain the impedance matching. Given a value for the characteristic impedance, Z_0, the *w/d* ratio can be calculated as follows:

$$\frac{w}{d} = \begin{cases} \dfrac{8e^{A}}{e^{2A}-2} & if \ \dfrac{w}{d} \leq 2 \\ \dfrac{2}{\pi}\left[B-1-\ln(2B-1)+\dfrac{\varepsilon_r-1}{2\varepsilon_r}\left(\ln(B-1)+0.39-\dfrac{0.61}{\varepsilon_r}\right)\right] & if \ \dfrac{w}{d} > 2 \end{cases}$$

(2.18)

where:

$$A = \frac{Z_0}{60}\sqrt{\frac{\varepsilon_r+1}{2}}+\frac{\varepsilon_r-1}{\varepsilon_r+1}\left(0.23+\frac{0.11}{\varepsilon_r}\right)$$

(2.19)

$$B = \frac{377\pi}{2Z_0\sqrt{\varepsilon_r}}$$

(2.20)

2.3.a. The inverted-microstrip line structure

The goal of this work is the design of tunable devices where LC is used as dielectric substrate, in order to take advantage of the anisotropic properties of these materials. As the LC is a fluid material, a cavity is necessary for confining it. Therefore, for LC-based devices, a variant of the microstrip line structure, called inverted-microstrip line structure, is employed. The use of this structure for LC devices has been reported [2.15], [2.16].

Fig. 2.6 shows a typical inverted-microstrip line structure. It consists of a conductor of width *w* supported by a dielectric substrate of thickness *a* and dielectric constant ε_r, separated from the ground plane by an air region of thickness *b* [2.17].

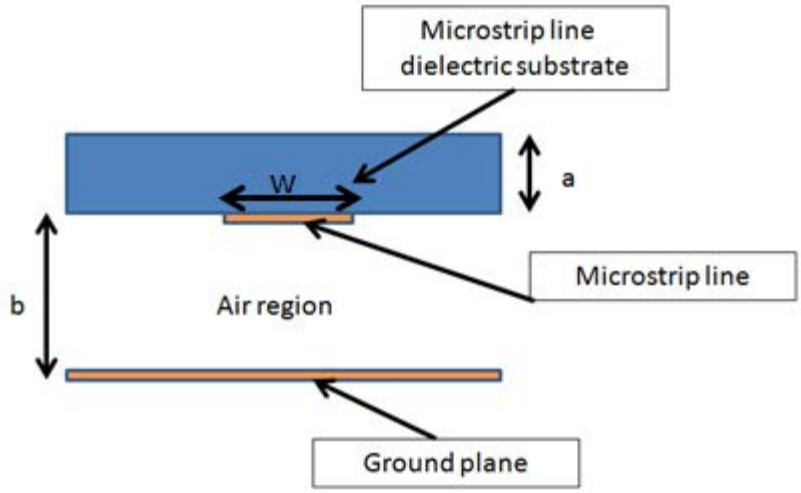

Figure 2.6. Typical inverted microstrip line geometry.

As happens in a conventional microstrip line, if the dielectric substrate and the air region are thin enough ($a << \lambda$ and $b << \lambda$), the electromagnetic field can be considered as a quasi-TEM wave where:

$$v_p = c/\sqrt{\varepsilon_{eff}} \tag{2.21}$$

$$\beta = k_0\sqrt{\varepsilon_{eff}} \tag{2.22}$$

In the case of an inverted-microstrip line, ε_{eff}, whose value is also between 1 and ε_r and depends on ε_r and the structure dimensions, is calculated as:

$$\varepsilon_{eff} = 1 + \frac{a}{b}\left(A - B\ln\frac{w}{b}\right)\left(\sqrt{\varepsilon_r} - 1\right) \tag{2.23}$$

where:

$$A = \left(0.5173 - 0.1515\ln\frac{a}{b}\right)^2 \tag{2.24}$$

$$B = \left(0.3092 - 0.1047\ln\frac{a}{b}\right)^2 \tag{2.25}$$

In the same way, the characteristic impedance (Z_0) of the inverted microstrip line is expressed as follows:

$$Z_0 = \frac{60}{\sqrt{\varepsilon_r}} \ln\left[\frac{f(u)}{u} + \sqrt{1 + \left(\frac{2}{u}\right)^2}\right] \tag{2.26}$$

where:

$$u = w/b \tag{2.27}$$

$$f(u) = 6 + (2\pi - 6)e^{-\left(\frac{30.666}{u}\right)^{0.7528}} \tag{2.28}$$

A typical inverted microstrip line structure for LC-based devices is shown in Fig. 2.7. The air region is replaced by a cavity which is filled with a LC material. In order to delimit the LC cavity, spacers of thickness *b* are inserted.

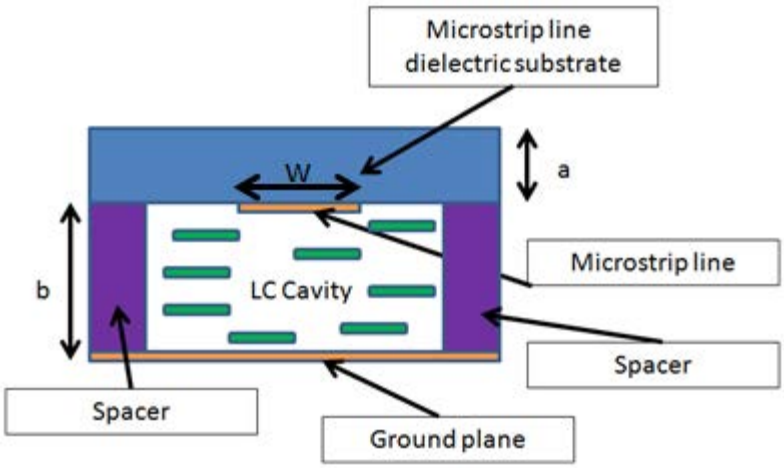

Figure 2.7. Inverted microstrip line geometry for LC-based devices.

The value of the effective permittivity (ε_{eff}) of the structure presented in Fig. 2.9 depends on the geometry and, also, on the dielectric constants of the different used materials: substrate which supports the microstrip line, spacers, and LC. As it was detailed in section 2.1, LC permittivity can be varied by applying an external voltage due to the LC anisotropic properties. Therefore, the value of ε_{eff} can be tuned correspondently.

2.4. References

[2.1] J. C. Torres "Caracterización, modelado eléctrico y desarrollo de nuevas aplicaciones de dispositivos basados en cristales líquidos". Juan Carlos Torres Zafra. Tesis Doctoral. Universidad Carlos III de Madrid, 2009.

[2.2] V. Urruchi, "Dispositivos electroópticos para aplicaciones fotónicas y domóticas". Apuntes asignatura Dispositivos electroópticos para aplicaciones fotónicas y domóticas. Máster en Sistemas Electrónicos Avanzados. Departamento de Tecnología Electrónica. Universidad Carlos III de Madrid. Curso 2010/2011.

[2.3] G. C. Temes, J. W. LaPatra, "Circuit Synthesis and design", McGraw-Hill Book Company, 1977.

[2.4] R. J. Cameron, C. M. Kudsia, R.R. Mansour, "Microwave Filters for Communication Systems. Fundamentals", Design and Applications. Wiley Interscience, 2007.

[2.5] M. Salazar Palma, A. García Lampérez, "Síntesis avanzada de filtros paso banda para aplicaciones espaciales. Introducción al diseño de multiplexores complejos", Grupo de Radiofrecuencia, Dpto. de Teoría de la Señal y Comunicaciones, Escuela Politécnica Superior, Universidad Carlos III de Madrid, Febrero 2008.

[2.6] J. Torrecilla, "Diseño y ajuste de filtros en banda Ka construidos con resonadores dieléctricos", Proyecto Fin de Carrera, ETSIT-UPM, 2008.

[2.7] C. Wang, K. A. Zaki, "Dielectric Resonators and Filters", IEEE Microwave Magazine, Vol. 8, no. 5, pp. 115-127, 2007.

[2.8] A. Kumar, D. Arya, D. K. Srivastava, "Band width of microstrip antenna improved by using mushroom type EBG structure", International Conference on Multimedia, Signal Processing and Communication Technologies (IMPACT), p. 159-162, Aligahr, India, 2013.

[2.9] N. Lu, X. Xu, "Sierpinski carpet fractal antenna in third iteration", International Conference on Microwave Technology & Computational Electromagnetics (ICMTCE), p. 164-167, Quindao, China, 2013.

[2.10] H. Shaman, S. Almorqi, O. Haraz, S. Alshebeili, A. Sebak, "Butterfly-shaped slot coupled microstrip 90° hybrid couplers for K- and Ka-band millimeter-wave radar applications", 14th Mediterranean Microwave Symposium (MMS), p. 1 - 3, Marrakech, 2014.

[2.11] D. Ghosh, G. Kumar, “A four branch microstrip coupler with improved bandwidth and isolation”, Twenty First National Conference on Communications, p. 1 - 6, Mumbai, 2015.

[2.12] J. Andrew Yeh, C. Alex Chang, Chih-Cheng Cheng, Jing-Yi Huang, and Shawn S. H. Hsu, “Design of microstrip lossy filter using an extended doublet topology”, IEEE Microwave and Wireless Components Letters, Vol. 24, No. 5, p. 318-320, 2014.

[2.13] S. Kaur, P. D. Laforge, “Design of a four pole quasi-elliptic microstrip filter using the reflected group delay method”, IEEE MTT-S International Microwave Symposium (IMS), p. 1-4, Tampa, USA, 2014.

[2.14] D. M. Pozar, “Microwave Engineering”, Wiley Interscience, 3rd ed., pp. 143 – 149, 2005.

[2.15] C. Weil, S. Müller, P. Scheele, Y. Kryvoshapka, G. Lüssem, P. Best, R. Jakoby, “Ferroelectric- and Liquid Crystal- Tunable Microwave Phase Shifters”, 33rd European Microwave Conference, p. 1431-1434, Munich, Germany, 2003.

[2.16] Y. Garbovskyi, P. Krivosik, J. Lovejoy, “Liquid crystal phase shifters at millimeter wave frequencies”, Journal of Applied Physics, Vol. 111, No. 5, p. 054504 - 054504-4, 2012.

[2.17] K. C. Gupta, “Microstrip lines and Slotlines”, Artech House, 2nd ed., pp. 115 – 117, 1996.

CHAPTER 3. FABRICATION AND EXPERIMENTAL SET-UP

Once the main theoretical fundamentals have been presented in a previous chapter, the main practical considerations for the fabrication and the measurement of tunable devices based on LC are described in this chapter. Since in this Thesis work, some different kinds of devices have been manufactured and characterized, the manufacturing procedure can slightly change depending on the requirements of the different prototypes to fabricate. Nevertheless, in this chapter, the general and common steps for the manufacturing process of every LC-based device are presented and described.

This chapter is divided into two main sections. The first one is devoted to the process of the device manufacturing. The fabrication and assembly of the different parts of the devices are described. It includes the cutting of the using substrates, the developing of the microstrip electrodes (carrying out by using a milling machine or by photolithography), the deposition of the alignment layer, which is a key process for the alignment of the LC molecules, the device assembly and, finally, the device filling with LC.

On the other hand, the second main section is about the experimental set up in order to carry out the characterization and measurements of the devices. The main equipment used in the characterization at microwave frequencies is the network analyzer, which allows the device S-parameters to be measured. The used equipment characteristics, working and calibration are described in this section.

In LC based devices, the key aspect is the necessity of switching the LC molecules by an external excitation. In this work, the devices are excited by an external voltage from a waveform generator, which is the most common way to switch LC molecules, in spite of the existence of other ways to do it, such as the excitation by using a magnetic field [3.1]. The requirement of an external voltage signal (in this case, a sinusoidal AC signal of low frequency), leads to the presence of two different signals at the device input: the microwave signal from the network analyzer and the external voltage signal from the waveform generator. In order to overlap both signals at the device input, a bias-T is employed. This component is, therefore, very important in the characterization set-up of LC based devices and its characteristics are also described in this chapter.

Finally, the characterization protocol for the measurements is described. It is important into take into account that devices are always previously measured with the LC cavity empty (i. e. before the filling with LC). This measurement is carried out in order to study the viability of the designed device. Since the device is sealed after the LC filling, it would not be

possible to back out, and, additionally, it would lead to a waste of LC, which is a very expensive material. Therefore, the device is first characterized without LC and then, if a good performance has been obtained, it is filling with LC.

3.1. Manufacturing process of microwave devices

This section is devoted to the main general considerations for the manufacturing of tunable devices based on liquid crystal (LC) technology.

As stated in the previous chapter, tunable LC devices for this work of thesis are implemented by inverted-microstrip line structures which are provided with a cavity specially designed for housing a LC mixture. The geometry of microwave devices is outlined in Fig. 3.1. It comprises a set of three different substrates: the substrate where is printed the microstrip circuit, the substrate that supports the ground plane and the spacer (that sometimes consists in two parts) which delimits the thickness of the LC cavity.

Some of the processes involved in the manufacturing protocol have to be carried out in a clean room classified as class 100. The fabrication of the alignment layer of the LC molecules and the filling of the device are processes that are required to be free from pollutants and therefore completed only in a clean environment.

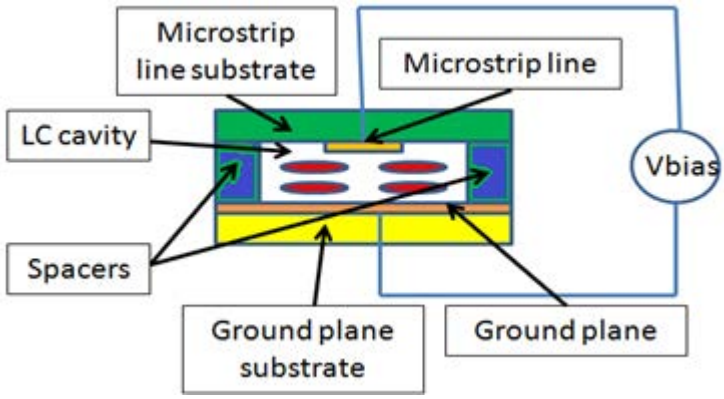

Figure 3.1. Inverted microstrip line geometry for LC-based devices.

A three-step protocol is followed for the device manufacturing:

- Firstly, the substrates are prepared: The dielectric material of the substrates is cut with the final size of the device, the pattern of the electrode is copper engraved with a specific shape and the treatment of the alignment layer is defined.

- The stack of layers that compose the device is assembled and sealed.

- Finally, the device is filled with the liquid crystal dielectric material.

The methods applied for the manufacturing processes are detailed in the following subsections.

3.1.a. Substrates manufacturing protocol

In this subsection manufacturing of the different parts or substrates of the device are presented. Next, the treatment of those substrates is described in terms of substrate cutting, printing the electrical conductors and aligning of the LC molecules. Before manufacturing, the design of the structure of the device: size, shape of the electrode pattern, etc., have been optimized by simulation though an electromagnetic software tool.

i) Cutting of the substrates

The substrates employed for building the filters are dielectric materials widely used in microwave frequencies. In this work, Taconic TLX-08 is used in the design of the devices. This material has a dielectric permittivity $\varepsilon_r = 2.55$, which is a very similar value compared to the estimated permittivity for certain LC´s at microwave frequencies [3.2]. In addition, this material has a good value of loss tangent ($\tan \delta = 0.0019$), which makes it very suitable to be used as dielectric substrate. The other material used is FR4 ($\varepsilon_r = 4.4$ and $\tan \delta = 0.02$), specifically employed as ground plane substrate due to its easiness of use.

Figure 3.2 shows various substrates depending on the degree of treatment; specifically, Fig. 3.2 a) illustrates a sheet of a raw Taconic TLX-08 dielectric substrate [3.1]. Usually, dielectric substrates are covered with a thin metallic layer that allows them connect electrically to a electronic circuit. The substrates we used in practice have a copper layer of 18 μm thick. At first, Taconic material is cut by a milling machine with the desired and optimized dimensions. Figure 3.2 b) shows a square piece of the substrate with the copper layer untreated. On the surface of this piece, several evenly distributed holes are drilled to make easier the alignment of the stack of layers later. Finally, last step involves the copper engraving and the generation of the pattern electrode of the microstrip line circuit (see Figure 3.2. c)).

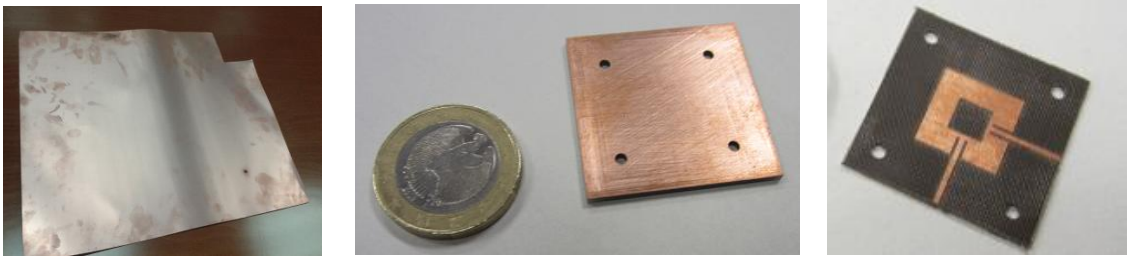

a) A sheet of the raw material.

b) A square piece of the dielectric with the copper layer.

c) Dielectric substrate with the microstrip circuit.

Figure 3.2. Taconic TLX-08 dielectric substrate for microwave frequencies.

ii) Developing the electrode pattern

The copper layer has to be selectively removed from the different substrates. It must remain in the ground plane and in the microstrip circuit. There are two procedures for removing the copper layer of the substrates: by using a milling machine and by photolithographic techniques.

Photolithographic methods are more accurate but, at the same time, they involve more steps and materials and ultimately are more expensive. This fact, coupled with a lack of infrastructure and the necessary tools to carry out the pattern with this technique, at the University Carlos III of Madrid, has led mainly to mechanical developments of the patterns. Photolitographic techniques have been only used for the manufacturing of the spiral notch filter (see section 4.3), whose fabrication was carried out in the facilities of the Universidad Miguel Hernández de Elche. Photolithography method consists of the following steps [3.3]:

- Mask preparation. A mask which corresponds to the electrode pattern of the microstrip line to use, depending on the desired circuit, is prepared.

- Photoresist deposition. The photoresist, which is a photosensitive fluid, is spread over the surfaces of the substrates by a spinning machine and cured in an oven.

- Insolation. The mask to print the electrode pattern is put on the substrate. Then, the substrate is exposed to UV light, which only affects to the parts of the substrate that have not been covered by the mask.

- Developing. The photorresist insolated is removed and the substrate is prepared to be attacked by acid.

- Attack with acid. The substrate is attacked with acid and the metallic layer is removed except the parts which were covered by the mask.

The generation of the electrode pattern by mechanical techniques through a milling machine is in fact a less fine process but that does not compromise the realization of the electrode patterns for the LC filters since the finer resolution is only 0.1 mm. So, most of the filters has been done with this procedure. University Carlos III of Madrid has machining equipment and numeric control machine for positioning the substrates to be shaped, engraved and drilled. The used milling machine is shown in Figure 3.3.

Figure 3.3. Milling machine.

iii) Treating the alignment layer

Once the electrode pattern is engraved on the dielectric substrates, a critical aspect to take into account is the alignment of the LC molecules within the cavity that house them. If LC mixture is inserted directly into the cavity without any preparation of it, molecules are not homogeneously oriented in nearly the same direction within the bulk. So, it is necessary to guide the molecules in a preferred direction through an additional process. This task usually is got by placing and treating an alignment layer on the substrates. In Fig. 3.4 is outlined the processes involved in the protocol of alignment.

In order to orient the LC molecules parallel to the microstrip line (homogeneous alignment), a thin film of polyimide is placed on the inner face of the substrates, that is, on top of the copper conductors of the device (microstrip circuit and ground plane) (Figure 3.4 a)). The polyimide is spread on the surfaces by using a spinner and the substrates are heated up in an oven (up to 200º C). Then, these surfaces are rubbed (Figure 3.4 b)) in one direction by using a rubbing machine. The direction of alignment is specific for each manufactured pattern (Figure 3.4 c)). For example, alignment direction is the same as the spurline length *a* for the conventional spurline structure and as shown in Fig. 3.3 c) in the other electrode patterns. Once surfaces are rubbed, micro-grooves are created in the conductor and the interaction between the polyimide and the LC involves the alignment of the LC molecules. Figure 3.4 d) represents a reference system diagram to set the direction of alignment on the microstrip line. It is important to take into account that the two rubbed substrates (for the microstrip circuit and for the ground plane) have to be antiparallel assembled for obtaining the right alignment. The LC molecules are oriented parallel to the microstrip line circuit (homogeneous alignment). In this way, when no voltage is applied, the LC permittivity for the microwave signal is $\varepsilon_{r\perp}$. As voltage is applied, the LC molecules are oriented in the electromagnetic field direction and at the saturation voltage value (V_{sat}), they are perpendicular to the microstrip line, and the LC permittivity for the microwave signal is, in this case, $\varepsilon_{r\parallel}$.

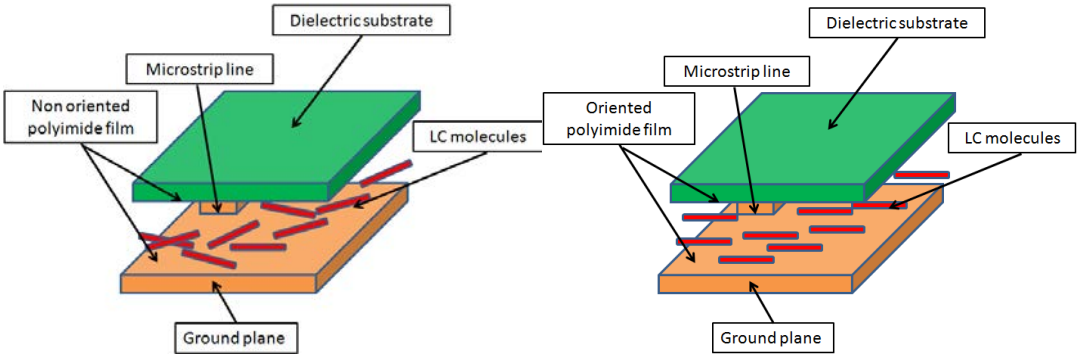

a) Inverted microstrip line structure with non oriented polyimide films

b) Inverted microstrip line structure with oriented polyimide films

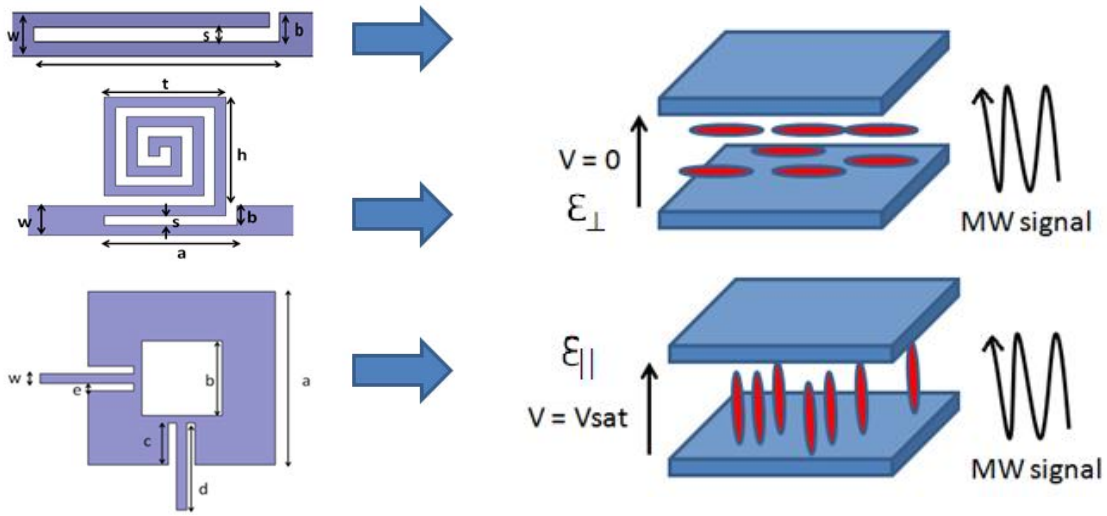

c) Direction of alignment for each used electrode pattern

d) Reference system diagram of the direction of alignment on the microstrip line.

Figure 3.4. Steps for treating the alignment layer of a LC filter for getting homogeneous alignment.

Due to the large thickness of the LC bulk in microwave devices, between 100 μm and 500 μm, orientation can be lost in the molecules which are far from the surfaces where polyimide is rubbed. Nevertheless, as it was suggested by previous experimental results of our research group [3.4], the LC director, $\hat{n}$, which is the vector that represents the local average orientation of LC molecules in the LC cavity, has an average tilt angle close to 0º when no voltage is applied to the device, so it is considered that a good homogeneous alignment of LC molecules is achieved.

In this work, homogeneous alignment is used in every manufactured device. Nevertheless, it is not the only kind of LC alignment possible to arise in this kind of devices. Other alignments such as homeotropic, where LC molecules are oriented perpendicular to the

substrates, or twisted alignment might be produced using specific mechanical or chemical procedures during the manufacturing process [3.5].

The deposition of the alignment layer, as well as the device assembly and the LC filling, are carried out in a clean room in order to avoid pollution in the process. People who work in this room always must wear a special dress, mask, latex gloves, bootees and head cap. Besides, the material introduced in the clean room has to be cleaned usually with alcohol or acetone. The devices manufactured in this work have been filled with LC material in the clean room of the Grupo de Fotónica Aplicada de la Escuela Superior de Ingenieros de Telecomunicación (Universidad Politécnica de Madrid). Examples of spinner machine and rubbing machine are shown in Figure 3.5.

a) Spinner machine. **b) Rubbing machine.**

Figure 3.5. Spinner machine and rubbing machine.

3.1.b. Device assembly

Once the process of manufacture of substrates is completed, the filter is assembled. As stated previously, the substrate of the microstrip circuit and the ground plane have to be antiparallel assembled for obtaining the right alignment of molecules., A spacer or a set of some spacers are inserted between both substrates for delimiting the LC cavity. As it was commented in section 3.1.a, the different substrates have been drilled in order to be aligned in stack. For this alignment, and also for the attachment of the different layers, set screws manufactured of nylon are used. The holes drilled for the screws have been implemented far enough from the LC cavity for not interfering in the device response. Additionally, two lineal guides are built on the spacer substrate for allowing the device to be filled with the LC mixture from the outer sides.

In order to connect the filters with the outer (i. e., with the measuring equipments and with the external voltage to switch the LC molecules), SMA connectors are used and soldered in the input and in the output of the device to serve as electrical interface. A SMA connector is a RF coaxial connector extensively used in microwave frequencies. It uses a

polytetrafluoroethylene PTFE dielectric and presents a characteristic impedance of 50 Ω [3.6]. Pictures of Figure 3.6 show SMA connectors (Fig. 3.5. a)) and a final manufactured and assembled LC filter (Fig. 3.5 b)). The assembled device is sealed by an epoxy resin coating and, then, by a photosensitive glue, except the guides on the spacer which must keep open to introduce the LC.

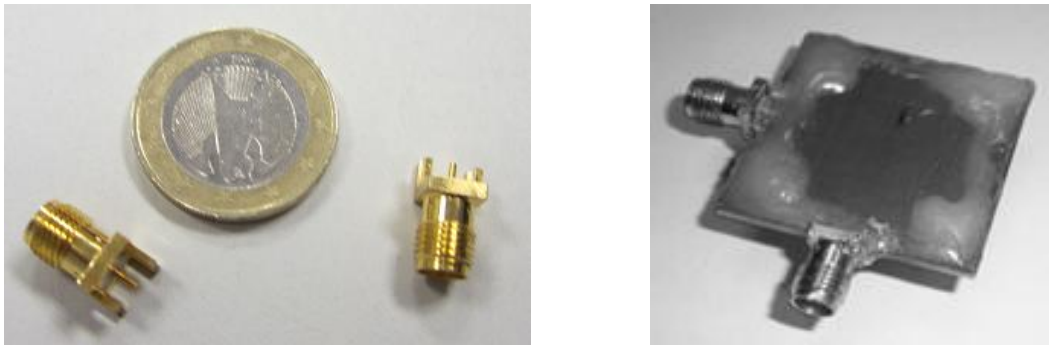

a) SMA connectors. **b) Example of manufactured device.**

Figure 3.6. SMA connectors and set of layers for a LC filter implementation.

3.1.c. Device filling

After the filters are assembled, they must be filled with the LC mixtures. The nematic liquid crystals, which are employed in this work of Thesis, are introduced in the devices by capillarity at room temperature. The material is inserted into the cavity from the outside of the filter through some guides built in the spacers.

Additionally, to avoid vapors inside the cavity, the LC is degassed before being introduced into the filter. The degassing process consists of heating the LC (up to 80º C) in vacuum regime [3.3] during about 30 minutes.

Once the filter is filled, the guides are sealed with an epoxy adhesive and, also, with a photosensitive glue and the device is ready to be experimentally characterized.

3.2. Experimental set-up

In this section the measurement process or experimental set-up of the manufactured devices is described. Since the work of this Thesis is focused on tunable filters and, as it was mentioned in the previous chapter, the electrical response of a microwave filter is characterized by its scattering matrix, it is necessary to measure the filter S-parameters. The

equipment used to measure these parameters is the network analyzer, which is described in depth in sub-section 3.2.a.

This section is organized as follows: first, the different components of the experimental setup are described, as well as the connections among them. It is important to take account that, as network analyzer is the equipment for the measurements of the S-parameters, it is important to assure its right working. For this purpose, network analyzer needs to be calibrated and this process is explained next. Finally, the measurement protocol is presented.

3.2.a. Components of the experimental set-up

A general schematic of the components that are included in the experimental set-up is shown in Fig. 3.7. The frequency response of the LC filters is measured through the S-parameters with a network analyzer. Simultaneously to the measuring process, filters are excited by low frequency alternating voltage (LC driving voltage) to test the ability of them to tune the spectral response by controlling voltage.

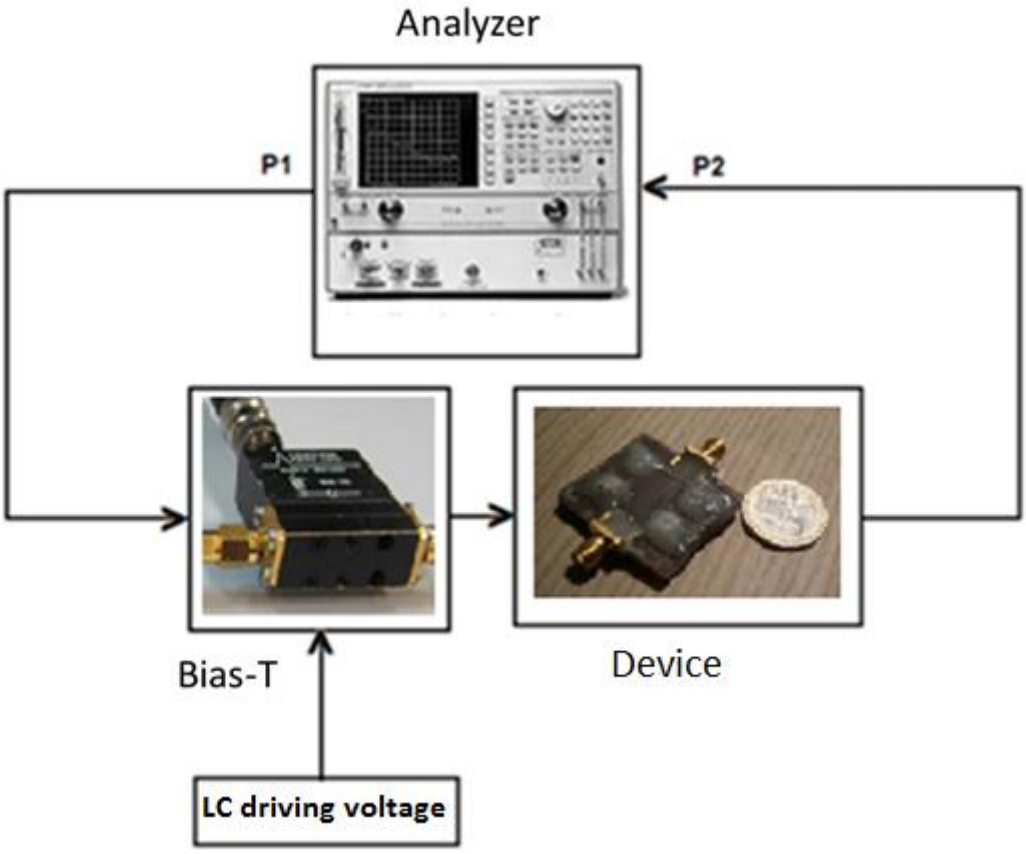

Figure 3.7. Experimental set-up.

A DC block, which is a device which not allows the external driving voltage to be passed to the network analyzer, is sometimes connected between the device output and the port 2 of the network analyzer. Since the LC driving voltage does not reach the maximum voltage supported by the analyzer (40 V, while the maximum voltage used for switching the LC filters is 15 V_{rms}), it is not necessary the use of a DC block. Nevertheless, it was used in the first prototypes of LC devices, when higher voltages were supplied to the devices in order to study their behavior with high DC voltages and AC voltages of low frequency [3.7].

The key of the measuring system core is a network analyzer. This measuring equipment, among other features, characterizes the S-parameters of devices under test in modulus, phase, group delay, etc. in a certain range of microwave frequencies. It is connected with samples to be measured through two interfaces or ports: an input port (port 1, P1) and an output port (port 2, P2). Through port 1 the microwave signal is applied to the test sample; port 2 receives the response of the system on the analyzer to process it.

Network analyzer available to Universidad Carlos III de Madrid is a 8703B network analyzer from Agilent Technologies (Fig. 3.8). Main features of this equipment are [3.8]:

- Frequency range up to 20 GHz. This parameter is not a limitation for the devices of this Thesis work, since every designed device works at a frequency lower than 10 GHz.

- Maximum voltage supported: ±40 V. This is not a limitation for this Thesis Work. The maximum voltage used to switch the devices has been 15 V_{rms}.

- Operating temperature: 20º C – 30º C. The network analyzer displays an error message if temperature conditions are not achieved.

- Maximum resolution: 1601 points. The resolution depends on the span chosen for carrying out the different measurements. For example, for a span of 1 GHz the resolution would be 1 GHz/1601 points, i. e., 0.625 MHz.

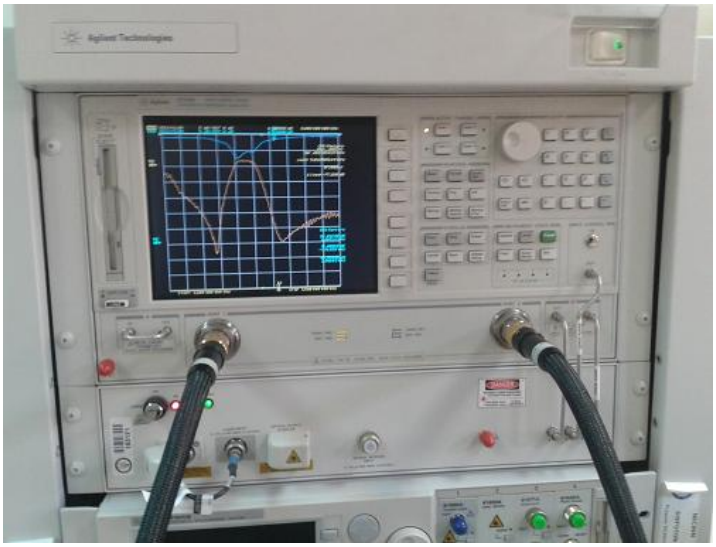

Figure 3.8. 8703B network analyzer from Agilent Technologies.

As schematized in Figure 3.7, there are two different signals at the LC filter input: a microwave signal from the network analyzer and a low frequency AC signal to switch the LC. Both signals overlap before driving the filter by a bias-T. It is connected between the network analyzer, the LC driving generator waveform and the filter input.

A bias-T is a three-port network which can be modeled as an ideal capacitor that allows passing high frequency signals (for instance, microwave signals) and blocks low frequency signals and an ideal inductor that blocks high frequency signals while allows low frequency signals. Reciprocally, its function is the opposite, that is, it overlaps the inputs, as shown in Fig. 3.9 a). So, it is employed for setting a bias voltage without disturbing other electrical signals that flow by the test cell. Thus, to the filters regards, it is used for overlapping MW signal and LC driving voltage. Typically, a Bias-T has a nominal characteristic impedance of 50 Ω. A 5575A Bias-T [3.9] from Picosecond has been used in this work of Thesis (see Fig. 3.9 b)).

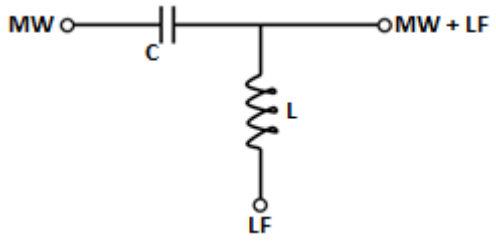

a) General schematics of a bias-T. MW: microwave signal. LF: Low frequency signal.

b) Picture of a 5575A Bias-T from Picosecond.

Figure 3.9. Three-port network for overlapping electrical signals.

To drive the LC a 33120A waveform generator from Agilent Technologies [3.10] is used; it is connected to the input for low frequency signals of the Bias-T. Initially, DC driving signals were used for switching the LC. This kind of signals were applied in the first designed prototypes of LC-based tunable devices [3.7] developed in the GDAF group (Grupo de Displays y Aplicaciones Fotónicas). However, that alternative was not suitable because the saturation voltage value was not reached maybe due to ionic effects in the LC bulk. Therefore, AC voltage of low frequency is employed as the LC driving voltage, specifically, sinusoidal signals of 1 kHz. The signal amplitude depended on the specific filter but always within a range between 12 V_{rms} and 15 V_{rms} for a nearly linear behavior.

3.2.b. Calibration of the microwave measuring equipments

Before characterizing a device with a network analyzer, it has to be calibrated in order to obtain a correct measurement. The network analyzer provides a calibration kit, as well as different calibration options, to make this process. Figure 3.10 shows a picture of the calibration kit for the Network Analyzer Agilent 8703B. The different components of this kit are connected to the network analyzer to make the calibration. These components are the "short", the "open", the "load" and the "thru".

Figure 3.10. Network Analyzer Agilent 8703B Calibration kit.

First, it is important to take into account that the characterization set-up includes connectors, the bias-T and, optionally, the DC-block. For a right measurement the calibration has to be done including all of these items, which means that they have to be connected to the network analyzer for making the calibration, in order to do the calibration in the device input and output.

There are different kinds of calibration depending on the measurement to carry out (port 1, response, etc.). The most accurate calibration option for measuring S-parameters (specifically, S_{11} and S_{21}) is the "Full-two-port" calibration. It consists of three different

phases: reflection, transmission and isolation. Isolation phase, however, is usually omitted. In the reflection phase, the calibration components “open”, “short” and “load” are connected to the port 1 of the network analyzer (including connectors and bias-T) and measured. The same process is done for the port 2. Then, in the transmission phase, the “thru” component is connected between the ports of the analyzer and measured. Figure 3.11 shows the calibration set-up for reflection and transmission. Note that bias-T is connected to port 1 during the calibration process.

Finally, it is important to mention that the calibration of the network analyzer usually expires after three days. Nevertheless, it is strongly recommended to do the calibration process every day before the measurements.

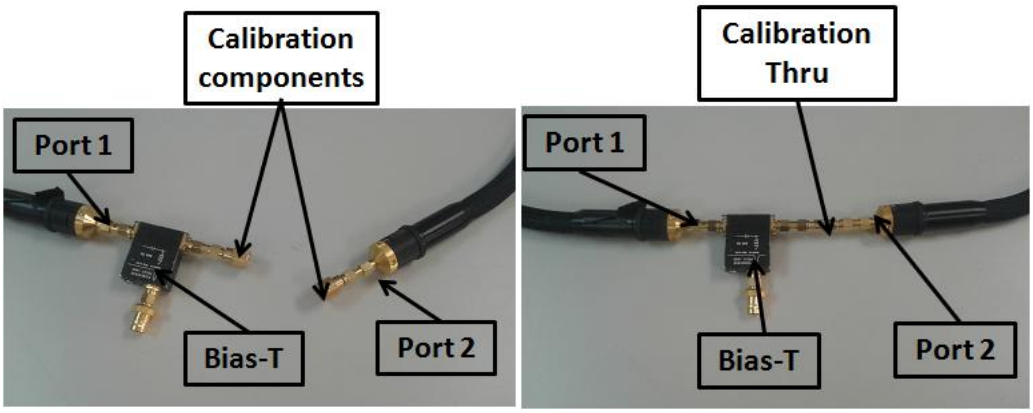

a) Reflection **b) Transmission**

Figure 3.11. Calibration set-up for reflection and transmission.

3.2.c. Characterization protocol

Once the network analyzer has been calibrated, it is ready to do the measurements of the device. For the characterization protocol, the next steps are considered:

a) Connection of components. The different components of the characterization set-up shown in Figure 3.x are connected as it was indicated.

b) Measurement of the empty device. Before the filling with LC, the device S-parameters are measured with the LC cavity empty in order to demonstrate the viability of the design. It is important to take into account that once the LC is introduced in the device, it is sealed, so in this point it is not possible to back out. If the results are satisfactory, the device is filled with LC.

c) Measurement of the LC device. The device filled with LC is characterized by measuring its S-parameters. The obtained response is studied, discussed and compared to other previous results, as well as improvements are proposed.

3.3. References

[3.1] P. Pieranski, F. Brochard, E. Guyon, "Static and dynamic behavior of a nematic liquid crystal in a magnetic field. Part II : Dynamics", Journal de Physiques France, Vol. 34, No 1, pp. 35 - 48, 1973.

[3.2] TLX high volume fiberglass reinforced microwave substrate, www.taconic-add.com.

[3.3] D. Pérez, "Liquid cristal photonic devices based on conductive polymers". PhD Doctoral Thesis. Universidad Politécnica de Madrid, 2010.

[3.4] J. Torrecilla, V. Urruchi, J. M. Sánchez-Pena, N. Bennis, A. García, D. Segovia, "Improving the pass-band return loss in liquid crystal dual-mode bandpass filters by microstrip patch reshaping", Materials, Vol. 7, No. 6, pp. 4524-4535, 2014.

[3.5] J. C. Torres "Caracterización, modelado eléctrico y desarrollo de nuevas aplicaciones de dispositivos basados en cristales líquidos". PhD Doctoral Thesis. Universidad Carlos III de Madrid, 2009.

[3.6] SMA 50 Ohm End Launch Jack Receptacle - Tab Contact Data Sheet. Johnson Components.

[3.7] C. Marcos, J. Torrecilla, V. Urruchi, J. M. Sánchez-Pena, "Dispositivo de fase sintonizable para microondas basado en cristal líquido", XXVI Simposiun Nacional Unión Científica Internacional de Radio (URSI), Leganés, Spain, 2011.

[3.8] Agilent 8703B Lightwave Component Analyzer, Technical Specifications, 2001.

[3.9] Picosecond pulse labs Inc., Spec 4040045, Rev. 4, June 2009 (www.picosecond.com).

[3.10] Agilent 33120A Function/Arbitrary Waveform Generator Data Sheet, 2004.

CHAPTER 4. TUNABLE NOTCH FILTERS BASED ON LIQUID CRYSTAL TECHNOLOGY

Filters are two-port networks used to control the frequency response in a system. They permit good transmission of determined signal frequencies while rejecting unwanted frequencies. Filters can be classified in four types: low-pass, high-pass, band-pass, and band-stop. Microwave filter design has been a very active topic for investigation in the last decades. The design of tunable filters, whose selected or rejected frequency band can be voltage-controlled, is a key point in new telecommunication systems.

As it is well known, tunable filters can be made by using different kinds of technology. The microwave filter is a component which provides frequency selectivity in many kind of applications such as mobile and satellite communications, radar, electronics warfare, and remote sensing systems operating. In general, the electrical performances of the filter are described in terms of insertion loss, return loss, frequency-selectivity (or attenuation at rejection band), group-delay variation in the passband, among others.

A band-stop filter is a device that attenuates a frequency band, while the rest of frequencies remain constant. A notch filter is a particular kind of band-stop filter with a very narrow stop-band and a high quality factor. Notch filters are used at microwave frequencies to reject spurious bands or noise signals. For example, they are used in satellite telecommunication systems in order to eliminate spurious signals which can interfere the transmitted signal.

In this chapter, two different microstrip tunable notch filters at microwave frequencies based on LC technology are presented. The first prototype is a tunable notch filter with conventional *spurline* structure based on LC technology which has been designed, simulated and characterized. Then, as some different alternative spurline structures were previously studied in order to improve the filter performance, a notch filter with spiral meander spurline structure is fabricated, measured and studied in depth.

This chapter is organized into the following main parts:

- First, microstrip spurline technology for notch filters is introduced in a section, explaining the configuration of the electrode pattern for the conventional spurline structure. Then, the structure dimensions are optimized by simulation and two spurline variants are presented: the meander spurline structure and the spiral meander spurline structure. Comparisons among these structures are made in order to determine the advantages and disadvantages of each one. Finally, the filters to be manufactured are presented.

- A tunable notch filter based on LC with conventional spurline structure has been manufactured and characterized and its design, simulation and experimental results are presented and discussed. The used LC has been the experimental mixture 1631F, which exhibits high dielectric anisotropy, which involves the management of a large tuning range for the rejection frequency of the notch filter. As its dielectric properties had not been tested at microwave frequencies, an estimation of these properties is pone parting from the experimental results.

- The following device presented is a LC-based tunable notch filter with spiral meander spurline structure, which is expected to improve the performance of the conventional strucuture. The design, simulation and characterization of this filter are described and the main results are discussed. In this case, LC 1631E is used, which is another experimental mixture from the same family of 1631F, and its dielectric properties are also estimated.

- Finally, the main conclusions of the chapter are summarized and discussed.

4.1. Notch filter configurations

A typical frequency response of a notch filter is shown in Figure 4.1. As stated in Chapter 2, an ideal spectral response of a notch filter should offer high insertion loss (S_{21}) that is signal attenuation (commonly expressed in positive dB's) greater than a certain value in the stop-band. Consequently, the higher the insertion loss would provide the sharper or narrower the bandwidth. Of course, minimum attenuation is required outside the stop-band.

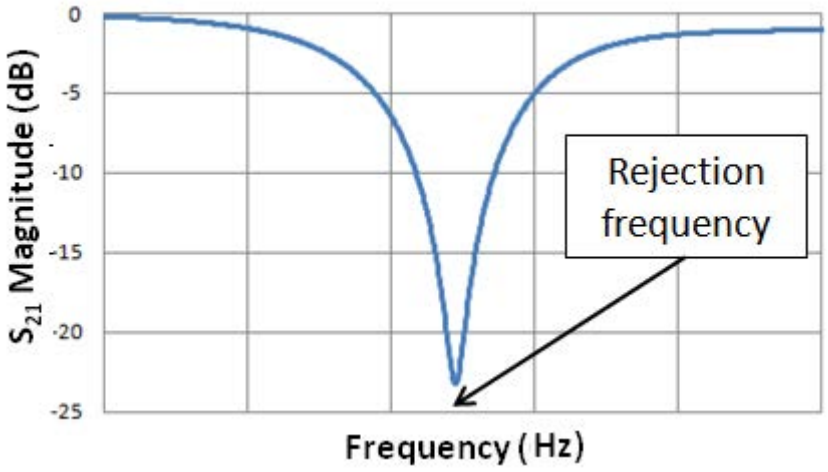

Figure 4.1. A typical frequency response of a notch filter.

Specifically, three parameters that evaluate the performance of the frequency response for a notch filter are: the insertion loss just at rejection frequency (f0), the quality factor (Q) and the filter selectivity.

- *Insertion loss at rejection frequency f_0*: The signal attenuation at this frequency is expected to be as high as possible.

- *Quality factor (Q).* It is defined as the ratio between the rejection frequency, f_0, of the filter and the bandwidth of the stop-band ($Q = f_0 / BW$).

- *Filter selectivity*: A filter exhibits better selectivity if signal attenuation at the rejection frequency, f_0, is very high while it is very low at nearby frequencies. This concept is closely related to the quality factor, Q.

Moreover, in LC-based devices is very important the size of the LC cavity described in the Chapter 2. Since LC is an expensive material, it is desirable not to employ a large amount of LC. Therefore, designing a cavity as small as possible while a good device performance is obtaining is a key issue.

This section describes some topologies based on spurline structures over microstrip technology for notch filters. A thorough description of a conventional spurline structure is included. First, the dimensions of the electrode pattern for a conventional spurline structure are optimized in order to achieve improvements in filter performance mainly in terms of increasing attenuation at rejection frequency and quality factor. In the optimization process, marks of each dimension are swept within a range of values to find a practical embodiment. Additionally, further two approaches by reshaping the microstrip spurline structure have suggested. Specifically, some benefits have been recognized in meander and spiral meander spurline structures, in front of structures with conventional format. Their profits on decreasing the cavity volume are substantial, without jeopardizing the filter performance. Discussion of the best configuration is included and a selection of devices for manufacturing is argued.

4.1.a. Conventional spurline structure

In order to obtain a notch filter characteristic, a spurline topology is used as the shape for the microstrip line over the dielectric substrate. A spurline structure is a notch filter widely used in microwave applications as distributed element filter due to its compact design and ease of integration. A typical spurline structure is shown in Figure 4.2.

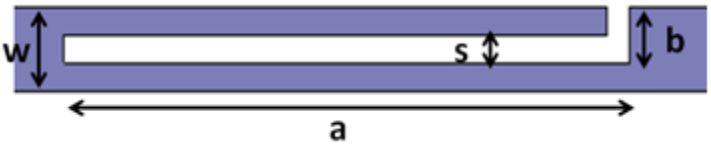

Figure 4.2. Shape of the electrode pattern for a conventional spurline structure.

It consists of a microstrip line based on two asymmetrical coupled lines, where one of the resonating lines is open-ended. The spurline length ($a = \lambda_0/4$) is one quarter the vacuum wavelength, λ_0. Besides, the spurline height and gap are b and s, respectively, while w is the microstrip line width. It works as a rejection-band filter with a fixed rejection frequency (f_0) [4.1] defined as

$$f_0 = \frac{c}{4a\sqrt{\varepsilon_{reff}}} \tag{4.1}$$

where c is the velocity of light, a the spurline length, and ε_{eff} the effective relative permittivity of the microstrip line substrate. For a fixed spurline length *a*, the rejection frequency only depends on the effective permittivity. The other spurline dimensions, *b*, *w* and

s, (Fig. 4.2), do not affect the filter rejection frequency; nevertheless, as explained next, dimensions *s* and *b* will affect the bandwidth of the stop-band.

The contribution of liquid crystal (LC) technology to microwave filters is mainly focused to add the ability of tuning the rejection frequency. Taking advantage of the electrically controlled permittivity of these materials, the filter design can improve strongly compared to conventional microwave filters. The frequency response of the new filters, with emphasis on the generation of analogue adaptive rejection frequencies, provides enormous versatility on the devices.

4.1.b. Improving conventional spurline structure

Different strategies for modeling the conventional spurline structure have been proposed. As stated previously, the design of the electrode pattern dimensions are intended to give optimized performance. This option has been the first line of study. It was performed by using mainly the electromagnetic software tool Ansoft. The frequency response was outlined through a batch of simulations based on programmable loops; every variable dimension was updated in every step of the loop. It should be warned that, this first analysis does not concern the dielectric material of the microstrip substrate. In this way, filter schemes for simulations featured with a special geometry owning a cavity for housing the tunable liquid crystal later, but defining the permittivity of the cavity equal to the air permittivity, $\varepsilon_r = 1$, (that is, with the empty filter).

The main two filter parameters that have been evaluated in the simulation phase are: Insertion loss at rejection frequency f_0, that is designed to achieve a value as high as possible, quality factor (Q) that leads to more selective filters and device volume focusing the design improvements to the final tunable filter based on liquid crystal.

Researchers involved in the design of conventional spurline notch filters have just explored the variation of the spurline gap, *s*, as a simple and easy strategy for enhancing filter selectivity. Initial guidelines for the notch filter design of our work have been extracted from literature [4.2]. Loo-Yau et.al in this work use a notch filter with a non-inverted microstrip spurline and, specifically, the theoretical response of a notch filter for some values of the spurline gap, *s*, is studied. By reducing *s*, the filter selectivity increases and the losses outside the stop-band decreases. This result is very attractive for the final notch filter performance; however, insertion loss (signal attenuation) at rejection frequency f_0 decreases. It is also tested that, by changing the spurline gap *s* about one order of magnitude, does not alter substantially the position of the rejection frequency f_0 at the stop-band.

The study of the spurline gap (*s*) dependence of the frequency response for a notch filter with inverted-microstrip structure is a new contribution of this work. Some simulations based on programmable loops have been run for several values of *s*, while *a, b* and *w* remained constant. These magnitudes unchanged have been previously optimized by simulation to obtain a rejection frequency close to 5 GHz. The thickness of the cavity for housing the LC

later is chosen of 250 μm. The simulation results are presented in Fig. 4.3. It is observed that they are fairly in agreement with the response given in [4.2].

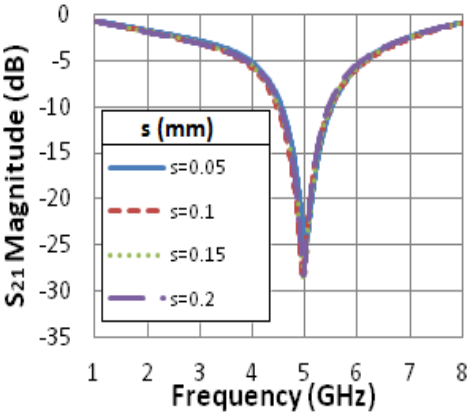

a) **Simulation of frequency dependence of S_{21} parameter.**

***a* (mm)**	***b* (mm)**	***w* (mm)**
11.2	0.4	0.6

***Gap s* (mm)**	**Q = f_0/BW**	**Attenuation (dB)**
0.05	2.13	-24
0.10	**2.08**	**-26**
0.15	2.03	-26
0.20	2.03	-26

b) **Filter performance.**

Figure 4.3. Optimization of the pattern design for a notch filter with conventional spurline structure. Several values of the spurline gap *s* are tested.

A proper design for the spurline gap *s* has been detected that ranges within the interval 0.1 mm – 0.2 mm; signal attenuation at rejection frequency is maximum and quality factor very close to the better performance with this structure. Higher values of *s* would lead to a growing trend of signal attenuation at rejection frequency, but decreasing slightly the quality factor and, additionally, s values too much high could be limit the value of the height *b*. In the other direction of variation of the spurline gap *s*, quality factor enhances slightly but minor spurline gap can compromise the accuracy of the rigorous manufacturing process in this area of the electrode.

The optimization process of the dimensions has also dealt with the spurline height *b* dependence of the notch filter performance in an inverted-microstrip structure. The spurline width *w* conditions the spurline height *b*. Width *w* is designed of 0.6 mm in order to obtain input impedance about 50 Ω for a thickness device of 250 μm, as it is calculated by using the microstrip equations shown in Chapter 2, and spurline gap *s* has been set to 0.1 mm to broaden the range of variation of *b*. In fact, the filter response is more sensitive to changes in the height *b* than in the gap *s*. Fig. 4.4 shows the simulation results achieved for different values of *b*, remaining *a*, *s* and *w* constant. The outcome suggests that height *b* also affects to the selectivity of the notch filter through both the quality factor and the attenuation at rejection frequency. It can be observed from the plots that reducing the dimension *b*, the filter selectivity improves, but the attenuation at rejection frequency decreases. So, again a trade-off solution between both parameters should be attained for the filter design. Height *b* has been designed of 0.4 mm.

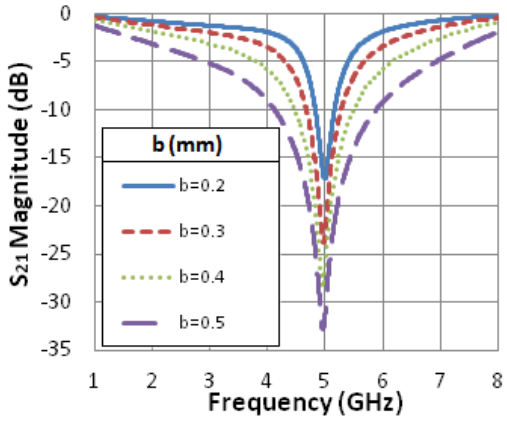

a) Simulation of frequency dependence of S_{21} parameter.

a (mm)	*s* (mm)	*w* (mm)
11.2	**0.1**	0.6

Height b (mm)	Q = f_0/BW	Atten. (dB)
0.2	4.36	-17
0.3	2.75	-24
0.4	**2.03**	**-26**
0.5	1.24	-33

b) Filter performance.

Figure 4.4. Optimization of the pattern design for a notch filter with conventional spurline structure. Several values of the spurline height *b* are tested.

4.1.c. Meander spurline structure

As summarized in the outline of this section, in a second line of work, we have contributed to the improvement of the notch filter performance described in previous section by reshaping the spurline structure included in the inverted-microstrip of the filter.

First approach uses a meandering technique. Traditionally, this method has been utilized for miniaturization of resonator devices at microwave frequencies, making each branch of the device transforms into multiple meanders (with or without different depths). Several embodiments have been described in literature of late 20th century, for example, in band-pass filters [4.3]. It has been reported a meander loop resonator that has a smaller size as compared with the other microstrip band-pass filters, the ring, the square patch, and the disk, with a size reduction of 53%, 68%, and 76%, respectively [4.4]. Very recently, some meander spurline resonators have been implemented in microwave oscillators also with this procedure [4.5], and specifically, in notch filters [4.6]. The size reduction of the circuit area can be significant if it is managed suitably and specifically at low microwave frequencies where size of devices is higher because of the inverse proportionality between the frequency and size.

A further approach assessed besides the area surface of the electrode pattern, which involves a new contribution for the present work, is related to the size reduction of the third dimension, that is, the device depth. This strategy is focused on the volume reduction of the cavity for housing the liquid crystal. In fact, the area reduction affects directly the device volume. This is a critical issue because of the volume reduction represents a reduction in the amount of liquid crystal used. As is known, liquid crystals are intrinsically expensive to

synthesize and, additionally, if experimental mixtures are employed, the purification processes suppose a supplementary cost. Therefore, this argument leads to include a new design hypothesis referred to the minimization of the LC cavity used in the manufacturing process.

a) Performance comparison between meander and conventional spurline structures.

In a first step, the meander spurline structure has been studied in depth, not only in terms of size reduction of the device, but also in reference to electrical performance. Figure 4.5 shows the microstrip pattern of conventional and meander spurline structures. Two new dimensions are added to the pattern definition: *meander width c* and *meander height d*. The meandering configuration of Fig. 4.5 b) is formed with six meanders.

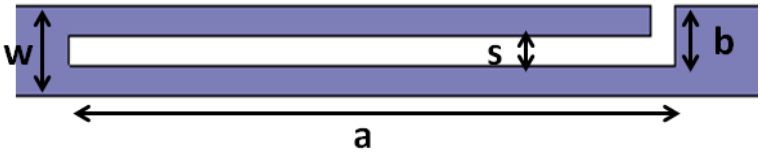

a) Conventional spurline struture.

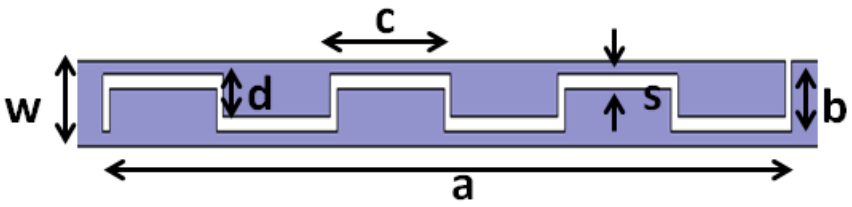

b) Meander spurline structure.

Figure 4.5. Definition of dimensions of the microstrip pattern for conventional and meander spurline structures.

The improvement of filter performance of meander spurline structures compared to conventional structures has been already reported in literature in reference to filter selectivity. Also, it has been tested that for a same value of the length *a* in both structures, the position of rejection frequency of the meander structure diminishes [4.6 (antes 4.10)]. This last outcome was applied to the design of the specifications of the meander notch filter for the present work. So, the structural dimensions of both approaches (conventional and meander) were optimized by simulation for achieving a rejection frequency close to 5 GHz (f_0 = 4.94 GHz).

As stated above, it is important to take into account that the geometry of the spurline structure limits the value of the dimensions. The width *w* remains 0.6 mm in order to obtain an input impedance about 50 Ω, the gap *s* also remains 0.1 mm. And, knowing the impact of

the height *b* on the filter performance from the previous results, the height *b* = 0.5 mm has been considered as an initial value for the design of the filter with meander configuration.

Figure 4.6 summarizes the performance comparison between meander and conventional spurline structures. The scheme and dimensions of the electrode patterns are shown in Fig. 4.6 a)). A size reduction of the length *a* arises from the simulation results: a length *a* = 11.2 mm for the conventional approach is turned into a length *a* = 9.6 mm for the meander approach with six meanders. It means a pattern size reduction of 14.2% (i. e., 9.6/11.2) for the approach with meander configuration. That is, a volume reduction of 14.2% of the LC cavity is achieved, which means a decrease of the total amount of LC used (including the guides for introducing the LC) about 9.6%. Additionally, the meander structure provides the filter with a significant improvement of the selectivity (Figures 4.6 b) and c)); however attenuation outside the stop-band gets worse. Those results certainly imply a tradeoff solution for these parameters.

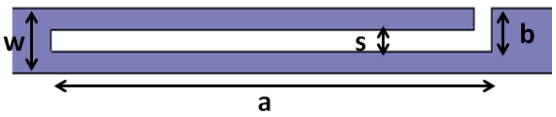

Conventional spurline struture.

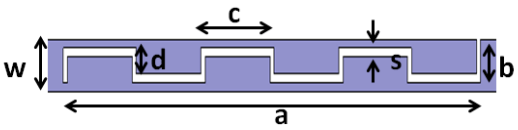

Meander spurline structure.

Dim.	Conventional (f_0 = 4.98 GHz)	6 Meanders (f_0 = 4.94 GHz)
a	**11.2 mm**	**9.6 mm**
b	0.5 mm	0.5 mm
c		1.65 mm
d		0.4 mm
s	0.1 mm	0.1 mm
w	0.6 mm	0.6 mm

a) Scheme and dimensions of the electrode patterns.

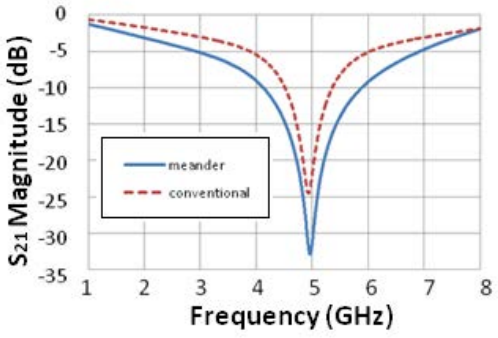

b) Frequency response.

Structure	Q = f_0/BW	LC volume (mm^3)	Atten. (dB)
Conventional	1.24	33.3	-33
6 Meanders	2.05	30.1	-25

c) Performance.

Figure 4.6. Performance comparison between meander and conventional spurline structures. LC volume includes the LC cavity and the guides for introducing LC.

The initial value of the height *b* = 0.5 mm used in the meander structure could be quite large for getting miniaturization of the filter. So, in order to evaluate the effect of reduction of the height *b*, frequency responses from Figures 4.4 and 4.6 have been superimposed (Figure

4.7 b)). Frequency responses for a conventional structure with b = 0.4 mm and the six meander structure with b = 0.5 mm are comparable in terms of filter selectivity, quality factor and attenuation at rejection frequency. However, in terms of volume reduction, reducing the height b in a conventional filter seems less effective than using the meander structure (Figure 4.7 c)).

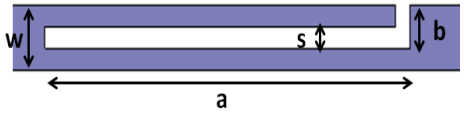

Conventional spurline struture.

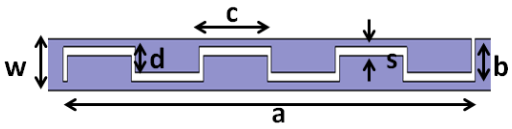

Meander spurline structure.

Dim.	Conventional (f_0 = 4.98 GHz)	6 Meanders (f_0 = 4.94 GHz)
a	11.2 mm	9.60 mm
b	0.2 - 0.50 mm	0.50 mm
c		1.65 mm
d		0.40 mm
s	0.1 mm	0.10 mm
w	0.6 mm	0.60 mm

a) Scheme and dimensions of the electrode patterns.

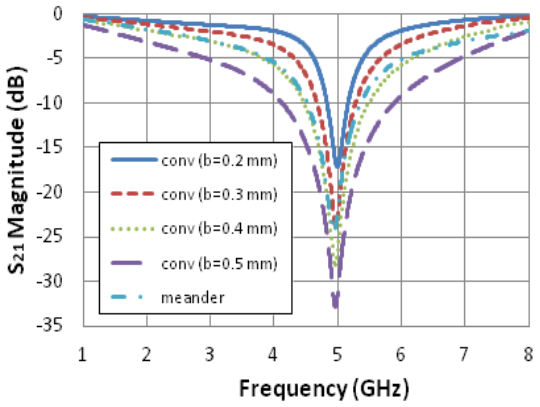

b) Frequency response.

Structure	Height b (mm)	Q = f_0/BW	LC volume (mm^3)	Atten. (dB)
Conventional	0.2	4.36	33.3	-17
	0.3	2.75	33.3	-24
	0.4	**2.02**	**33.3**	**-26**
	0.5	1.24	33.3	-33
6 Meanders	**0.5**	**2.05**	**30.1**	**-25**

c) Performance.

Figure 4.7. Performance comparison between meander spurline structure and conventional spurline structures for different values of the height *b*. LC volume includes the LC cavity and the guides for introducing LC.

b) Meander spurline approach changing the number of meanders

The meandering technique allows every branch of the spurline to consist of different number of meanders, by changing the dimension c. This new structure considered has 12 meanders, while the previous structure had 6 meanders; both microstrip patterns are shown in Fig. 4.8 a). The comparison between both meander structures reveals that there are not significant differences between them (Figures 4.8 b) and c)) except for a small variation of the rejection frequency (from 4.94 GHz to 4.80 GHz). Again, the new structure reduces the

size of the LC cavity compared to the spurline conventional structure, because the dimension *a* is again slightly smaller (a has the same value as the 6 meanders structure). The volume reduction from conventional to spurline with six meanders structure was about xx% and it is the same value for the 12 meanders structure, since the dimension *a* has the same value.

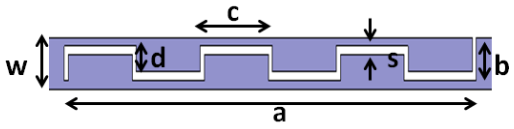

Spurline microstrip with six meanders.

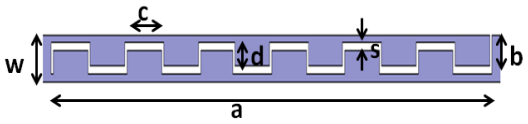

Spurline microstrip with twelve meanders.

Dim.	Spurline with 6 meanders (f_0 = 4.94 GHz)	Spurline with 12 meanders (f_0 = 4.8 GHz)
a	9.6 mm	9.6 mm
b	0.5 mm	0.5 mm
c	**1.65 mm**	**0.925 mm**
d	0.4 mm	0.4 mm
s	0.1 mm	0.1 mm
w	0.6 mm	0.6 mm

a) Scheme and dimensions of the electrode patterns.

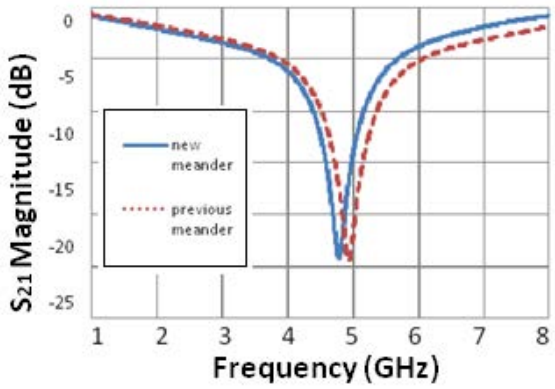

b) Frequency response. Poner en el eje y "S_{21} Magnitude (dB)"

Spurline structure	Q = f_0/BW	LC volume (mm^3)	Atten. (dB)
6 meanders	2.05	30.1	-25
12 meanders	2.12	30.1	-24

c) Performance.

Figure 4.8. Performance comparison between a filter with spurline microstrip technology based on six and twelve meanders. LC volume includes the LC cavity and the guides for introducing LC.

4.1.d. Spiral meander spurline structure

The favorable results described in the previous section for the meandering technique have been a key of our work to deepen further this beneficial strategy for implementing liquid crystal filters by creasing the cavity size.

A variant of the lineal meander spurline structure is the spiral meander spurline one. Recent research in this area proves that spiral meander scheme provide resonators with a significantly reduced size and an enhanced quality factor Q [4.7, 4.8]. High performance has been reported in microwave oscillators [4.9] and filters [4.10]. Figure 4.9 shows the microstrip pattern of conventional and spiral meander spurline structures. Two new dimensions are added to the electrode pattern definition: *spiral width t* and *spiral height h*. The spiral meander configuration of Fig. 4.9 b) is formed with twelve branches.

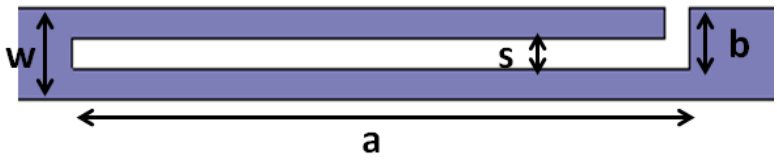

a) Conventional spurline structure.

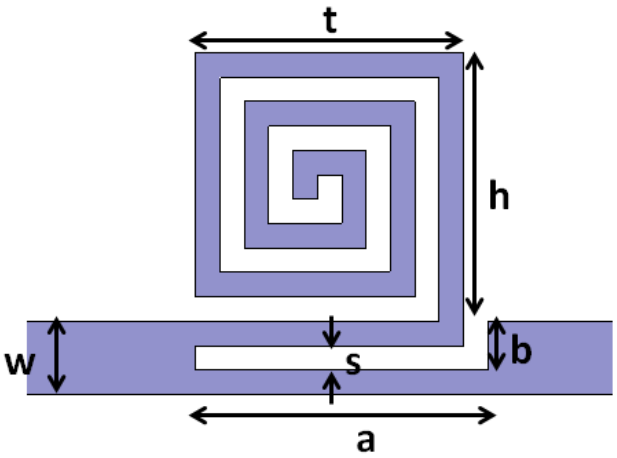

b) Spiral meander spurline structure.

Figure 4.9. Definition of dimensions of the microstrip pattern for conventional and spiral meander spurline structures.

The contribution of the present work in this matter is mainly focused in a new filter with a spiral meander spurline structure supported by the same hypothesis than that assumed for lineal meander structures. With these premises, simulation efforts have been made on this special arrangement guided to an advanced filter again with a tunable dielectric liquid crystal. The spiral meander structure is compared firstly to a lineal meander one and next to a conventional spurline. Simulation results have been the tool for the comparison.

a) Performance comparison between spiral and lineal meander spurline structures.

The spiral and lineal meander spurline structures have been compared. Since both kinds of electrode patterns are structurally different, the initial values of their dimension have been considered a little different for the comparison of them. Specifically, the gap *s* has increased,

from 0.1 mm to 0.2 mm, for the benefit of the spiral manufacturing; as a result, dimension b has reduced from 0.5 mm to 0.4 mm. A combination of a six meander structure for the lineal electrode pattern and a three full turns structure for the spiral pattern, has been chosen for comparing the filters' performance. Figure 4.10 summarizes the simulation results. Figure 4.10 a) shows the scheme and lists the optimized dimensions for filters with the same rejection frequency (5 GHz). The frequency response is graphed in Figure 4.10 b) and the performance of both structures in Figure 4.10 c). Two are the more significant effects on the filter performance:

a) The spiral meander structure reduces the LC volume by about 26.5% that is an important factor with respect to that of the filter based on a linear meander structure.

b) Additionally, the spiral meander spurline structure doubles the quality factor Q, which means an excellent successful property despite the attenuation level at rejection frequency is slightly lower.

These excellent results determine the decision for the present work of manufacturing a notch filter with spiral meander structure, as will be described in the next sections.

b) Performance comparison between spiral meander and conventional spurline structures.

It has just been shown that spiral configuration advantages frequency performance of linear meander one. Besides, previously was demonstrated that meander structures enhance the response of conventional spurline schemes. So, it does not seem unreasonable to suggest that spiral meander configurations give more favorable results than conventional spurlines. In view of that, a non-exhaustive but concluding analysis has been carried out for this comparison.

In order to compare the global performance of spiral meander and conventional spurline structures, the structure dimensions for two filters each with one type of these electrodes have been optimized by simulation for achieving the same rejection frequency, close to 5 GHz.

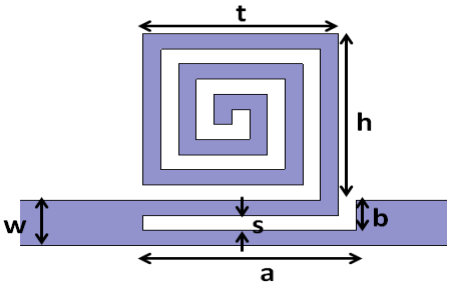

Spiral meander spurline structure.

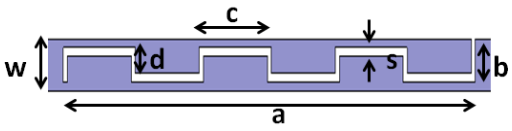

Meander spurline structure (6 meanders).

Dim.	6 meanders (f_0 = 4.94 GHz)	Spiral meander (f_0 = 4.96 GHz)
a	**9.6 mm**	**2.4mm**
b	**0.5 mm**	**0.4 mm**
c	1.65 mm	
d	0.4 mm	
s	**0.1 mm**	**0.2 mm**
w	0.6 mm	0.6 mm
t		2.2 mm
h		2.2 mm

a) Scheme and dimensions of the electrode patterns.

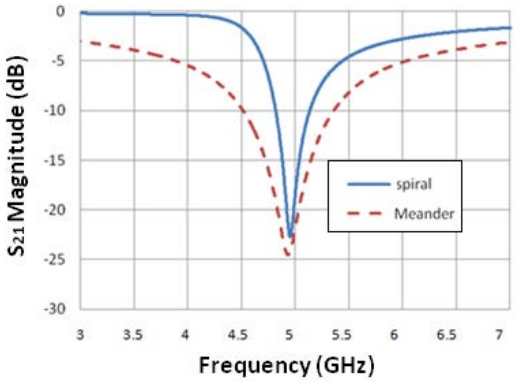

b) Frequency response.

Structure	Q = f_0/BW	LC volume (mm^3)	Atten. (dB)
Meander	2.05	30.1	-25
Spiral meander	3.88	21.12	-22

c) Performance.

Figure 4.10. Comparison between spiral meander and meander spurline structures. LC volume includes the LC cavity and the guides for introducing LC.

Figure 4.11 summarizes the outcome. Figure 4.11 a) shows the scheme and dimensions optimized for both structures, Figure 4.11 b) graphs a comparison between both frequency responses and the inset table of Figure 4.11 c) lists a performance comparison of the main parameters.

As expected, the dimension *a* is much smaller in the spiral meander spurline structure than in the conventional one for achieving the same rejection frequency of the notch filter. The size of the LC cavity depends strongly of the dimension *a*, so the reduction of the dimension *a* will imply a decrease of the volume of the cavity and also a diminution of the total amount of the LC used in the spiral meander structure. Particularly, a reduction of the size of the LC cavity of 50% is achieved, which means a decrease of the total amount of LC used (including the guides for introducing the LC) about 38%. It involves a larger reduction than that obtained with the meander spurline structure. As is known, this is an interesting

aspect since LC is an expensive material saving a significant cost in the device manufacturing process.

The main impact on the filter performance is the volume reduction caused by the change of dimension *a*. Other effects appeared to be of minor relevance. For example, the attenuation at rejection frequency gives slightly inferior performance in the spiral meander structure, although the filter has a little better selectivity and presents a better quality factor (Q). Additionally, it is also observed that frequency response of the spiral structure is a little asymmetrical caused by the own asymmetrical structure itself.

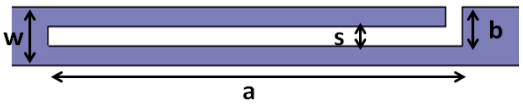

Conventional spurline structure.

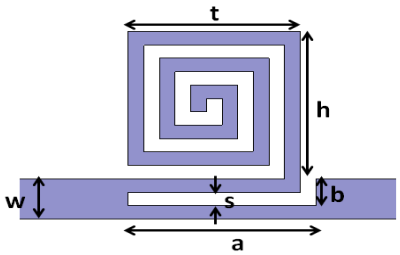

Spiral meander spurline structure.

a) Scheme and dimensions of the electrode patterns.

Dim.	Conventional (f_0 = 4.98 GHz)	Spiral meander (f_0 = 4.96 GHz)
a	**11.2 mm**	**2.4 mm**
b	0.4 mm	0.4 mm
s	0.2 mm	0.2 mm
w	0.6 mm	0.6 mm
t		2.2 mm
h		2.2 mm

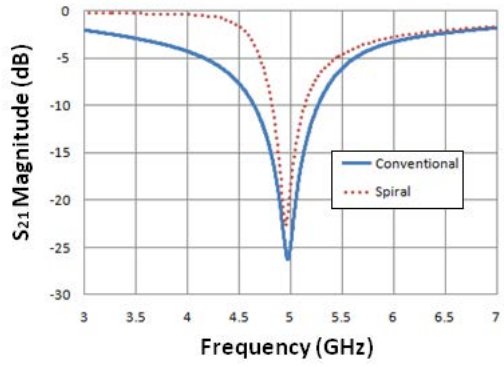

b) Frequency response.

Structure	Q = f_0/BW	LC volume (mm^3)	Atten. (dB)
Conventional	2.03	33.3	-26
Spiral meander	3.88	21.12	-22

c) Performance.

Figure 4.11. Performance comparison between spiral meander and conventional, spurline structures. LC volume includes the LC cavity and the guides for introducing LC.

Results obtained in simulation provide an important support to predict the practical behavior of the filters. With these premises, both configurations the conventional spurline and the spiral meander have been considered for the design of new notch filters.

4.1.e. Manufactured notch LC filters

The indicators of the filter performance have been stated as design premises for the manufacturing of notch filters with microstrip-inverted spurline structure.

Table 4.1 summarize the optimum values that would be required for the manufacture of the conventional spurline structure. However, a filter whose electrode dimensions were a bit different than these optimum values was implemented and taken as the jump off point. Nevertheless, this fact is not an inconvenient for studying the viability of this device as a notch filter.

Conventional spurline electrode pattern	Spurline dimension	Value
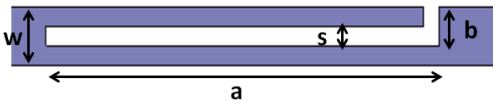	*Length a*	11.2 mm
	Height b	0.4 mm
	Gap s	0.1 mm
	Width w	0.6 mm
Thickness of the cavity		250 um

Table 4.1. Optimized values of the dimensions of the electrode pattern for the manufacturing of a notch filter with conventional spurline based on a microstrip-inverted structure.

The manufactured filter with conventional suprline structure was reported in a recent Thesis work [4.11] and the author of the present Thesis supported the design of this device, specially, in the electromagnetic simulation of the frequency response of the filter. Table 4.2 shows the device dimensions used in this previous work, which is considered a first approximation for the study of LC-based notch filters. In the present Thesis work, the estimation of the used LC permittivity, by using electromagnetic simulations, has been studied in depth. The used LC was the experimental mixture of high dielectric anisotropy 1631F supplied by Military University of Warsaw, which had not been tested at microwave frequencies.

Conventional spurline electrode pattern	Spurline dimension	Value
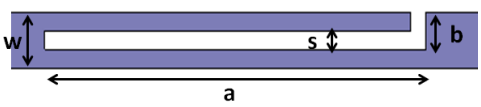	*Length a*	10 mm
	Height b	0.4 mm
	Gap s	0.2 mm
	Width w	0.6 mm
Thickness of the cavity		130 um
Experimental Liquid crystal		1631F

Table 4.2. Values of the dimensions of the electrode pattern for the designed notch filter with conventional spurline based on a microstrip-inverted structure. [4.11]

On the other hand, Table 4.3 summarizes the dimensions used in the fabrication of a notch filter with spiral meander spurline structure. The design, simulation, manufacturing and characterization of this device are original of this Thesis work. The used optimized dimension values of the electrode pattern have been derived from the previously presented study performed by simulations, taking into account the limitations in the manufacturing process (Figure 4.12).

LC 1631E, which is also a high dielectric anisotropy mixture developed by Military University of Warsaw, has been used and tested in this filter, and its dielectric properties at microwave frequencies have been also estimated by using electromagnetic simulations.

Conventional spurline electrode pattern	Spurline dimension	Value
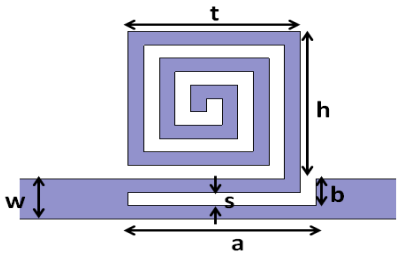	*Length a*	2.4 mm
	Height b	0.4 mm
	Gap s	0.2 mm
	Width w	0.6 mm
	h	2.2 mm
	t	2.2 mm
Thickness of the cavity		250 um
Experimental Liquid crystal		1631E

Table 4.3. Values of the dimensions of the electrode pattern for the manufacturing of the notch filter with meander spiral spurline based on a microstrip-inverted structure.

4.2. Notch filter on liquid crystal technology with conventional spurline structure

The study of theoretical simulations carried out until now has considered filter schemes owning a cavity for housing the tunable liquid crystal (LC) later, but defining the permittivity of the cavity equal to the air permittivity, $\varepsilon_r = 1$, (that is, with the empty filter). Simulations explored thorough the rest of this chapter will intend to design a tunable notch filter, thus considering the permittivity of the liquid crystal material in each case. Manufactured devices will fill with a high dielectric anisotropy LC mixture, so that, the mayor interest of the scheme will be its capacity of tuning the rejection frequency. This feature is especially attractive due to the possibility of generating higher tuning frequency ranges than that obtained with conventional nematic LCs.

This study is comprised of: the extension of the static spectral response of the notch filter designed to tunable, the characterization of this frequency response, the measurement of the driving voltage dependence of the filter rejection frequency and finally, the analysis and

discussion of the voltage tuning dynamic range. Additional discussions were devoted to the estimation of the permittivity and the loss tangent of the liquid crystal. This section is focused on the first implementation notch filter considered. It consisted on a LC tunable device with inverted microstrip spurline technology, specifically a conventional spurline electrode pattern engraved on an inverted microstrip substrate.

4.2.a. Choice of components for a practical implementation

Notch filters proposed for this work are based on inverted microstrip line technology (Figure 4.12) which was described in the Chapter 2. A conventional microstrip transmission line structure has been adapted for manufacturing the device containing a LC mixture inside, thus locating the microstrip line at the inner face of the top substrate (Figure 4.12 a)). Also, to fitting out a cavity for housing the liquid mixture, an additional spacer and a second bottom substrate (covered with the counter-electrode) were required. Thus, the LC acts as the dielectric substrate of the microstrip line. Figures 4.12 b) and c) show the steps for assembling the device, and a picture of the manufactured notch filter, respectively [4.12]. The top and bottom electrodes, that is, the microstrip line and the ground plane, were copper engraved. The microwave dielectric material of the substrates is Taconic TLX-8 with a thickness of 0.8 mm. This material is also used as the spacer, but with a thickness of 130 μm [4.12]. The inset table of Figure 4.12 d) summarizes the optimized dimensions.

Positions of LC molecules inside the cavity are conditioned by the alignment method used in the device manufacturing. Both electrodes are covered by a rubbed polyimide alignment layer for providing a homogeneous alignment to the LC molecules and glass substrates are antiparallel assembled. When no voltage is applied to the LC, molecules place in a near parallel position to the glasses. Effective permittivity of the whole structure in that stage is $\varepsilon_{r\perp}$ for the input microwave signal. By tuning the LC device with an external AC voltage, molecules tend to tilt their orientation under the electric field and rotate changing the permittivity between two extreme values, corresponding to $\varepsilon_{r\perp}$ and $\varepsilon_{r\parallel}$, respectively. When the permittivity reaches the minimum value, $\varepsilon_{r\parallel}$, molecules are placed in a near perpendicular position to the microstrip line. Therefore, by applying equation (4.1), as voltage increases, the rejection frequency of the filter decreases.

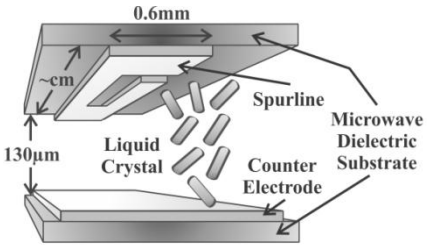

a) Microstrip inverted arrangement.

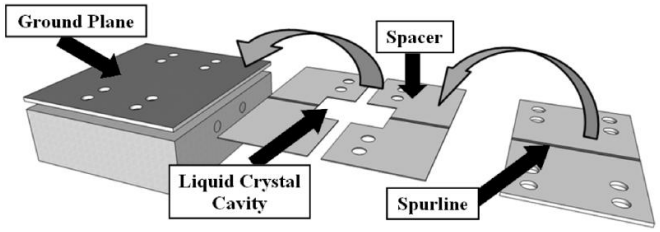

b) Detail of the steps for assembling the device.

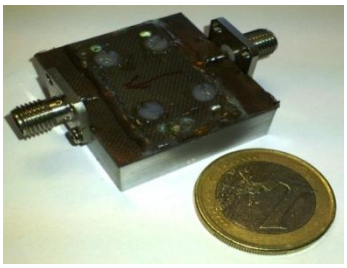

c) A picture of the manufactured notch filter.

Component	Material	Thickness (mm)
Microstrip line substrate	Taconic TLX-08	0.8
Spacers	Taconic TLX-08	0.25
Liquid crystal	Nematic LC 1631F	0.25
Microstrip line and ground plane	Copper	0.018
Ground plane substrate	Taconic TLX-08	0.8

d) Materials and dimensions of the structure.

Figure 4.12. Notch filter based on LC technology with conventional spurline structure.

A high-birefringence LC ($\Delta n = 0.3988$ at room temperature) has been used in this work, in order to achieve a high tunability of the notch filter. It is a nematic LC mixture, 1631F, synthesized by Spadlo et al. [4.13] and delivered by Military University of Technology. It is composed of fluorosubstituted alkyltolane and alkylphenyltolane isothiocyanates. This material presents the nematic phase from 0 to 102.5º C. The lateral isothiocyano group induces a large positive dielectric anisotropy ($\Delta\varepsilon = 9.51$ at 20º C and 10 kHz frequency). Unsubstituted cyclohexylbenzene and bicyclohexyl benzene isotiocyanates, biphenyl-, fluorosubstituted terphenyl-, tolane-, and phenyl tolane isothiocyanates are very useful liquid crystalline compounds for diverse applications because of their high polarity, low viscosity, and high birefringence [4.14 – 4.16]. The permittivity of the LC chosen has not been tested at microwave frequencies yet. However, this is a eutectic mixture of several isothiocyanatotolane liquid crystals. Those mixtures do have been tested at microwave frequencies giving rise to permittivities $\varepsilon_{r\perp} = 2.43$ and $\varepsilon_{r\parallel} = 3.49$ [4.17]. The affinity of the used LC with those mixtures already characterized allows those LC permittivity values to be employed in simulation in order to predict theoretically the filter frequency response. In this way, the device static spectral response obtained for the filter when the LC cavity was considered to be empty is extended to a tunable response considering the cavity filled with LC.

4.2.b. Extension of the static spectral response to tunable

The spurline bandstop filter has been simulated with the electromagnetic software tool Ansoft HFSS. Some simulation tests were programmed to obtain the S_{21} parameter of the scattering matrix. The frequency range was included between 3 GHz and 6 GHz. Filter rejection frequency was identified as the frequency in which the S_{21} parameter reached its minimum value.

The shape of the conventional spurline structure from the software tool is shown in Figure 4.13 a); the inset table shows the dimensions. Figure 4.13 b) shows a 3D detail of the conventional spurline for simulations. The spurline length a = 10 mm was chosen to obtain a filter with a rejection frequency f_0 within the range 4 GHz to 5 GHz, from equation (4.1) and the effective permittivities considered.

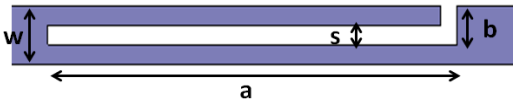

Dimension	Value
a	10 mm
b	0.4 mm
s	0.1 mm
w	0.6 mm

a) The shape and dimensions of the conventional spurline structure. Note that figure is not drawn to scale.

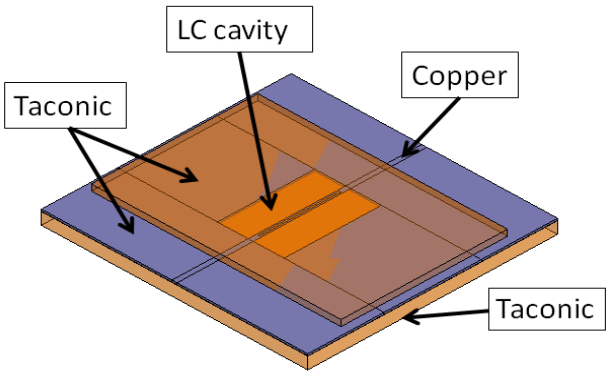

b) 3D detail of the conventional spurline for simulations.

Figure 4.13. Design of the conventional spurline structure for a microstrip inverted notch filter. The inset table shows the results for the optimized dimensions.

The evolution of the S_{21} parameter of the notch filter obtained in simulation is shown in Figure 4.14. As expected, the rejection frequency obtained in simulation with the cavity filled with LC is lower than the achieved for the empty filter (i. e. $\varepsilon_r = 1$; 5.75 GHz obtained in simulation for this case), since LC permittivity is considered to be greater than $\varepsilon_r = 1$. A frequency shift of $\Delta f_0 = 520$ MHz have been managed, which means a relative tuning range of $\Delta f / f_0 = 0.115$.

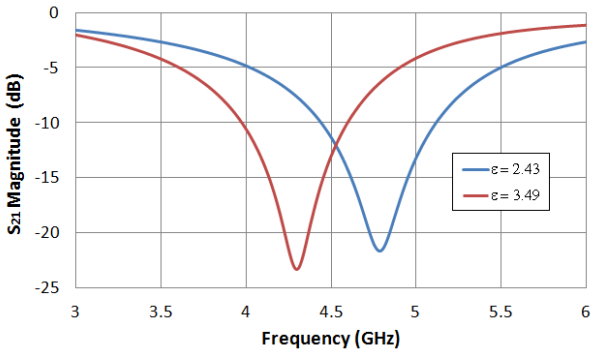

a) Simulation of frequency dependence of S_{21} parameter.

Permittivity	Rejection frequency (f_0, GHz)
$\varepsilon_\perp = 2.43$	4.79
$\varepsilon_\parallel = 3.49$	4.27

Relative tuning range $\Delta f / f_0$	520 MHz / 4.53 GHz = 0.115

b) Filter performance.

Figure 4.14. Simulation of the spectral tuning range of a LC notch filter with conventional spurline structure [4.17]

4.2.c. Characterizing the filter performance

Electric characterization of the designed notch filter is shown and discussed. Filter frequency response has been characterized by measuring the transmission coefficient S_{21} of the scattering matrix vs. microwave frequency. As is known, this parameter quantifies the insertion losses of the device and is the decibel (dB) expression of the ratio between the microwave output and input powers.

The experimental setup to measure the frequency response for this device is depicted in Figure 4.15. S_{21} parameter of the device has been measured by using an 8703B network analyzer from Agilent. Port 1 of the analyzer is coupled to a Bias-T, which is also connected to the input of the notch filter. Next, the filter output is connected to a DC-block input. Finally, the connection of the blocking coupler to the port 2 closes the microwave signal circuit towards the network analyzer. As previously mentioned, the Bias-T consists of a three-port network that makes it possible to drive the LC at lower frequencies without disturbing the flow of the microwave frequency signals.

Sinusoidal signals of 10 kHz have been applied in order to switch the LC molecules. The intermediate tunable voltage levels were comprised in the range of values from 0 V_{rms} to 15 V_{rms}.

Figure 4.15. Experimental set-up for the notch filter with conventional spurline structure. [4.11]

Experimental results of frequency response were obtained for the hypothesis previously described. Frequency dependence of insertion losses for the designed filter is graphed in Figure 4.16 a). It is shown that, without external voltage, the rejection frequency of the notch filter is about 4.84 GHz; molecules exhibit the lower value of permittivity, $\varepsilon_{r\perp}$. As LC driving voltage increases, permittivity also increases, so rejection frequency decreases. The minimum of the rejection frequency is 4.45 GHz, as 15 V_{rms} saturation voltage is applied to the filter, so permittivity reaches its maximum value, $\varepsilon_{r\parallel}$. Therefore, filter tunability relative to central rejection frequency achieves 8.4% (Δf_0 / f_0 = 0.39 GHz / 4.65 GHz), a very attractive feature compared to other commercial competitive technologies, such as MEMS, which do not obtain large tuning ranges as it was mentioned in the Chapter 1. Also, the stop-band filter attains a rejection of about 24 dB, a suited value that remains almost constant as voltage increases from 0 to 15 V_{rms}. Also, range of voltage for the rejection frequency 10% – 90%, shown in Figure 4.16 b), is 5.2 V_{rms}, just a few volts, therefore it can be generated using standard electronics. There is no dependence of the quality factor (Q) with the LC driving voltage. In spite of the fact that the filter bandwidth decreases, f_0 also diminishes as driving voltage is increased, so Q remains constant with a value about 2.5.

As it was mentioned in section 4.1.e, the design and measurement of this device was reported in a previous Thesis work [4.11] and in a JCR Journal article [4.12], which the author of the present Thesis work collaborated in its results, redaction and production. This device is considered to be the the jump off point of the LC based notch filters, since no LC notch filter had been reported before this device. Nevertheless, the discussion about the different topologies of spurline notch filters previously presented in chapter 1, as well the estimation of LC properties and the design, simulation and measurements of a meander spiral spurline notch filter that are described following are original of this work.

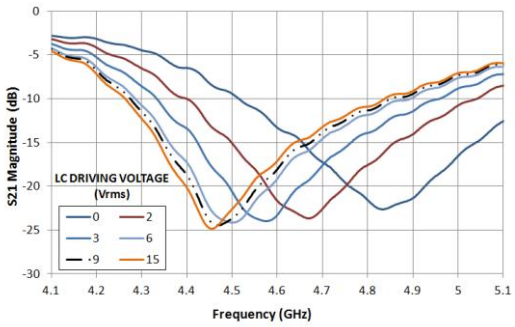

a) **LC driving voltage dependence of the filter spectral response.**

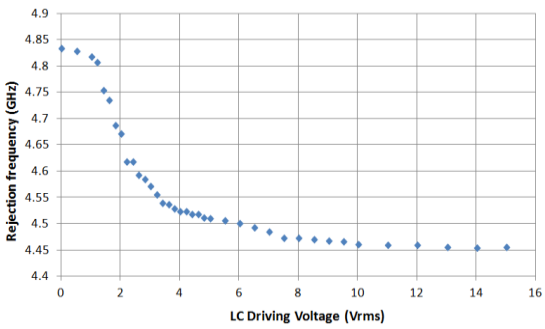

b) LC driving voltage dependence of the rejection frequency f_0.

V	ε_r	f_0	Relative tuning range $\Delta f / f_0$	Quality factor (Q)	Dynamic range (V_{rms})
0 V_{rms}	$\varepsilon_{r\perp}$	4.84 GHz	8.4%	2.5	5.2 V_{rms}
15 V_{rms}	$\varepsilon_{r\parallel}$	4.45 GHz			

c) Summary of the obtained results for the rejection frequency.

Figure 4.16. Spectral tuning range of a LC notch filter prototype with spiral meander spurline structure [4.11]

4.2.d. Estimating liquid crystal parameters by a notch filter

Due to the interest in using LC at microwave frequencies, it is very important to know its properties at these frequencies, specifically, its dielectric constant and loss tangent. However, the LC properties are often unknown at microwave frequencies and this aspect can be a problem for the precise design of microwave devices using this technology. A fairly good estimation can be achieved by using a resonant method [4.18]. A resonant method is a technique used for calculating material properties which consists of estimating these properties parting from experimental results by comparison with theoretical responses at a determinate frequency.

As commented previously, the nematic LC 1631F used for the notch filter with conventional spurline structure, is an experimental mixture with a high dielectric anisotropy, which has not been reported at microwave frequencies before. Thus, the extreme values of the permittivity, $\varepsilon_{r\perp}$ and $\varepsilon_{r\parallel}$, are initially unknown at these frequencies. For estimating these values, the experimental characterization of the notch filter frequency response has been considered as an initial hypothesis.

Ansoft HFSS electromagnetic software tool is used to simulate the notch filter. With this software the frequency response of the device can be simulated very accurately. Particularly,

S_{21} parameter of the notch filter is simulated including the different substrates and dimensions shown in previous chapters. The estimated values of LC permittivity and loss tangent for the LC 1631F are described following.

Since LC permittivity (ε_r) is unknown, several simulations considering successive values of ε_r are run. The minimum step considered for this input permittivity parameter has been 0.2 in the simulation loop. The evolution of the filter's rejection frequency obtained as a function of the LC permittivity is shown in Fig. 4.17.

These numerical results are employed to derive the value of the LC permittivity for each measured rejection frequency. In this case, it is enough with the estimation of the extreme values of the LC permittivity, $\varepsilon_{r\perp}$ and $\varepsilon_{r\parallel}$, which correspond, respectively, to 0 V_{rms} and 15 V_{rms}.

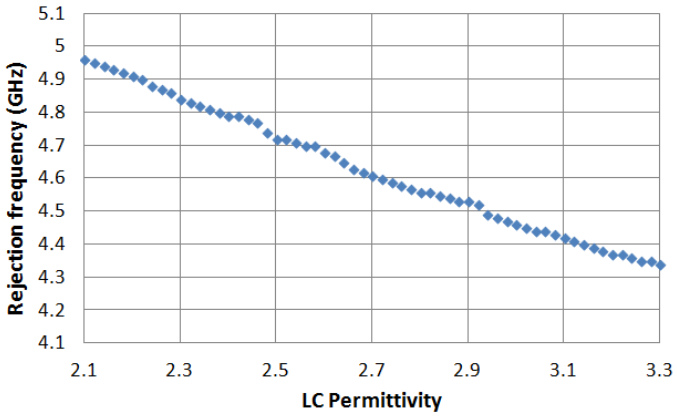

Figure 4.17. Simulation of the evolution of the rejection frequency as a function of the LC permittivity.

The method used to estimate the LC dielectric constant can be also employed for the estimation of the LC loss tangent (tan δ). This parameter is inherent to the material and it is related to device losses due to the LC. Therefore, the lower value of loss tangent, the lower value of filter losses. As happens with the permittivity, the LC loss tangent varies with the orientation of the LC molecules, due to the LC anisotropy, between two extreme values, tan $\delta_\perp$ and tan $\delta_\parallel$. Therefore, the estimation of both parameters: permittivity and loss tangent has been derived simultaneously.

Figure 4.18 includes a matching between the measurements and the simulation results of the spectral response for the LC spiral notch filter. Figure 4.18 d) summarizes the results. The superposition of the two responses has been achieved by nearly matching the rejection frequency, f_0, and the attenuation at this frequency, but leaving freedom to the slope of the branches and the attenuation at nearby frequencies.

Figure 4.18 a) illustrates the overlapping for 0 V_{rms}. As a result, the estimation of the LC permittivity and loss tangent are, respectively: $\varepsilon_{r\perp}$ = 2.3 and tan $\delta_\perp$ = 0.035. Similarly, in

Figure 4.18 b) it is graphed the overlapping of the simulated and experimental curves for 12 V_{rms}. This time the estimated parameters for the LC permittivity and loss tangent are, respectively: $\varepsilon_{r\parallel} = 3.02$ and $\tan \delta_{\parallel} = 0.02$. Therefore, the dielectric anisotropy of the nematic LC 1631E ($\Delta\varepsilon = \varepsilon_{r\parallel} - \varepsilon_{r\perp}$) is estimated to be $\Delta\varepsilon = 0.72$ at about 5 GHz. This value is higher than other previously characterized commercial liquid crystals at those frequencies [4.19, 4.20]. For example, LC K15 from Merck has a dielectric anisotropy of $\Delta\varepsilon = 0.3$ at GHz frequencies.

Just like the extreme values of permittivity are estimated, the intermediate values of permittivity, for the external voltage ranging from 0 V_{rms} to 15 V_{rms}, vary between $\varepsilon_{r\perp} = 2.3$ and $\varepsilon_{r\parallel} = 3.02$. In Figure 4.18 c), the variation of the estimated LC permittivity as a function of the LC drive voltage is shown.

Finally, the values of the loss tangent are very similar to the loss tangent values of other characterized LC at these frequencies [4.19, 4.20], which is about 0.01 - 0.06.

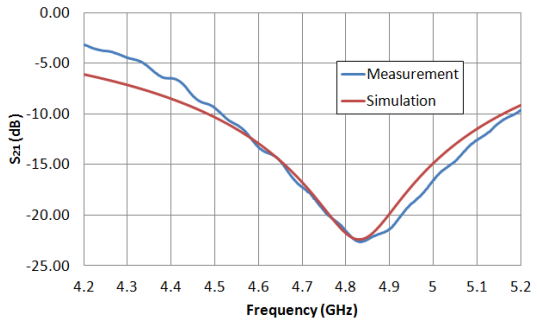

a) Measurement: 0 Vrms LC driving voltage. Simulation: $\varepsilon r_{\perp} = 2.3$ and $\tan \delta_{\perp} = 0.035$

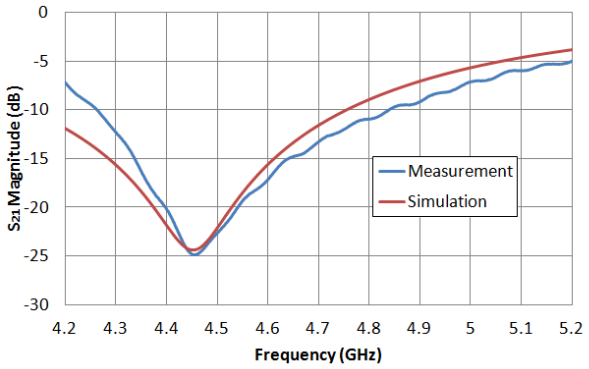

b) Measurement: 15 Vrms LC driving voltage. Simulation: $\varepsilon r_{\parallel} = 3.02$ and $\tan \delta_{\parallel} = 0.02$.

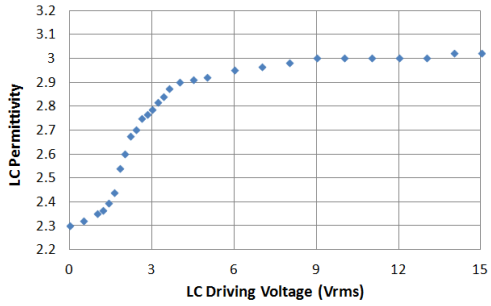

c) Evolution of the estimated LC dielectric permittivity as a function of the LC driving voltage.

LC Driving Voltage	f_0	Estimated	
		ε_r	tan δ
0 V_{rms}	4.84 GHz	$\varepsilon_{r\perp} = 2.3$	$\tan \delta_{\perp} = 0.035$
15 V_{rms}	4.45 GHz	$\varepsilon_{r\parallel} = 3.02$	$\tan \delta_{\parallel} = 0.02$

d) Summary of the estimated parameters.

Figure 4.18. Matching between the measurements and the simulation results of the spectral response for the nematic LC 1631F spiral notch filter.

4.3. Notch filter on liquid crystal technology with spiral meander spurline structure

In section 4.1 of this chapter, the spiral meander spurline structure was studied in depth. The simulated filter with the dimensions of the electrode pattern and LC cavity already optimized are used as the jump off point of the device design. As it was mentioned, this notch filter is implemented by employing the LC 1631E, which is also an experimental mixture of high dielectric anisotropy from the same family as 1631F.

The rejection frequency of the designed notch filter satisfies equation (4.1) by replacing *a* by the spiral equivalent length. Hence, for fixed dimensions of the spurline, the rejection frequency of the filter can be modified by changing the value of ε_{eff}. This can be accomplished by tuning the LC permittivity between two extreme values $\varepsilon_{r\perp}$ and $\varepsilon_{r\parallel}$ through applying an external voltage.

This section includes the choice of components and materials for the filter implementation and, then, electromagnetic simulations are done in order to study the device viability and predict the frequency response of the filter S-parameters. Once simulations are done, the filter is manufactured and experimentally measured. The experimental results for the tuning of the rejection frequency and the negative group delay are shown in sub-section 4.3.c.

Finally, the experimental results of the filters are employed to estimate, by using a resonant method, the LC dielectric permittivity extreme values, which are, initially, unknown at microwave frequencies. This method is also used to estimate the LC dielectric loss tangent.

The design and characterization of this device is a colaborative work between Grupo de Displays y Aplicaciones Fotónicas (GDAF) from Universidad Carlos III de Madrid and Grupo PROMETEO (Procesado de Materiales y Tecnologías Optoelectrónicas) from Universidad Miguel Hernández de Elche. The researching lines of this group include the design of optical filters, optoelectronic modulators and optical characterization techniques. The manufacture of the filter has been done in the facilities of this university.

4.3.a. Choice of components for a practical implementation

The choice of the components for a practical implementation of the notch filter is summarized in the inset table of Figure 4.19 c). The structure of the filter (Figure 4.19 a)) has the same microstrip inverted arrangement than that of the notch with conventional spurline electrode, previously described. The dimensions of the pattern of the spiral meander spurline structure have been determined by the limitations of the manufacturing process. Therefore, the spurline gap *s* dimension cannot be lower than 0.2 mm and it limits the other dimensions of the structure. A picture of the notch filter based on LC technology with spiral meander spurline structure is shown in Figure 4.19 b). The implementation of this device is an original contribution of this work of Thesis.

The filter is fabricated using Taconic TLX-8 as the supporting substrate for the microstrip line and spacer. The cavity is then filled with the LC 1631E and sealed. The dielectric substrate attached below the ground plane is FR4 ($\varepsilon_r = 4.4$) with a thickness of 1.52 mm. This substrate is only used to provide support for the metallic plane, so it will not affect the filter behavior. The spurline width (w) is 0.6 mm in order to have an input impedance of about 50 Ω by using the microstrip line equations [4.21]. Remember that, taking into account these initial constraints, the dimensions of the structure were optimized in order to obtain a rejection frequency nearby 5 GHz considering that the LC cavity is empty.

The LC employed to fill the 250 μm thick cavity has been another experimental mixture of high birefringence in order to obtain a high tuning range of the rejection frequency. It is a nematic LC, named 1631E, again synthesized and delivered by Military University of Technology [4.14], whose behavior at microwave frequencies has not been previously studied, that is, its loss tangent and permittivity extreme values are unknown at these frequencies.

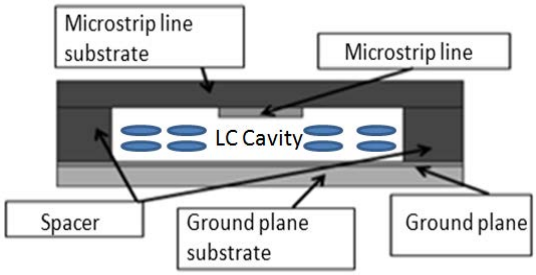

a) Microstrip inverted arrangement.

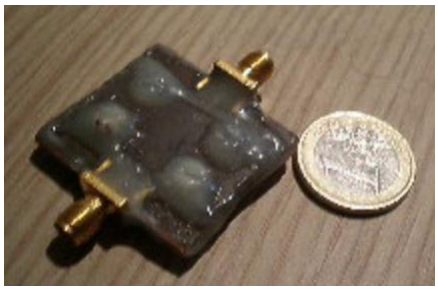

b) A picture of the manufactured notch filter.

Component	Material	Thickness (mm)
Microstrip line substrate	Taconic TLX-08	0.8
Spacers	Taconic TLX-08	0.25
Liquid crystal	Nematic LC 1631E	0.25
Microstrip line and ground plane	Copper	0.018
Ground plane substrate	FR4	1.52

c) Materials and dimensions of the structure.

Figure 4.19. Notch filter based on LC technology with spiral meander spurline structure.

4.3.b. Extension of the static spectral response to tunable

The simulations of the S_{21} parameter of the notch filter, by using the electromagnetic software tool Ansoft HFSS, are presented. The notch filter with spiral meander spurline structure is simulated considering the materials and dimensions aforementioned. The shape of the spiral meander spurline structure from the software tool is shown in Figure 4.20 a); the inset table shows the dimensions. Figure 4.20 b) shows a 3D detail of the structure for simulations.

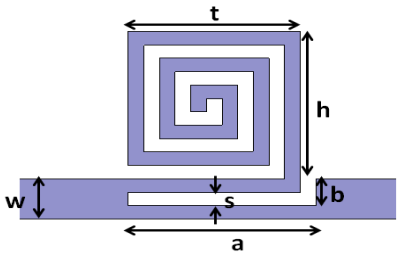

Dimension	Value
a	2.4 mm
b	0.4 mm
s	0.2 mm
w	0.6 mm
t	2.2 mm
h	2.2 mm

a) The shape and dimensions of the spiral meander spurline structure. Note that figure is not drawn to scale.

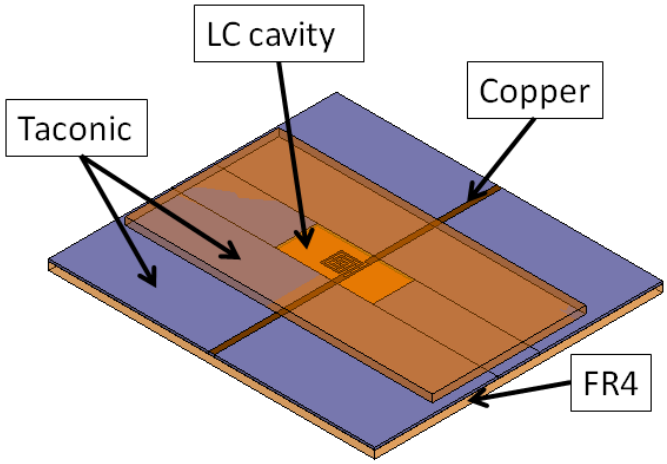

b) 3D detail of the spiral meander spurline for simulations.

Figure 4.20. Design of the spiral meander spurline structure for a microstrip inverted notch filter. The inset table shows the results for the optimized dimensions.

The evolution of the filter S_{21} parameter with the frequency, between 2.5 GHz and 5 GHz, is shown in Fig. 4.21. The rejection frequency obtained is f_0 = 3.73 GHz when $\varepsilon_{r\perp}$ = 2.43 (blue line) is considered. When $\varepsilon_{r\parallel}$ = 3.49 (red line), the rejection frequency reaches its minimum value, f_0 =3.25 GHz.

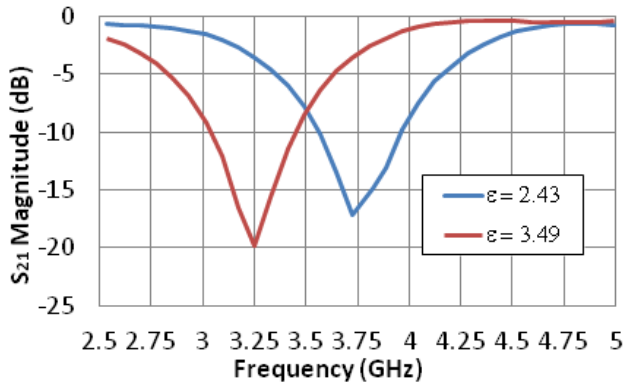

a) Simulation of frequency dependence of S_{21} parameter.

Permittivity	Rejection frequency (f_0, GHz)
$\varepsilon_{r\perp} = 2.43$	3.73
$\varepsilon_{r\parallel} = 3.49$	3.25

Relative tuning range $\Delta f / f_0$	480 MHz / 3.49 GHz = 0.138

b) Filter performance.

Figure 4.21. Simulation of the spectral tuning range of a LC notch filter with spiral meander spurline structure [4.17].

As expected, the rejection frequency of the filter considering the cavity filled with the liquid crystal is lower than that of the empty filter (with $\varepsilon_r = 1$). In fact, the simulation results for an spiral meander spurline structure with optimized dimensions achieved a rejection frequency nearby 5 GHz. Finally, a frequency shift of $\Delta f_0 = 480$ MHz have been achieved, which means a relative tuning range of $\Delta f / f_0 = 0.138$.

4.3.c. Characterizing the filter performance. Tuning of the filter parameters

In the following sections, the experimental results related to the device designed are detailed and the most important aspects of these are discussed as well. The used experimental set-up is the same as the employed in the LC notch filter with conventional spurline structure. The schematic is reproduced in Fig. 4.22 but specifically for this new filter.

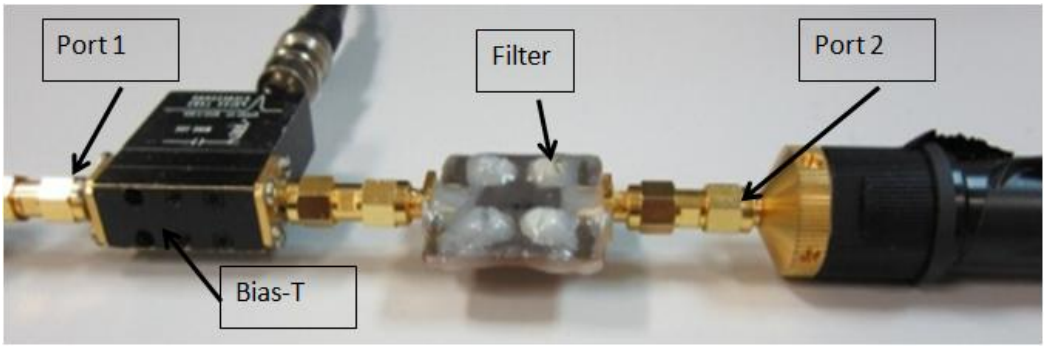

Figure 4.22. A general experimental set-up for characterizing LC samples at microwave frequencies. The picture illustrates a notch filter with spiral meander structure connected to the microwave signal flow.

Before filling the filter with LC, the device was measured with the LC cavity empty. Figure 4.23 shows the frequency response of the empty filter and a comparison with the theoretical response obtained in simulation. The measured rejection frequency appears at 5.05 GHz, which is a value a bit higher than the obtained in simulation (4.96 GHz). Nevertheless, it is a not significant difference and it could be due to error tolerances in the manufacturing process presented in Chapter 3. Once the filter has been measured with the LC cavity empty and it response is validated, the device is filled with LC 1631E. The measurements with LC are presented next.

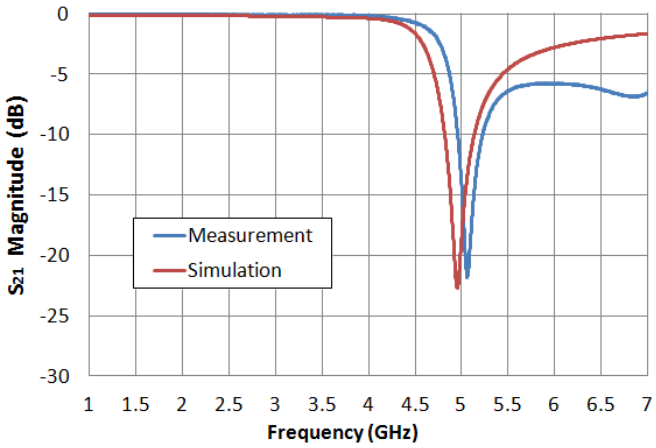

Figure 4.23. Measured frequency response obtained for the empty filter. Comparison with the theoretical response in simulation.

a) Tuning of the rejection frequency

The magnitude of the S_{21} parameter of the notch filter was characterized by using a LC driving voltage that ranges between 0 V_{rms} and 12 V_{rms}. Figure 4.24 summarizes the characterization results. The LC driving voltage dependence of the filter spectral response is illustrated in Figure 4.24 a). Again, as expected, the rejection frequency value f_0 is shifted to lower frequencies as voltage increases. Of course, the value expected for the LC relative permittivity is greater than 1. In Figure 4.24 c) is inset a table with the main result parameters. Without external voltage, f_0 = 3.75 GHz; upon applying 12 V_{rms}, f_0 reaches its minimum value, 3.40 GHz. Both values are minor than 5 GHz for the empty filter. This behavior means a variation of the rejection frequency of 350 MHz across the tuning range, that is, a relative tuning range (with respect to the medium central frequency) of 9.8%.

LC driving voltage dependence of the rejection frequency, f_0, is shown in Figure 4.24 b). It is noticed that the profile of this behavior is not linear at all. The filter rejection frequency does not change while the applied voltage is lower than 1 V_{rms}. Then, two sections of the curve can be distinguished nearly linear. Between 1 V_{rms} and 4 V_{rms}, f_0 varies with a rate of 97 MHz/V_{rms}. From 4 V_{rms}, f_0 decreases very slowly with a rate of 10 MHz/V_{rms}. The dynamic range of the applied external voltage, for f_0 varying from 10% to 90%, is

approximately 4.5 V_{rms}. In addition, it is observed that as the driving voltage is increased, the rejection level of f_0 also increases.

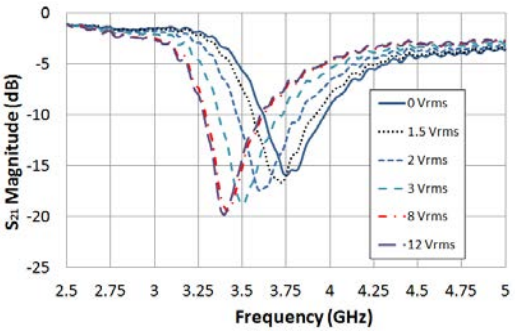

a) LC driving voltage dependence of the filter spectral response.

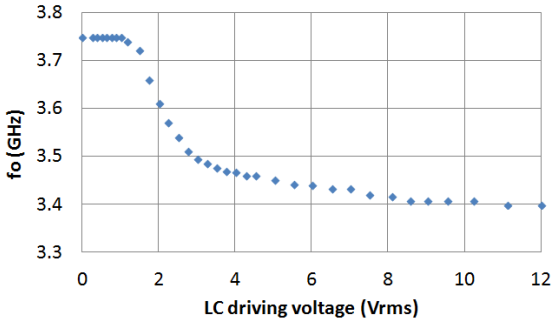

b) LC driving voltage dependence of the rejection frequency f_0.

V	ε_r	f_0	Relative tuning range $\Delta f / f_0$	Quality factor (Q)	Dynamic range (V_{rms})
0 V_{rms}	$\varepsilon_{r\perp}$	3.75 GHz	9.8%	3.2	5 V_{rms}
12 V_{rms}	$\varepsilon_{r\parallel}$	3.40 GHz			

c) Summary of the obtained results for the rejection frequency.

Figure 4.24. Spectral tuning range of a LC notch filter prototype with spiral meander spurline structure.

A significant result is attained about the quality factor Q of the notch filter. That is, there is no dependence of the quality factor (Q) with the LC driving voltage. Although the filter gets narrower as driving voltage is increased, f_0 also decreases, so Q remains constant. A Q value about 3.2 is obtained, which is a higher value than the achieved by the notch filter with conventional spurline structure shown in section 4.2.

b) Tuning of the negative group delay (NGD)

An interesting aspect of notch filters is the existence of a negative group delay region at f_0. Research Group PROMETEO from Universidad Miguel Hernández de Elche has contributed to the development of negative group delay (NGD) systems [4.22]. NGD systems allow the propagation of pulses, at a zero transmission frequency, to be delayed. Due to a notch filter exhibits a transmission zero at the rejection frequency, f_0, it exhibits NGD at this frequency. Therefore, just like the rejection frequency is voltage controlled, NGD can also be frequency-shifted. Because of the increasing interest in microwave applications for NGD circuits [4.24 - 4.26], the group delay, τ_g, of the notch filter is also evaluated. It is calculated as the frequency derivative of the S_{21}-parameter phase, ϕ_{12}.

$$\tau_g = -\frac{\partial \phi_{21}}{\partial \omega} \tag{4.2}$$

where $\phi_{21}(\omega)$ is the phase of the S_{21} parameter and ω the angular frequency.

The frequency evolution of τ_g for several values of the LC driving voltage is shown in Fig. 4.25 a). As f_0 is tuned from 3.40 to 3.75 GHz, the NGD region is accordingly shifted. This shift is accompanied by a variation of the group delay value at f_0, ranging from -1.6 ns at 3.40 GHz to -1.0 ns at 3.75 GHz (Figure 4.25 b)). This is a consequence of the non-constant rejection level at f_0 as the LC drive voltage is changed.

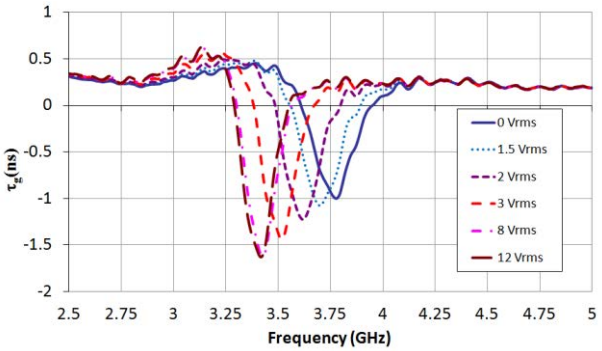

a) LC driving voltage dependence of the negative group delay.

V	ε_r	τ_g (f_0)
0 V_{rms}	$\varepsilon_\perp$	-1 ns
12 V_{rms}	$\varepsilon_\parallel$	-1.6 ns

b) Summary of the voltage controlled negative group delay at the rejection frequency.

Figure 4.25. Tuning of the negative group delay for a LC notch filter.

As the LC driving voltage increases, NGD also increases, while the group delay bandwidth is narrower. This behavior is characteristic of passive NGD circuits. Moreover, because of the fact that NGD appears at transmission zero frequencies, where the attenuation has a maximum, it would be necessary to add an active component (e.g. a FET) in order to amplify the signal at the rejection frequency. This solution has been already used in research [4.25] obtaining a good performance. In this case, a tunable capacitance or inductance would be needed in order to control the NGD level.

4.3.d. Estimating liquid crystal parameters by a notch filter

The nematic LC 1631E used for the notch filter with spiral meander structure, is also an experimental mixture with a high dielectric anisotropy developed by Military University of Warsaw (Poland), whose dielectric properties (LC permittivity and loss tangent) were initially unknown at microwave frequencies.

In order to estimate these properties, the same resonant method used for LC 1631F in section 4.2.d has been carried out. The manufacturing error tolerances has been taken into account in the simulations. Fig. 4.26. shows the evolution of the filter's rejection frequency obtained by simulating with Ansoft HFSS as a function of the LC permittivity.

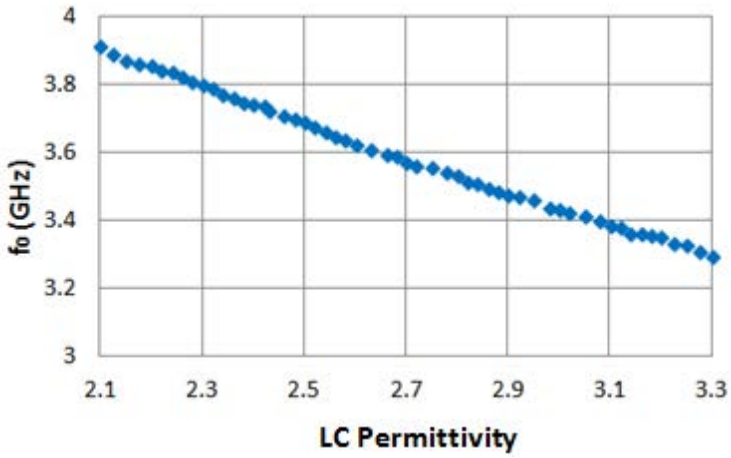

Figure 4.26. Simulation of the evolution of the rejection frequency as a function of the LC permittivity.

The results are used to infer the value of the LC permittivity for each measured rejection frequency as it was derived for LC 1631F, estimating the extreme values of the LC permittivity, $\varepsilon_{r\perp}$ and $\varepsilon_{r\parallel}$, which correspond, respectively, to 0 V_{rms} and 15 V_{rms}.

Figure 4.27 a) shows the measured and simulated curves for 0 V_{rms} and the estimation of the LC permittivity and loss tangent are, respectively $\varepsilon_{r\perp} = 2.38$ and $\tan \delta_{\perp} = 0.04$, while Figure 4.27 b) shows the graphics for 12 V_{rms}, obtaining $\varepsilon_{r\parallel} = 3.08$ and $\tan \delta_{\parallel} = 0.02$. Thus, the dielectric anisotropy of the nematic LC 1631E ($\Delta\varepsilon = \varepsilon_{r\parallel} - \varepsilon_{r\perp}$) is estimated to be $\Delta\varepsilon = 0.7$ at about 3.5 GHz.

The values of LC permittivity and loss tangent obtained in this estimation for LC 1631E are similar to the estimated for LC 1631F, as it was expected since both LC are from the same family.

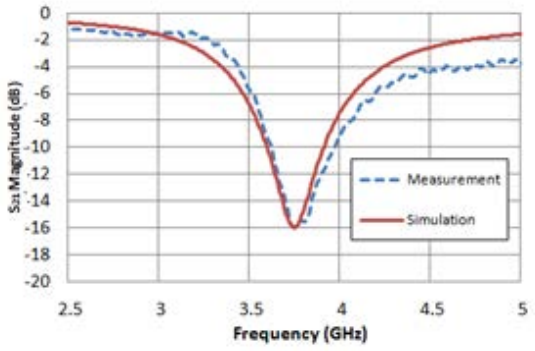

a) Measurement: 0 Vrms LC driving voltage. Simulation: $\varepsilon r_{\perp} = 2.38$ and $\tan \delta_{\perp} = 0.04$.

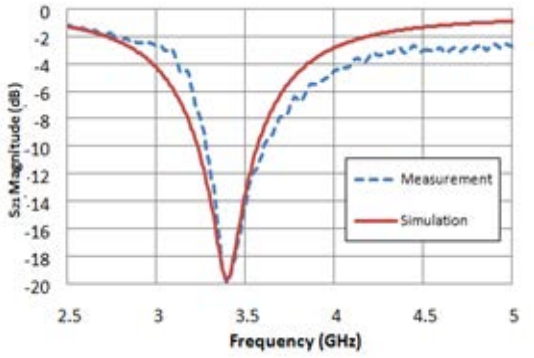

b) Measurement: 12 Vrms LC driving voltage. Simulation: $\varepsilon r_{\parallel} = 3.08$ and $\tan \delta_{\parallel} = 0.02$.

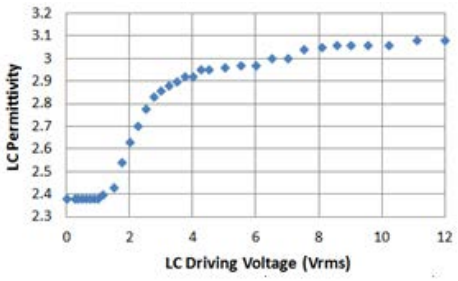

c) Evolution of the estimated LC dielectric permittivity as a function of the LC drive voltage.

LC Driving Voltage	f_0	Estimated	
		ε_r	tan δ
0 V_{rms}	4.84 GHz	$\varepsilon_{r\perp} = 2.3$	$\tan \delta_{\perp} = 0.035$
15 V_{rms}	4.45 GHz	$\varepsilon_{r\parallel} = 3.02$	$\tan \delta_{\parallel} = 0.02$

d) Summary of the estimated parameters.

Figure 4.27. Matching between the measurements and the simulation results of the spectral response for the nematic LC 1631E spiral notch filter.

4.4. Conclusions

Stop-band filters or notch filters are very important devices in telecommunication systems at microwave frequencies due to its ability of attenuating a determined frequency or band of frequencies. The possibility of designing reconfigurable notch filters, whose rejection frequency can be externally changed, is very interesting in order to obtain more flexible telecommunications systems.

This chapter deals with tunable notch filters based on LC. Concretely, spurline structure, which is a very common topology in microstrip band-stop filters at microwave frequencies because of its easy design and good performance, has been studied in depth and it has been employed for the design of the devices. A theoretical study of the spurline structure, including the conventional structure and two variants of it, the meander structure, and the spiral meander structure, has been carried out in order to optimize the structure for the filters to manufacture.

The jump off point has been the design, manufacture, simulation and characterization of a tunable notch filter with a conventional spurline structure. An experimental high anisotropic mixture developed by Military University of Warsaw (1631F) has been employed as the LC material. Due to high dielectric anisotropy, a high relative tuning range of 8.4% has been achieved for the filter rejection frequency, which is a very promising value. Additionally, the experimental results of this device have been used for the estimation of the LC dielectric properties, which were unknown at these frequencies, by using a resonant method. A dielectric anisotropy $\Delta\varepsilon = 0.72$ has been estimated at 5 GHz, which is a larger value than other commercial LC´s.

The next characterized device was a tunable notch filter implemented in inverted-microstrip line technology using a spiral meander spurline structure. This new structure provides an improvement of the filter performance and an important reduction of the device size with respect the conventional spurline topology. The key point is that the cavity volume is reduced by a factor of two and, consequently, the amount of the LC required is also reduced, saving a relevant cost in the manufacturing process of the device.

A rejection frequency tuning range about 10% upon applied voltage has been obtained, along with the corresponding frequency-shift of the NGD region. These experimental results of this device have been also employed to estimate the used LC (in this case, 1631E) permittivity and loss tangent by using the same procedure employed for the LC 1631F. A dielectric anisotropy $\Delta\varepsilon = 0.7$ has been estimated at about 3.5 GHz.

4.5. References

[4.1] C. Nguyen, K. Chang, “On the analysis and design of spurline bandstop filters”, IEEE Trans. Microw. Theory, Vol. 33, p. 1416–1421, 1985.

[4.2] R. Loo-Yau, O.I. Gómez-Pichardo, F. Sandoval-Ibarra “Spurline structures and its application on microwave coupled line filter”. Revista Mexicana de Física, Vol.57, No 3, p. 184–187, 2011.

[4.3] Z. M. Hejazi, P. S. Excell, and Z. Jiang, “Compact dual-mode filters for HTS satellite communication systems”, IEEE Microwave and Guided Wave Letters, Vol. 5, No. 11, p. 275 - 277, Aug. 1998.

[4.4] J. S. Hong, M. J. Lancaster, “Microstrip bandpass filter using degenerate modes of a novel meander loop resonator”, IEEE Microwave and Guided Wave Letters, Vol. 5, No. 11, p. 371 – 373, Nov. 1995.

[4.5] B. Shrestha, N. Y. Kim, “Spurline resonators design and its implementation to microwave oscillators”, Microwave and Optical Technology Letters, Vol. 54, No. 1, p. 171-174, Jan. 2012.

[4.6] H. Liu, Reinhard, H. Knoechel, Klaus F. Schuenemann, "Miniaturized bandstop filter using meander spurline and capacitively loaded stubs", ETRI Journal, Vol. 29, No. 5, p. 614-618, Oct. 2007.

[4.7] S. J. Cho, N.Y.Kim, "A novel spiral meander spurline resonator and its implementation to a low-phase noise oscillator", Microwave and Optical Technology Letters , Volume 53, Issue 10, p. 2258-2262, Oct. 2011.

[4.8] J.V.S. Hari Krishna, "Compact spiral folded spurline for low frequency applications", Electronic Letters, Vol. 47 No. 15, p. 1508-1509, 2011.

[4.9] S. J. Choa, N. Y. Kim, "Miniaturisation and high quality factor of spiral meander spurline resonator for microwave oscillator", International Journal of Electronics, Vol. 100, No. 4, p. 563-574, 2013.

[4.10] B. Shrestha, N. Y. Kim, "Slot meander spurline bandstop filter using integrated passive device technology", Microwave and Optical Technology Letters, Vol. 57, No. 1, p. 168-172, 2015.

[4.11] C. Marcos, "Contribución al desarrollo de sensores y sistemas sintonizables eléctricamente basados en cristal líquido para aplicaciones en la industria aeroespacial". PhD Doctoral Thesis. Universidad Carlos III, Leganés, 2011.

[4.12] V. Urruchi, C. Marcos, J. Torrecilla, J.M. Sánchez-Pena, R. Dąbrowski, "Tunable notch filter based on liquid crystal for microwave applications", XIX Conference on Liquid Crystals, Międzyzdroje, Poland, 2011.

[4.13] A. Spadło, R. Dabrowski, M. Filipowicz, Z. Stolarz, J. Przedmojski, S. Gauza, C. Y. H. Fan, and S.-T. Wu, "Synthesis, mesomorphic and optical properties of isothiocyanatotolanes, Liq. Cryst. Vol. 30, No. 2, p. 191–198, 2003.

[4.14] R. Dabrowski, J. Dziaduszek, A. Ziólek, L. Szczuciñski, Z. Stolarz, G. Sasnouski, V. Bezborodov, W. Lapanik, S. Gauza, S. T. Wu, "Low viscosity, high birefringence liquid crystalline compounds and mixtures", Opto-Electronics Review, Vol. 15, p. 47-51, 2007.

[4.15] A. Spadlo, R. Dabrowski, J. Dziaduszek, E. Scibior, S. Urban, S. Gauza, S. T. Wu, "Liquid crystalline materials with high birefringence", Journal of Optical Technology, Vol. 72, No 9, p. 659-661, 2003.

[4.16] Dabrowski, J. Dziaduszek, K. Garbat, M. Filipowicz, S. Urban, S. Gauza, and G. Sasnouski, Liquid Crystals, Vol. 37, no 12, p. 1529, 2010.

[4.17] F. Dubois, et al., "Large Microwave Birefringence Liquid-Crystal Characterization for Phase-Shifter Applications", Japanese Journal of Applied Physics, Vol. 47, No 5 p. 3564-67, 2008.

[4.18] M. Yazdanpanahi, S. Bulja, D. Mirshekar-Syahkal, R. James, S. E. Day, F. A. Fernández, "Measurement of dielectric constants of nematic liquid crystals at mm-Wave Frequencies Using Patch Resonator", IEEE Transactions on Instrument Measurement, vol. 59, no. 12, pp. 3079-3085, Dec. 2010.

[4.19] S. Bulja, D. Mirshekar-Syahkal, R. James, S. E. Day, F. A. Fernández, "Measurement of dielectric properties of nematic liquid crystals at millimeter wavelength", IEEE Transitions on Microwave Theory and Techniques, vol. 58, No 12, pp. 3493-3501, Dec. 2010.

[4.20] C. Weil, S. Müller, P. Scheele, Y. Kryvoshapka, G. Lüssem, P. Best, and R. Jakoby, "Ferroelectric- and liquid crystal- tunable microwave phase shifters", 33rd European Microwave Conference, p. 1431-1434, Munich, Germany, 2003.

[4.21] D. M. Pozar, "Microwave engineering", 3rd ed. Ed. John Wiley & Sons, p. 143-149, 1999.

[4.22] A. Sánchez-Meroño, M. M. Sánchez-López, J. Arias, "Fast light in unbalanced low-loss Mach-Zehnder interferometers", Physical Review A, Vol. 89, 043828, 2014.

[4.23] J. Arias, A. Sánchez-Meroño, M. M. Sánchez-López, I. Moreno, "Slow and fast light in three-beam interferometers: Theory and experiment", Physical Review A, Vol. 85, 033815, 2012.

[4.24] O. F. Siddiqui, M. Mojahedi, G. V. Eleftheriades, "Periodically loaded transmission line with effective negative refractive index and negative group velocity", IEEE Transactions on Antennas Propagation Vol. 51, No. 10, p. 2619-2625, Oct. 2003.

[4.25] B. Ravelo, A. Pérennec, M. Le Roy, Y. G. Boucher, "Active microwave circuit with negative group delay," IEEE Microwave and Wireless Components Letters, Vol. 17, No. 12, p. 861-863, Dec. 2007.

[4.26] A. Sánchez-Meroño, E. Ávila, J. Arias, M. M. Sánchez-López, "Control del retardo de grupo en reflectores de Bragg para amplificadores feedforward", *XXV Simposiun Nacional Unión Científica Internacional de Radio* (URSI), 2010.

CHAPTER 5: TUNABLE DUAL-MODE BAND-PASS FILTER BASED ON LIQUID CRYSTAL TECHNOLOGY

Notch filters based on LC technology, as stated in the previous chapter, have already studied in depth and assessed their performance in terms of some parameters that evaluate its viability in practical applications. In this chapter, novel advanced proposals of filter configurations are considered. Some configurations of passive band-pass filters are devised. These filters allow wavelengths within a certain microwave range to be transmitted while reject (attenuate) frequencies outside that range. Again, all configurations have a cavity to house the liquid crystal (LC) material. Only filter structures that previously showed better performance were manufactured. The final choice was made according to its optimal frequency behavior. Spectral responses were simulated through a batch of tests programmed in some commercial softwares. The performance of the manufactured devices was examined and analyzed its viability for a real application.

Band-pass filters are very important in telecommunication systems because these devices allow the signals to be channeled. As already mentioned, we have focused our interest only in the frequency bands ranged from 5 GHz to 10 GHz. Again, planar structures with microstrip configuration have been chosen owing to they have advantages over waveguide filters mainly in terms of repeatability, compact size and low cost. A wide series of new and highly compact microstrip tunable LC-based band-pass filters are proposed with dual-mode configuration. A detailed study of every microstrip geometric shape is carried out for this kind of resonators from the conventional structure. Particularly, strategic parameters are pass-band return loss and ripple, group delay and power linearity. All of them are measured, compared its values to the theoretical predictions and discussed the results.

An important constraint detected from the filter measurements is a low value of pass-band return loss. As it is known in filter designing, in a band-pass filter, the larger the value of pass-band return loss, the better quality of the device under test. Some modifications to the microstrip requirements have been done in the original structure for enhancing the pass-band return loss of the filter, by narrowing its bandwidth. A new filter with improved frequency response has been predicted by electromagnetic simulations. In this regard, a practical embodiment of a novel filter confirmed the possibility of a solution that alleviated the problem. The strategy for the pass-band return loss increase was the reshaping of the patch of the microstrip structure. Best performance was achieved; the discussion of the improvements is also detailed.

This chapter is organized into the following main parts:

- First, dual-mode technology for band-pass filters is introduced in a section, explaining the dual-mode operation and why this technology has been chosen as one of the favorite configurations for developing band-pass filters in this work.

- A microstrip dual-mode configuration has been assessed initially on a FR4 microwave dielectric substrate with non-tunable permittivity. The performance of a first filter prototype manufactured using this substrate is analyzed in depth.

- The main sections of the chapter are devoted to the design, electromagnetic simulation and manufacture of a dual-mode band-pass filter on liquid crystal technology. The device is carefully probed and the measured results and main conclusions are presented.

- Improved performance in liquid crystal dual-mode band-pass filters is tested in new filters. Details of the design and test carried out on the manufactured filter are encompassed in the chapter.

- Also, an estimation of the permittivity of the commercial LC MDA-98-1602, at microwave frequencies, has been considered a key issue to solve for considering in future works based on the same material.

5.1. Dual-mode band-pass filter configuration

A typical frequency response of a band-pass filter is shown in Figure 5.1. An ideal spectral response of a band-pass filter should offer low passband insertion loss (S_{21}) within the passband, high return loss (S_{11}) and steep rejection skirts at the passband edge.

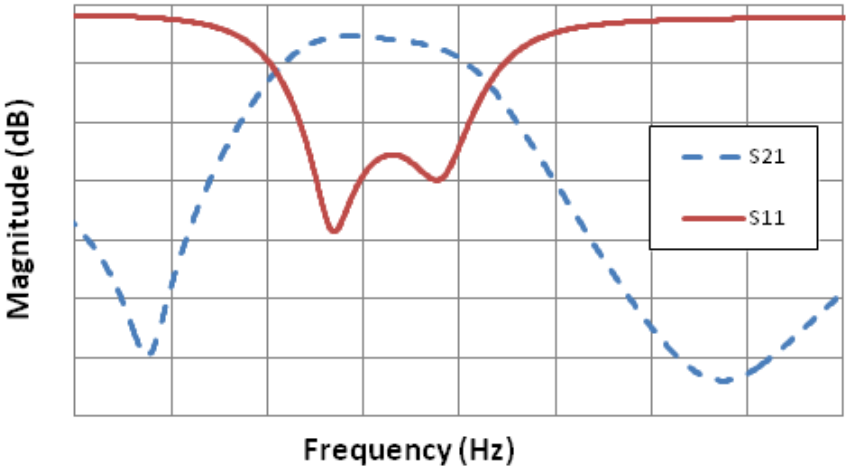

Figure 5.1. A typical frequency response of a band-pass filter.

This section describes first, dual-mode technology for band-pass filters. Next, improvements of filter performance are suggested by reshaping the conventional dual-mode geometry of the microstrip in order to achieve higher quality frequency responses.

5.1.a. Conventional filter structure

There is a wide variety of new filters that have been developed from lumped element (LC) resonators to distributed resonators, such as waveguide, coaxial and microstrip. Particularly, dual-mode operation for resonators is well known on microstrip structures since it was introduced by I. Wolff in 1972 [5.1]. Nowadays, this technology is widely used in the design of microwave band-pass filters because of its advantages in size and compactness. The interest generated by dual-mode technology is focused mainly on its simple and flexible design. Different structures have been studied to design dual-mode filters: ring resonators [5.2 - 5.4], loop resonators [5.5 - 5.7], cross-slotted patch resonators [5.8], etc.

A dual-mode resonator is devised from a simple square patch resonator, see Figure 5.2 a). The geometrical symmetry of that resonator gives rise to degenerate modes that means they resonate at the same frequency. Also, these modes are orthogonal, that is, they can be excited independently without microwave power exchange between them. However, by changing the geometrical symmetry of the structure can allow the modes to be coupled between them and consequently, two modes arise simultaneously at slightly split frequencies. For example, a

perturbation that breaks the symmetry can be the typical feed lines of the resonator placed orthogonally, Figure 5.2 b).

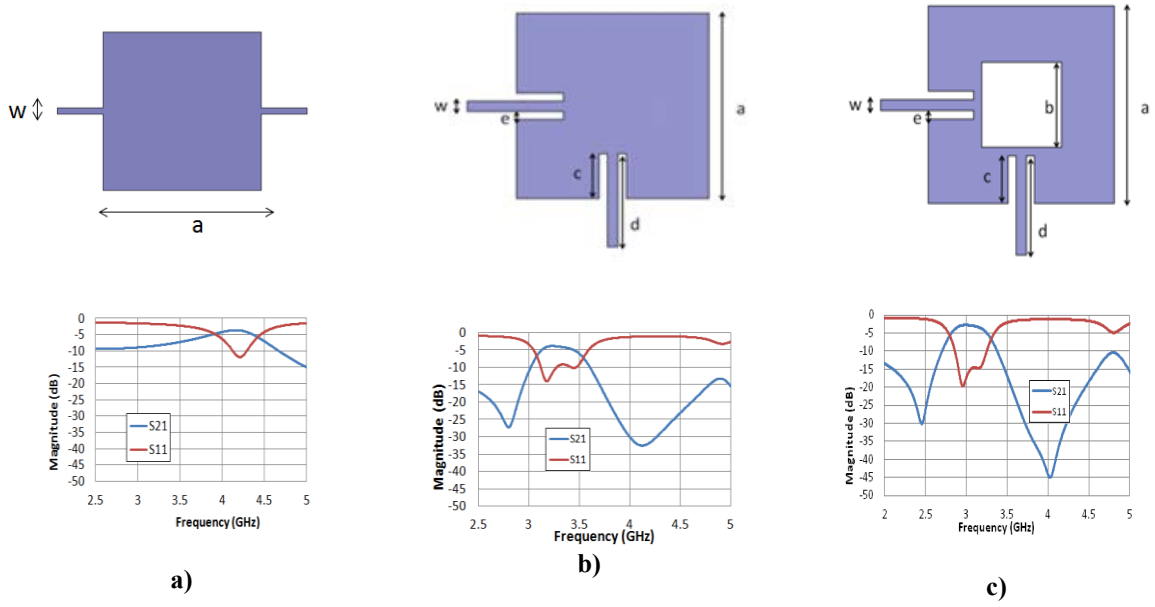

Figure 5.2. The conception of a dual-mode resonator devised from a simple square patch resonator.

With this guideline, the filter geometry chosen for this work have consisted of the previous configuration but introducing a square notch symmetric perturbation, Figure 5.2 c). This structure was introduced by S. Li *et al* [5.9] for a filter with non-tunable permittivity. The detail of the geometry of the microstrip patch is drawn in Figure 5.3. It consists of a microstrip metallic square with side whose length is *a* and a central square notch of side length *b*. The structure also connects two feed orthogonal lines which perturb the electromagnetic fields of the metallic patch. The two electromagnetic degenerated modes excited are coupled by the square notch. This couple is designed relatively weak in order to improve the return loss and insertion loss of the filter.

Figure 5.2 shows the simulation results obtained for this topology considering a conventional non-tunable FR4 microstrip structure. Fig. 5.2 a) is not a dual-mode filter, but a conventional microstrip square patch resonator. As it is shown in its frequency response, an only resonant frequency appears. The topology presented in Fig 5.2 b) consists of a square patch with two orthogonal feed lines which excite the two degenerated modes. This structure, which has not a square notch, is a dual-mode filter, as it is shown in the graphic. Finally, Fig. 5.3 shows the topology and frequency response of the filter proposed by Li *et al*, including a central square notch. It is observed that the insertion loss decreases while the return loss increases, as it was expected as effect of adding a square notch as a perturbation [5.10].

Central frequency of the filter is very sensitive to changes in *b* dimension, while filter bandwidth is sensitive to *a, c* and *e* dimensions. In addition, both magnitudes depend on the

permittivity of the dielectric substrate. *w* is referred directly to the feed lines and affect the impedance mismatch at the filter input and output. Finally, it is important to take account that frequency response of the filter exhibits two transmission zeros whose frequency location depends on the dimensions of the structure, specifically *b*.

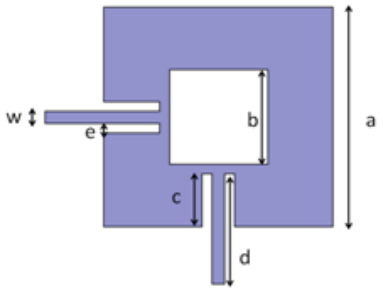

Figure 5.3. Detail of dual-mode filter geometry for a band-pass filter. Note that the drawn in not to scale.

Liquid crystal technology provides a significant added value to band-pass filters with dual-mode operation. One selection criteria for considering dual-mode geometry in filter design of this work has been an important reduction of size of devices. It is a critical issue affecting final arrangement of LC-based devices. Compact and small structures mean the saving of a certain amount of the material required. The easiest band-pass filter based on LC technology would consist of a single resonator, that is, a first order filter. Dual-mode technique can work as an alternative solution for the generation of two-degree filters, comprising two LC resonators coupled between them, without adding too much complexity to the structures. Further, low complexity implementations facilitate the design of new microstrip approaches.

5.1.b. Improving filter performance

The introduction of some controlled perturbation in the geometry of the microstrip electrode has been proposed. It has identified as a key strategy in achieving improved performance from the basic dual-mode configuration previously described. In taking forward this objective, the following design rules have thought about. First, a microstrip electrode with a pattern with continuous conductor is a mandatory requirement for a LC device, if non-complex manufacturing processes are demanded. Split electrodes would require through holes for guiding driving signals towards LC material, becoming more difficult the manufacturing processes; so this approach has not been contemplated. Likewise, two types of disturbances, the distortions that break symmetry of the conventional dual-mode structure with a square notch and those that do not, have been considered in the design. Some of them have been described in literature which can be implemented in order to reduce the coupling factor between the two modes [5.11, 5.12]. They consist of reshaping the conventional dual-mode structure presented in Fig. 5.3. An assessment of every configuration is given bellow.

Main parameters of interest focused on are filter pass-band return loss that can be increased by narrowing filter bandwidth. Filter bandwidth gets narrower if the coupling factor of the two degenerated modes gets lower. In this way, the difference between the resonant frequencies of the two electromagnetic orthogonal modes is also lower and, therefore, the filter bandwidth is reduced. Simulations of some of the most relevant results are presented following. Figure 5.4 summarizes the shape of the microstrip patches proposed for the simulated structures. The experimental nematic LC 1631E with permittivity extreme values $\varepsilon_{r\perp} = 2.38$ and $\varepsilon_{r\parallel} = 3.08$ [5.13] has been employed for this purpose.

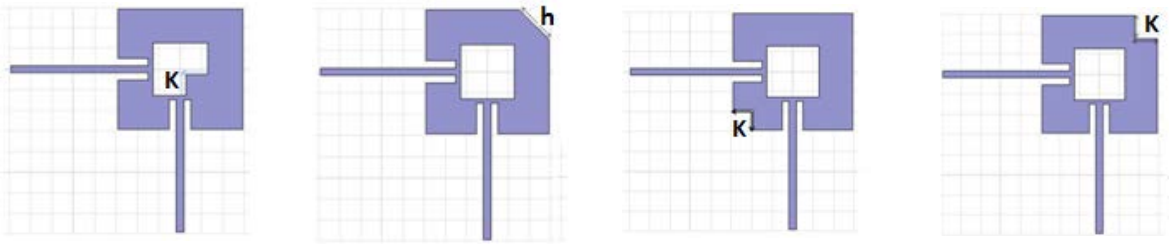

a) b) c) d)

Figure 5.4. Shapes of the microstrip patches proposed for improving filter performance.

The detail of the frequency response of the microstrip patch resonator of Fig. 5.4 a) is shown next. This first approach of a patch reshaping breaks the symmetry of the conventional structure. Intuitively, this perturbation predicts an asymmetry in the frequency response. Figure 5.5 summarizes this behaviour and the simulations achieved considering $\varepsilon_{r\perp} = 2.38$ for several values of k are presented.

Effectively, by increasing the value of k return loss increases within the passband. However, as k makes bigger there is a greater asymmetry between the two zeros of the S_{21} parameter and the same asymmetry is noticeable in the S_{11} parameter.

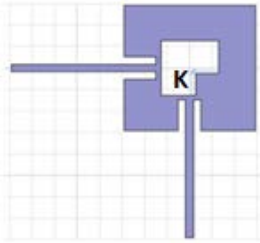

a) New geometry of the microstrip resonator.

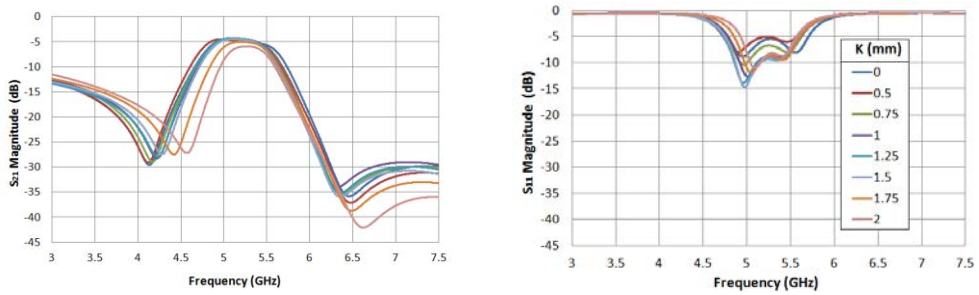

b) Frequency dependence of S_{21} and S_{11} parameters for several values of k considering $\varepsilon_{r\perp}$.

Figure 5.5. Microstrip dual-mode patch resonator with a central square notch including a square cut in a corner that breaks the symmetry.

Another alternative of microstrip reshaping is shown in Fig. 5.6 a). Possibly, one of the most common perturbations is a reshape that consists of a triangular cut on the original square patch resonator of hypotenuse h in the opposite corner to the feed lines. On the contrary to the previous perturbation, this approach does not break the symmetry of the microstrip. The spectral simulations for several values of h considering $\varepsilon_{r\perp}$ = 2.38 are presented in Fig. 5.6 b). Results advise that perturbations with triangular cuts require higher values of dimension h to obtain similar outcomes to those of the previous distortion. This can become a problem if the cut triangle is too near to the central square notch. However, it is observed a light improvement in the symmetry of the responses especially in the S_{11} parameter.

By incorporating the last guidelines, the following two geometries have been proposed; they do not break the symmetry of the dual-mode microstrip and are based on square cuts.

In the first case, an etched squared cut is introduced in the patch resonator in the corner between the feed lines, as shown in Fig. 5.7 a). Frequency response (S_{21} and S_{11}, respectively) achieved by simulation for some values of k, again with LC permittivity $\varepsilon_{r\perp}$ = 2.38, is depicted in Figure 5.7 b). This configuration also achieves a filter return loss improvement within the passband, but compared to the first approach (Fig. 5.5), it seems to be a slight major symmetry in the frequency response.

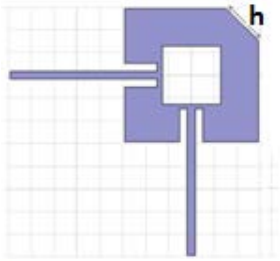

a) New geometry of the microstrip resonator.

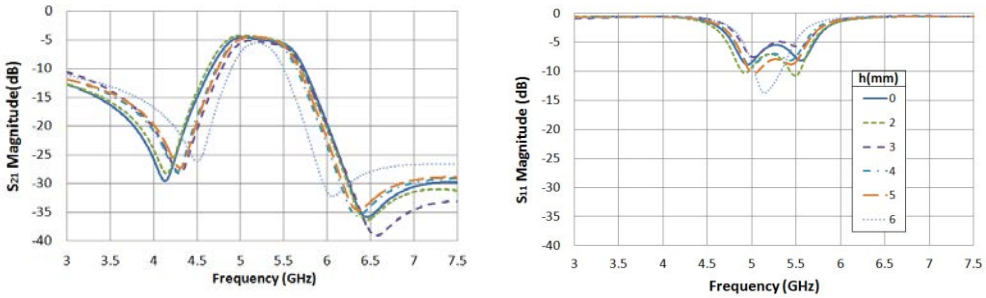

b) Frequency dependence of S_{21} and S_{11} parameters for several values of h considering $\varepsilon_{r\perp}$.

Figure 5.6. Microstrip dual-mode patch resonator with a central square notch including a triangular cut.

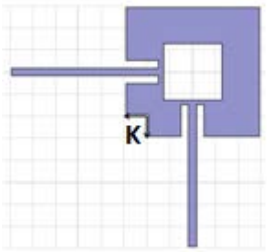

a) New geometry of the microstrip resonator

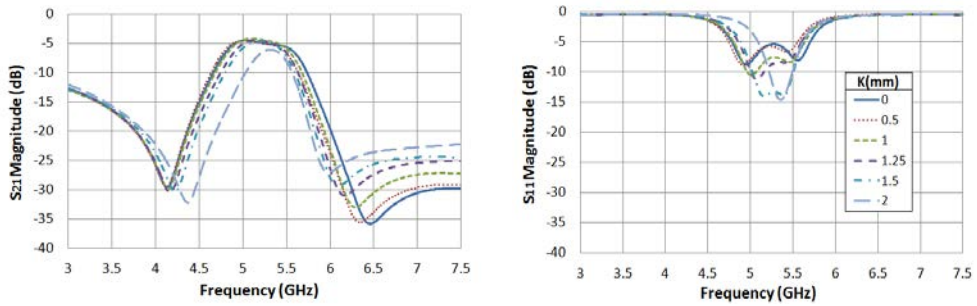

b) Frequency dependence of S_{21} and S_{11} parameters for several values of k considering $\varepsilon_{r\perp}$.

Figure 5.7. Microstrip dual-mode patch resonator with a central square notch including a square cut in the corner between the feed lines.

The last solution has the same configuration, a square cut of side length k in a corner, but in the opposite corner to the feed lines, as shown in Figure 5.8 a). This structure is again simulated by using an electromagnetic software tool for several values of k. Figures 5.8 b) and c) show the filter frequency response, this time considering $\varepsilon_{r\perp} = 2.38$ and $\varepsilon_{r\parallel} = 3.08$. Notice that the case k = 0 mm corresponds with the original structure, that is, without any square cut.

Results of the two last geometries are similar. Again, filter bandwidth decreases, while return loss increases, as value of k increases. Of course, a too large value is not adequate because filter bandwidth would become too much narrow, although return loss improves; a compromise solution must be set. Any of these approaches would be a fair geometry for implementing a new filter design. On the other hand, making a square cut in the other two geometry corners involves the contrary effect (bandwidth increase and return loss decrease), so these modifications are rejected. In this work, the last approach has been selected and used for designing a new dual-mode tunable bandpass filter with LC technology. Final sections of this chapter are dedicated to study in depth of such arrangement.

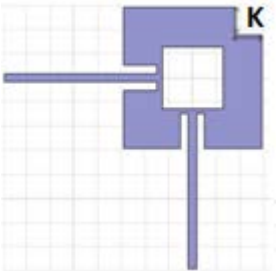

a) New geometry of the microstrip resonator.

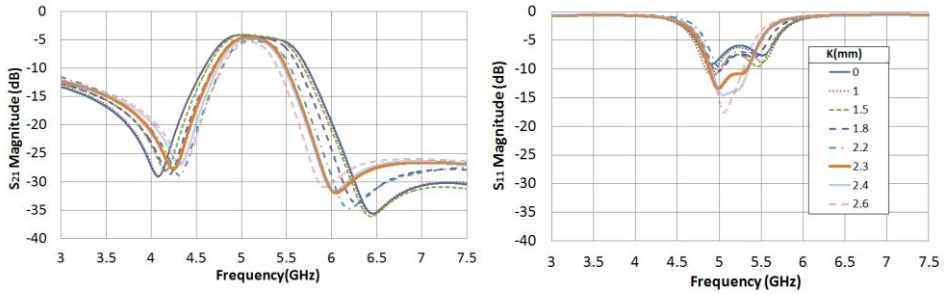

b) Frequency dependence of S_{21} and S_{11} parameters for several values of k considering $\varepsilon_{r\perp}$.

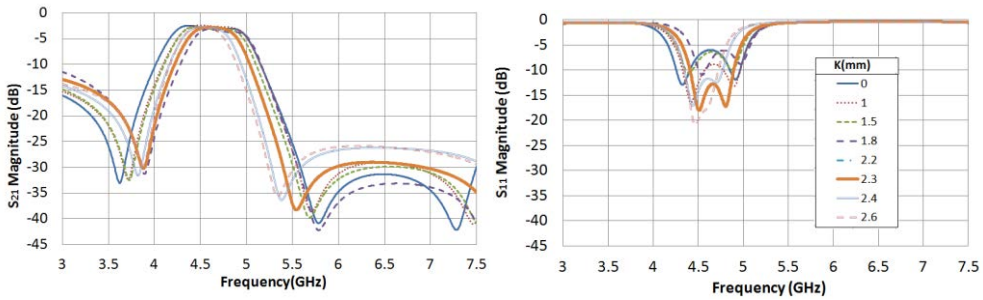

c) Frequency dependence of S_{21} and S_{11} parameters for several values of k considering $\varepsilon_{r\|}$.

Figure 5.8. Microstrip dual-mode patch resonator with a central square notch including a square cut in the opposite corner to the feed lines.

5.2. Dual-mode band-pass filter on FR4 substrate

As stated above, the filter geometry chosen in this work for band-pass filters at microwave frequencies is a dual-mode configuration with a square notch. From this basic geometry, two types of embodiments have been manufactured and tested their performance:

i) Filters based on the conventional structure.
ii) Filters with improved performance constructed by reshaping the microstrip resonator.

In order to study the feasibility of this two arrangements described in the previous section, for a band-pass filter, a first prototype has been developed. Its specific feature is the inclusion of FR4 as a microwave dielectric substrate and thus, carrying out a filter with non-tunable central frequency. The steps to developing this first band-pass filter embodiment are: the design of the constructive parameters linked to the spectral response simulations, the manufacture and the parameters characterization. The main results and conclusions about the

performance of this first prototype are presented in this section. The second phase will be the application of the outcomes of this study for the design of the filters with LC technology.

5.2.a. Designing the filter by spectral response simulation

The design of the constructive parameters of the filter consisted in programming a strategic batch of simulations by using the electromagnetic software tool Ansoft HFSS. The shape of the microstrip resonator from the software tool is shown in Figure 5.9. The objective was to dimension the size of the microstrip patch. The design of the structure dimensions has been optimized in order to achieve a filter with central frequency about 3 GHz. The filter uses FR4, 1.52 mm thick, as the dielectric substrate (ε_r = 4.4, tan δ = 0.02) of the microstrip structure. The suitability of the substrate FR4 is limited to frequencies less than 4 GHz due to restrictions of the material, so this is the reason why filter is designed about 3 GHz. Nevertheless, this material is used due to its ease and ability of manufacturing conventional microstrip designs. The feed lines of the patch are designed to have a 2.4 mm width (*w*) to allow the input impedance to be about 50 Ω (see Chapter 2). The inset table of Figure 5.9 shows the results for the optimized dimensions.

The magnitude of the scattering parameters S_{21} and S_{11}, as a simulation result, is shown in Fig. 5.10. A central frequency of 3.03 GHz and a bandwidth of 590 MHz have been achieved. There is a good match between the passband center and the predicted theoretically.

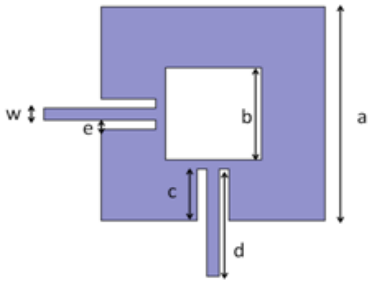

a) The shape and dimensions of the microstrip patch. Note that figure is not drawn to scale.

Dimension	Value
a	17.4 mm
b	6 mm
c	5 mm
d	20 mm
e	1.8 mm
w	2.4 mm

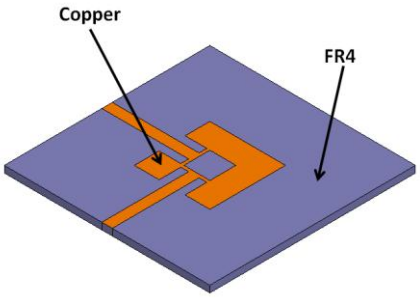

b) 3D detail of the microstrip patch for simulations.

Figure 5.9. Microstrip patch for a dual-mode band-pass filter on FR4 substrate. The inset table shows the results for the optimized dimensions.

The benefit of this simulation outcome is that the spectral response of the filter can be shifted to close neighbor microwave frequencies and to center the passband filter in other band for a specific application.

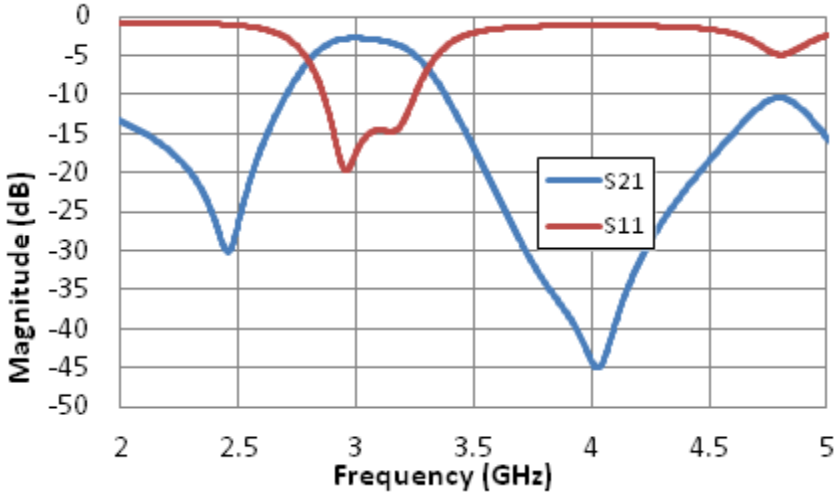

Figure 5.10. Frequency response of a dual-mode band-pass filter on FR4 substrate obtained in simulation.

5.2.b. Characterizing the filter performance

A filter with the specifications of the inset table of Figure 5.9, was implemented. The manufacturing process followed the protocol detailed in Chapter 3. A photo of the manufactured device, a dual- mode band-pass filter on FR4 substrate, is shown in Fig. 5.11.

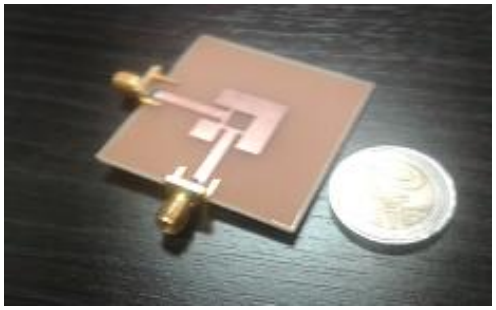

Figure 5.11. Manufactured dual-mode band-pass filter on FR4 substrate.

The experimental set-up is the usual one used in this work to take measurements of the devices, described in Chapter 3. S-parameters are measured by using a network analyzer 8703B from Agilent; the frequency response is shown in Fig. 5.12. A central frequency of 3.19 GHz and a filter bandwidth of 690 MHz have been measured. A two-pole filter with two transmission zeros and a high return loss of 17.5 dB has been achieved. These results validate

the proposed dual-mode microstrip structure for filtering purposes with conditions of impedance coupling, prior to the manufacture.

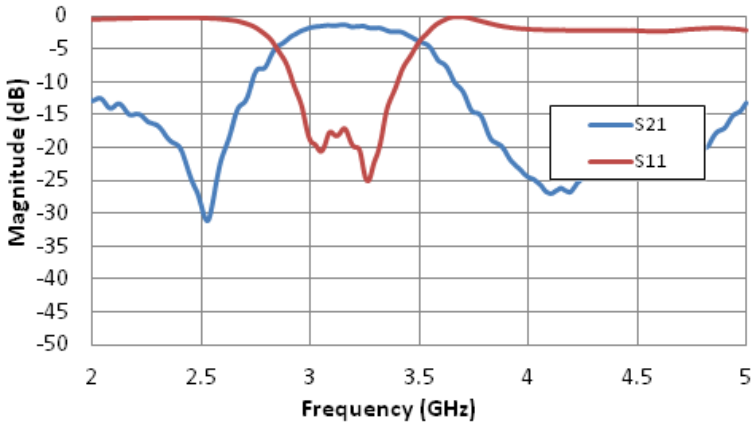

Figure 5.12. Frequency response of a dual-mode band-pass filter on FR4 substrate.

The design is also supported by simulations. Figure 5.13 shows a comparison between simulations and measurements. There is a good agreement between the simulations and the measurements. However, the experimental frequency response is shifted towards higher frequencies. It suggests that filter response is highly sensitive to the tolerance of the microstrip dimensions, thus detecting small changes mainly in small dimensions such as *c* or *e*. The manufacture process has little limitations and an error tolerance is assumed. A variation of 0.1 mm, which is the error tolerance, of these dimensions may involve a variation of a 5% of the bandwidth value. A first successful prototype has been demonstrated that yields valid filter features and warrants further study on this issue but further considering the ability of central frequency tunability.

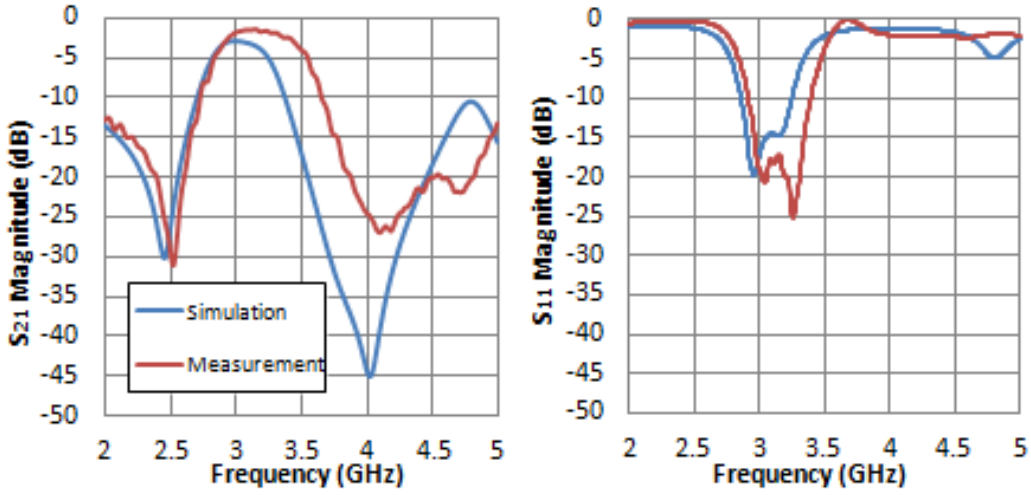

a) S_{21} parameter. **b) S_{11} parameter.**

Figure 5.13. Comparison between simulations and measurements of frequency response for a dual-mode band-pass filter on FR4 substrate.

5.3. Dual-mode band-pass filter on liquid crystal technology

Once again, novelty of this approach is the construction of a hybrid structure that combines some conventional dielectric layers with LC materials for this kind of filters. LC becomes a singular dielectric used as the microstrip line substrate of the structure. As stated above, inverted microstrip line structures (see Chapter 2) similar to this have been already reported in previous LC devices [5.14, 5.15].

5.3.a. Designing the filter by spectral response simulation

As is well-known for LC researchers, due to the anisotropic behavior of the LC molecules, permittivity of these materials can be tuned by applying an external electric field. In the absence of an electric field, LC molecules remain aligned parallel to the microstrip line and the microwave signal experiences the so-called perpendicular permittivity, $\varepsilon_{r\perp}$. When LC saturation voltage is reached, molecules are placed perpendicular to the microstrip line and permittivity in the microwave signal path is the parallel permittivity, $\varepsilon_{r\parallel}$. So, a filter with analogue tuning of the central frequency can be generated as a voltage is applied between the two permittivity extreme values, $\varepsilon_{r\perp}$ and $\varepsilon_{r\parallel}$. In order to design the frequencial tuning range, the dependences of central frequency have been identified. Central frequency of the bandpass filter (*fc*) depends on the effective permittivity (ε_{eff}), such that as permittivity increases, *fc* decreases. Besides, central frequency is determined by the structure dimensions and is especially sensitive to changes in *b* dimension [5.9]. With these premises and taking advantage of the LC tunable permittivity, the design of the constructive parameters of the filter consisted, once again, in programming a strategic batch of simulations by using the electromagnetic software tool Ansoft HFSS. It was used for predicting the response of the proposed filters.

Figure 5.14 shows an inverted microstrip line structure for a dual-mode band-pass filter on liquid crystal technology. From the bottom to the top of the sandwich, FR4 ($\varepsilon_r = 4.4$) of 1.56 mm thick is employed as the dielectric substrate for the ground plane. Next, a dielectric substrate TLX-8 ($\varepsilon_r = 2.55$) from Taconic of 0.25 mm thick is used for the spacer that delimit the LC cavity. This material is also used as the dielectric substrate which supports the microstrip line, but of 0.8 mm thick, on top of the filter. The same highly birefringent experimental nematic LC mixture employed for the notch filters has been also used for filling the band-pass filter. The estimated relative permittivity and loss tangent (tan δ) at 5 GHz for this material (see Chapter 4) are summarized in Table 5.1. [5.14].

Taking account these values, the dimensions of the filter layout (Table 5.1) have been optimized by simulation in order to achieve a central frequency close to 5 GHz and a 3 dB bandwidth (BW) about 800 MHz. The microstrip line is designed to have a 0.65 mm width (*w*) to allow the input impedance to be about 50 Ω (see details in Chapter 2).

Simulation tests have been focused on exploring the filter tuning capability. LC permittivity values considered were $\varepsilon_{r\perp} = 2.38$ and $\varepsilon_{r\parallel} = 3.08$. Figure 5.15 shows the frequency

dependence of S-parameters, S_{11} and S_{21}, for the filter considering both permittivities. Simulator allows us to emulate the ideal frequency response of the LC band-pass filter, but without considering any applied voltage.

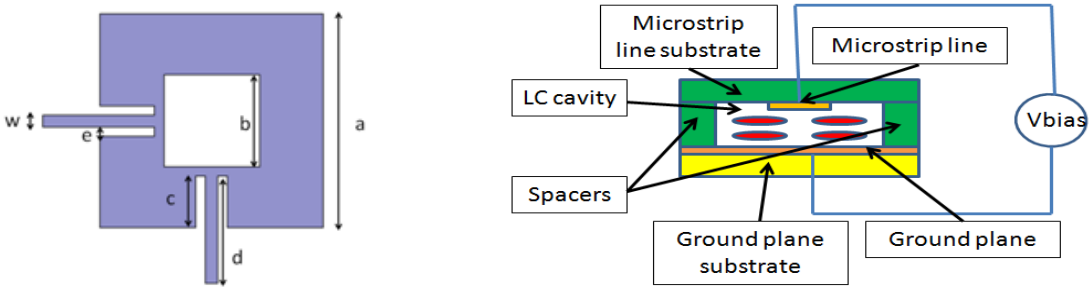

a) The shape of the conventional microstrip patch.

b) A simplified diagram of the filter.

Figure 5.14. An inverted microstrip line structure for a dual-mode band-pass filter on LC technology.

PARAMETERS OF MATERIALS		
	Dielectric constant (ε_r)	***Loss tangent (tan δ)***
Highly birefringent nematic LC (*)	$\varepsilon_{r\perp} = 2.38$	$\tan\delta_{\perp} = 0.02$
	$\varepsilon_{r\parallel} = 3.08$	$\tan\delta_{\parallel} = 0.04$
Taconic TLX-8	$\varepsilon_r = 2.55$	$\tan\delta = 0.02$
FR4	$\varepsilon_r = 4.4$	$\tan\delta = 0.02$

(*) Values estimated at 5 GHz.

MICROSTRIP DIMENSIONS	
Dimension	***Value***
a	11.6 mm
b	5 mm
c	2.8 mm
d	10 mm
e	0.5 mm
w	0.65 mm

Table 5.1. Materials and optimized microstrip dimensions for a dual-mode band-pass filter on LC technology.

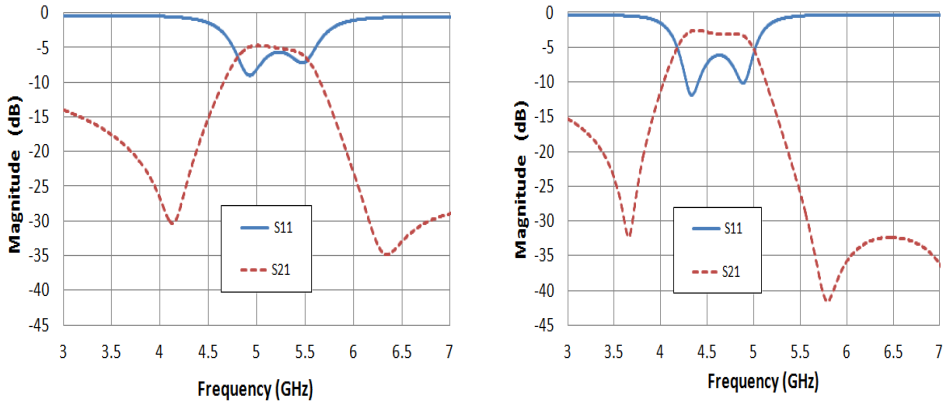

a) Considering $\varepsilon_{r\perp} = 2.38$. **b) Considering $\varepsilon_{r\parallel} = 3.08$.**

Figure 5.15. Frequency dependence of the filter response in simulation.

Table 5.2 shows a summary of the most significant values that describe the filter performance for both permittivities $\varepsilon_{r\perp}$ and $\varepsilon_{r\parallel}$. Two band-pass filters, which are centered at 5.16 GHz and 4.59 GHz, respectively, have been generated. A central frequency shift of 570 MHz is achieved in simulation, which means a relative tuning range of $\Delta f_c/f_c = 11.7\%$, a very promising feature. In special, if it is compared to the performances of other tunable filters that use commercial LC´s, which is about 6% [5.16]. Deviation of specifications of each filter is tolerable: band-pass attenuations differ minor than 3dB and the relative bandwidth parameter, defined as BW/f_c, is quite similar.

LC dielectric constant	*Central frequency (f_c)*	*Bandwidth (BW)*	*Relative bandwidth (BW/f_c)*
$\varepsilon_{r\perp} = 2.38$	5.16 GHz	840 MHz	0.163
$\varepsilon_{r\parallel} = 3.08$	4.59 GHz	800 MHz	0.174

Table 5.2. Summary of the relevant simulation results for performance of a dual-mode band-pass filter on LC technology (LC 1631E).

5.3.b. Manufactured LC dual-mode band-pass filters

Once the LC filters with the new geometry of microstrip patch has been studied in depth, some LC filters have been manufactured and characterized. All these filters are included in a set of two types: Filters based on the conventional microstrip dual-mode structure and filters with improved performance constructed by reshaping the microstrip patch resonator. Both arrangements consist on a pile of three layers that are stacked as a sandwich to build the device with a cavity and the LC housed inside. All the components that make up each of the manufactured devices are described in Fig. 5.16. The example shown is that of a LC

conventional dual-mode filter with square notch. From the bottom to the top of the filter, constituent layers are: A ground plane to the left of the figure with four through holes for assembling the final device; a dielectric substrate layer acting as a spacer for housing the LC is shown in the centre of the figure. The spacer is split into two parts because two tracts, an entrance and an exit, have been prepared to enable the insertion of the LC by capillarity. The third layer is the microwave substrate on which the microstrip line is formed. SMA connectors will be soldered to feed lines of the filter. They connect the filter to the exterior circuit.

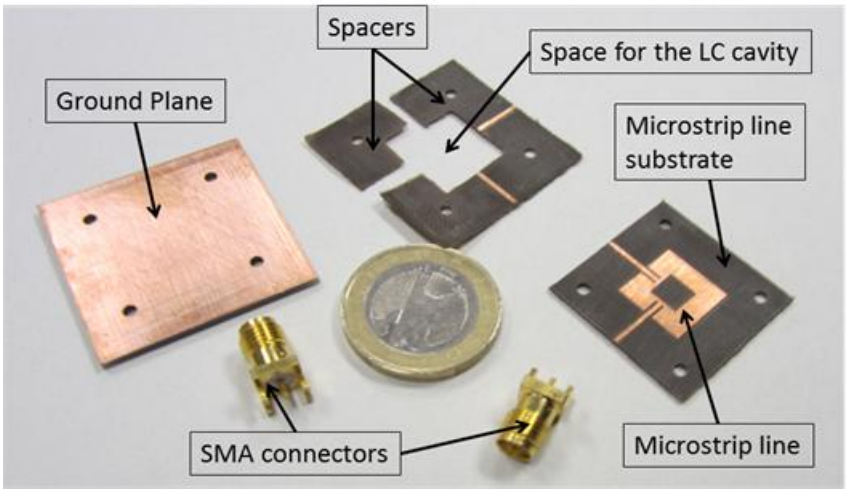

Figure 5.16. Detail of the components for assembling a conventional dual-mode band-pass LC filter with square notch.

Table 5.3 summarizes the characteristics: the materials of the dielectrics, the liquid crystals, the permittivities and the thicknesses for the set of two LC band-pass filter types: some filters based on the conventional microstrip dual-mode structure and other filters with improved performance.

	LAYERS			***CONVENTIONAL FILTER***	***IMPROVED FILTER***
	Microstrip line substrate	***Spacer***	***Ground plane substrate***	***Liquid crystal***	
Material	Taconic TLX-08		FR4	1631E	MDA-98-1602
Permittivities	$\varepsilon_r = 2.55$		$\varepsilon_r = 4.4$	$\varepsilon_{r\parallel} = 3.08$	$\varepsilon_{r\parallel} = 3$
				$\varepsilon_{r\perp} = 2.38$	$\varepsilon_{r\perp} = 2.6$
Thickness (mm)	0.8	0.25	1.56	0.25	0.25

Table 5.3. Summary of materials and layout dimensions for the two LC band-pass filter types.

Figure 5.17 shows two examples of the manufactured devices. Figure 5.17 a) is a conventional LC dual-mode band-pass filter with square notch; Figure 5.17 b) is an improved

LC dual-mode band-pass filter with square notch including a square cut in the opposite corner to the feed lines. Following sections are devoted to measure performance of LC filters.

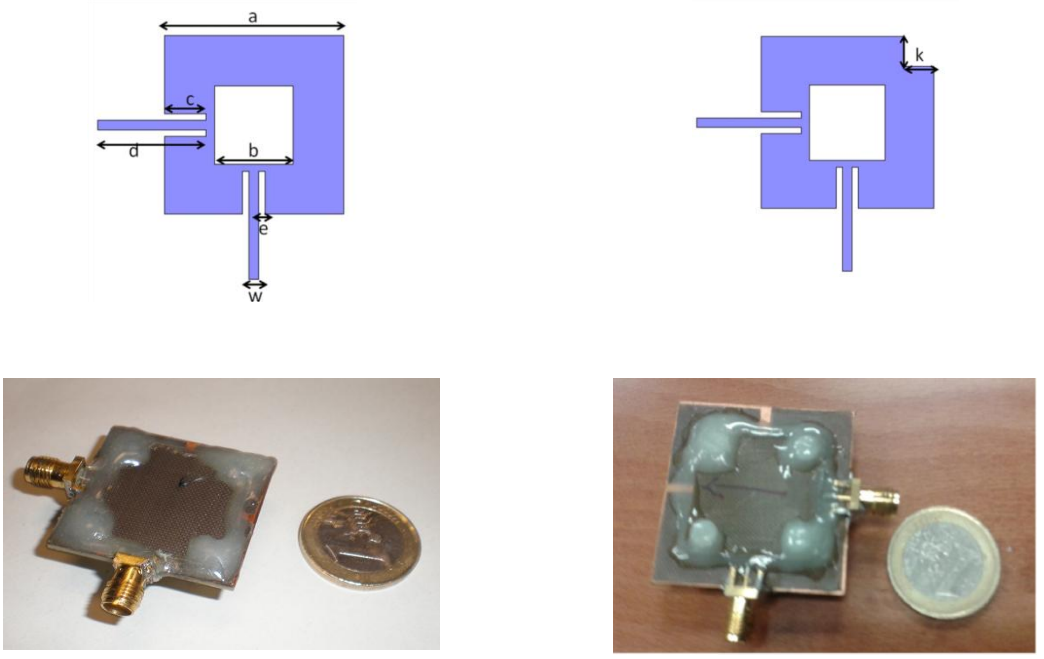

a) Conventional LC dual-mode band-pass filter with square notch.

b) Improved LC dual-mode band-pass filter with square notch including a square cut in the opposite corner to the feed lines.

Figure 5.17. Manufactured dual-mode band-pass LC filters.

5.4. Performance of liquid crystal dual-mode band-pass filters

In this section the measurements of the characterization of a tunable band-pass filter are detailed. This is a band-pass filter with a conventional dual-mode microstrip and a square notch. First, the experimental set-up is presented. Next, significant parameters, such us insertion and return loss, tunable group delay, band-pass ripple, roll off factor and filter power linearity, are described by subsections. These are identified as being a way to assess the filter quality. More representative results are included in the document.

Characterization of frequency response has been carried out with the experimental set-up depicted in Figure 5.18. S-parameters are the main result from which some other parameters are derived. As stated previously, experimental set-up has a traditional schema for microwave frequency measurements. Frequency response of the filter is measured by a two-port network analyzer 8703B from Agilent. Again, in order to superimpose the microwave signal and the external voltage for switching the LC, a bias-T is used. A sinusoidal AC signal of 1 kHz drives the LC device. Bias-T is connected between port 1 of the analyzer and the filter input, while the filter output is coupled to the port 2 of the analyzer.

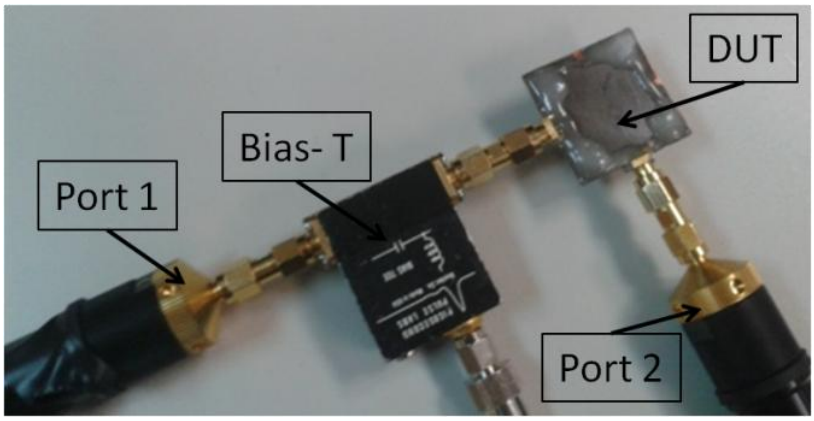

Figure 5.18. Picture of a detail from the experimental set-up to characterize a conventional dual-mode LC band-pass filter.

5.4.a. Frequency response

In order to obtain a complete characterization of the filter, firstly the device has been measured in a broad spectrum of frequencies from 1 GHz to 20 GHz. Next, a study in depth focusing on the evaluation of the environment of the objective central frequency, close to 5 GHz, has carried out.

The broad spectrum response advertises the existence of some significant events. The frequency response of the filter when no voltage is applied is shown in Fig. 5.19. Most noticeable effects under this voltage condition are located about 8 GHz and 12 GHz. Around 8 GHz, the first spurious band appears, far away enough from the filter band-pass and therefore does not affect the filtering feature. The other effect of S-parameters profile observed on the frequency response was two attenuation peaks that appeared simultaneously in S_{21} and S_{11} near 12 GHz. An explanation of this outcome may be radiation losses. This hypothesis is also supported by the fact that peak of S_{21} remains at the same frequency even if voltage applied to the LC changes, see Figure 5.20.

Frequency profile of S_{21} parameter has been chosen to illustrate LC switching dependence of the location of spurious peaks. Different values of external voltage applied to the LC cause distinctive shifts of those frequencies.

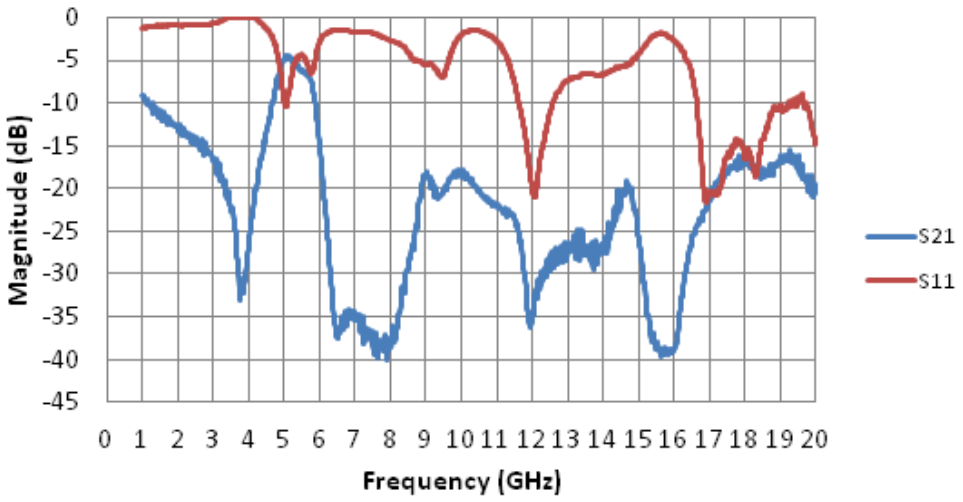

Figure 5.19. Frecuency evolution of parameters S_{21} and S_{11} in the range 1 GHz - 20 GHz. No voltage is applied to LC filter.

For a more detailed study of the LC filter, the signal amplitude of the LC driving voltage has been swept from 0 V_{rms} to 13 V_{rms} with a minimum increment of 0.1 V_{rms}. Within this interval, the frequency response of all the filters generated (one for each voltage), has shown a band-pass-like characteristic. Specifically, the pass-band insertion loss (S_{21} parameter) for each filter, has been extracted from the broad spectrum response for the interval from 3 GHz to 7 GHz. It is graphed in Fig. 5.21 a) and there it is illustrated the tunability of the central frequency.

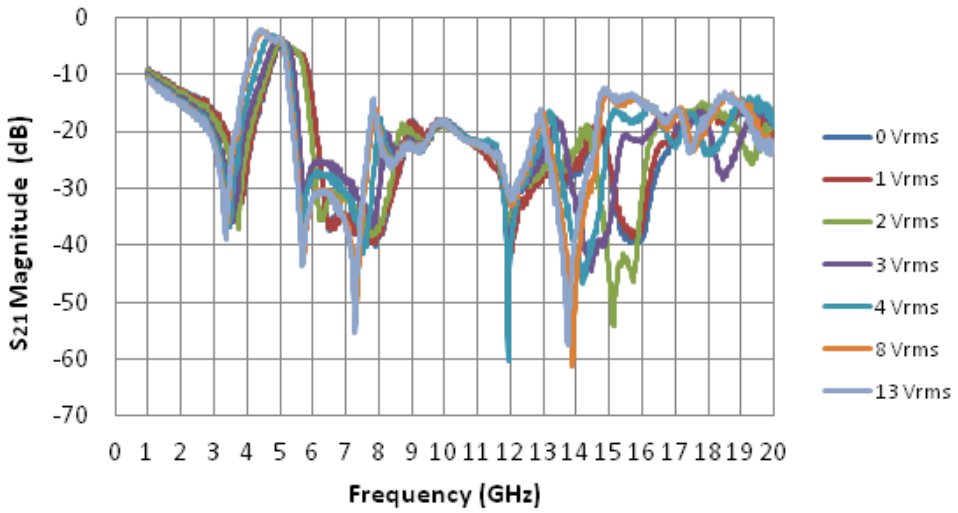

Figure 5.20. Evolution of filter S_{21} parameter with the frequency for several values of external applied voltage.

In particular, in the absence of LC voltage, a 5.19 GHz central frequency and 860 MHz bandwidth are measured. As LC voltage increases, LC permittivity also increases and central frequency decreases. By applying 13 V_{rms}, LC permittivity reaches the highest value and central frequency the minimum one, 4.54 GHz (and a 790 MHz filter bandwidth). A central frequency shift of 650 MHz is measured, which means a relative tuning range of $\Delta f_c/f_c$ = 13.4%. This value is slightly higher than that obtained in simulation, what reveals the manifestation of some tolerances of manufacturing. In Table 5.4 is compiled the experimental results of the frequency response of the LC filter. It is shown that the characterization results of Table 5.4 and the previous simulation results of Table 5.2, are fairly in agreement in regard to main parameters. However, again, magnitude of S_{21}, similar to the simulation results, changes slightly from a filter to another (Fig. 5.21 a)) due to the fact that the dielectric loss tangent (tan δ) also varies by applying an external voltage between the two extreme values, $tan\ \delta_{\perp}$ and $tan\ \delta_{\parallel}$. Collecting all the data, voltage dependence of the central frequency has been depicted in Fig. 5.21 b). Range of voltage for the central frequency, 10%–90%, is about 3 V_{rms}, just a few volts.

Finally, Fig. 5.22 shows a comparison between S_{11} and S_{21} parameters obtained in simulation and the same from characterization measurements. Profiles near the band-pass of the filter are reasonably in agreement.

LC drive voltage	***LC dielectric constant***	***Central frequency (f_c)***	***Bandwidth (BW)***	***Relative bandwidth (BW/f_c)***
0 V_{rms}	$\varepsilon_{r\perp}$	5.19 GHz	860 MHz	0.165
13 V_{rms}	$\varepsilon_{r\parallel}$	4.54 GHz	790 MHz	0.173

Table 5.4. Summary of the relevant experimental results for performance of a dual-mode band-pass filter on LC technology (LC 1631E).

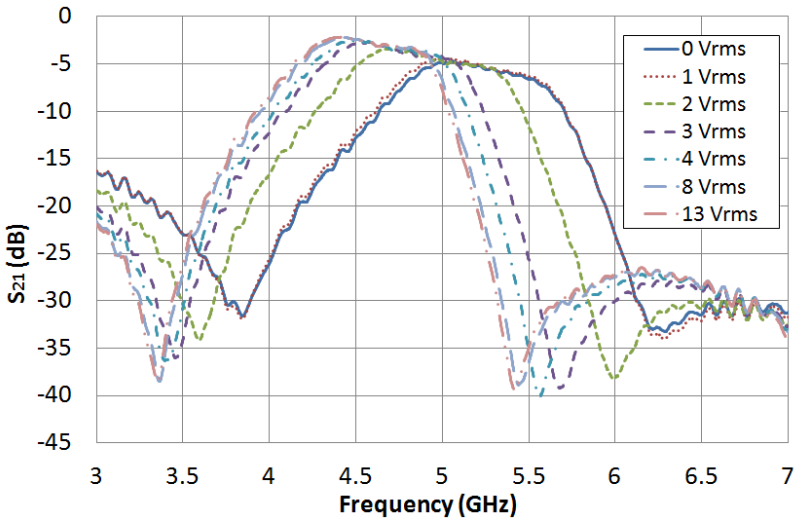

a) Frequency dependence of the S21 parameter.

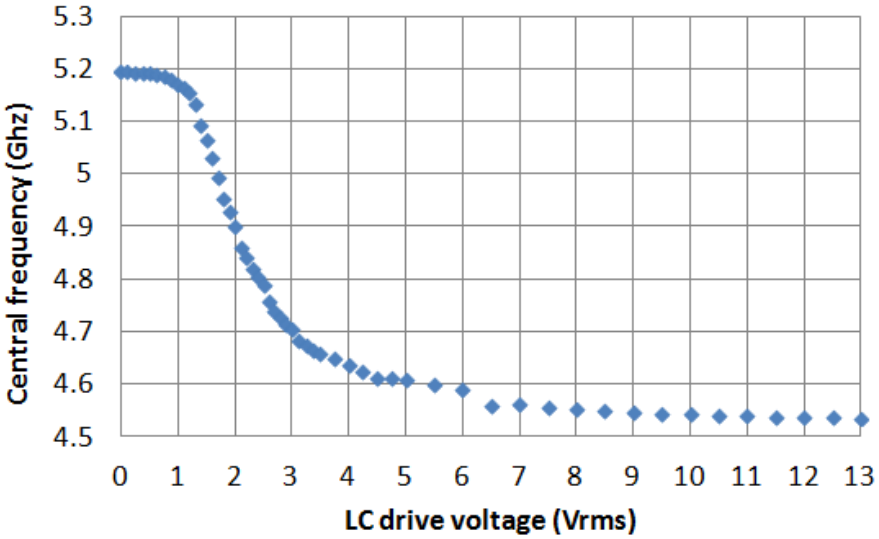

b) LC driving voltage dependence of the central frequency.

Figure 5.21. Tunability of central frequency in a LC dual-mode band-pass filter (LC 1631E).

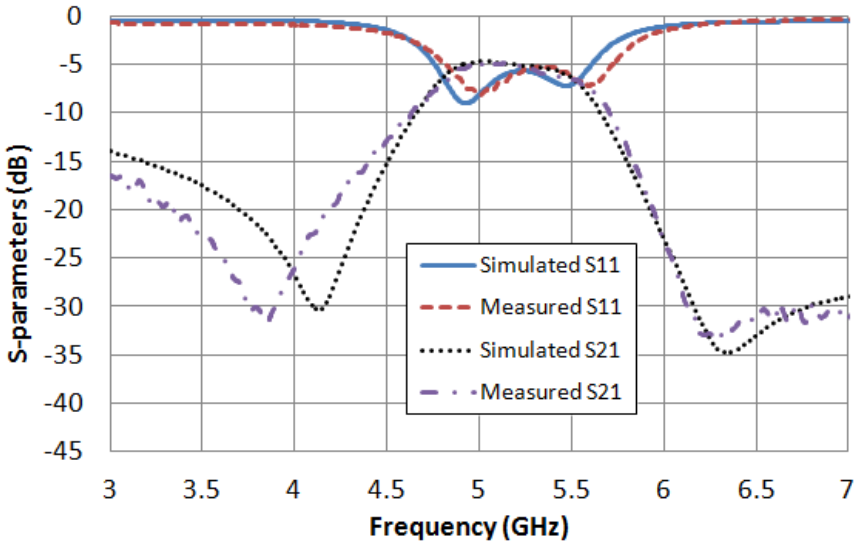

a) For $\varepsilon_{r\perp}$.

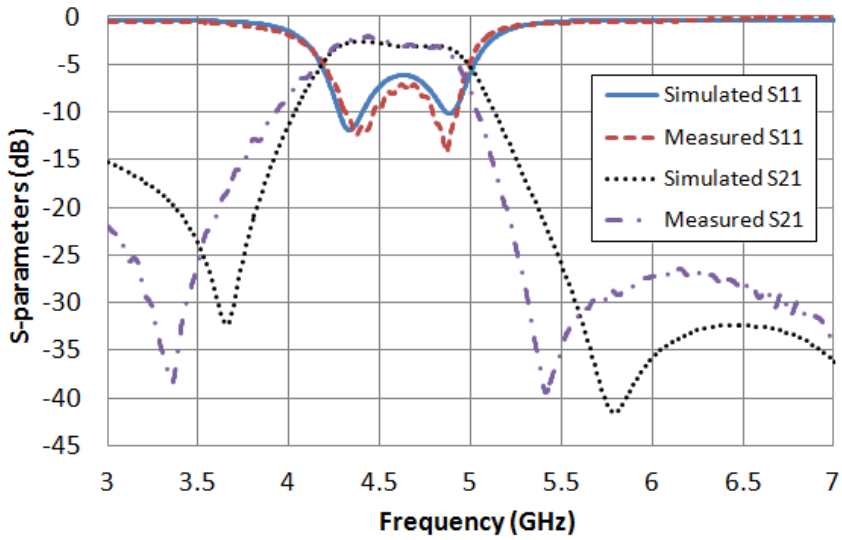

b) For $\varepsilon_{r||}$.

Figure 5.22. Comparison between simulated and measured S_{21} and S_{11} parameters in a LC dual-mode band-pass filter.

5.4.b. Tunable group delay

The group delay of a device is defined as the transmission time delay of the amplitude envelopes of the sinusoidal components of the signal through the device. The group delay of the S_{21} parameter (τ_g) is calculated as:

$$\tau_g = -\frac{\partial \phi_{21}}{\partial \omega} \tag{5.1}$$

where $\phi_{21}(\omega)$ is the phase of the S_{21} parameter and ω the angular frequency. In band-pass filters, the goal is to manage a group delay at the pass-band as constant as possible. A low value of the group delay variation avoids distortion and degradation of the microwave signals [5.17]

Figure 5.23 shows the evolution of the filter group delay with the frequency when no voltage is applied.

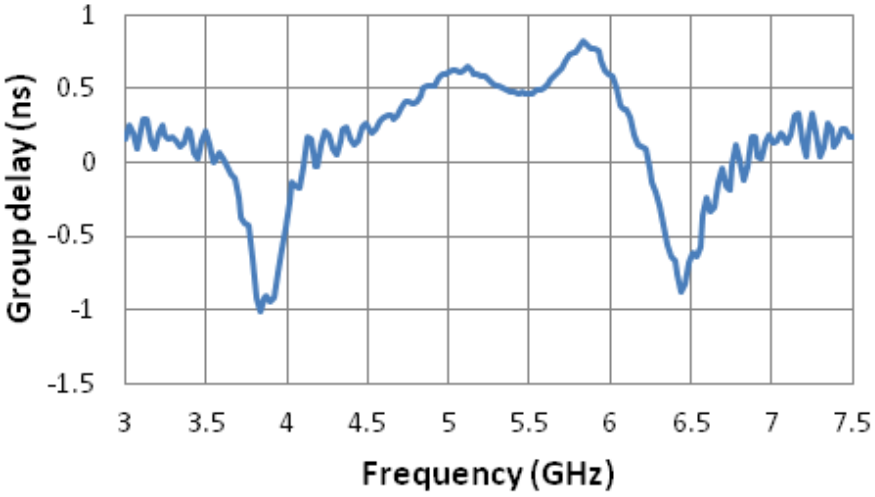

Figure 5.23. Evolution of the filter group delay with frequency when no voltage is applied.

Fig. 5.24 shows the evolution of the filter group delay for several values of applied external voltage.

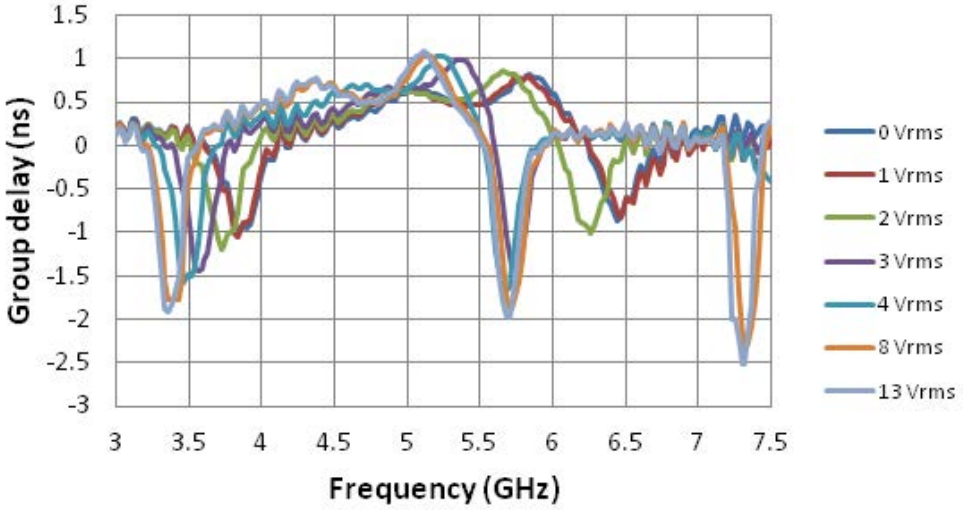

Figure 5.24. Evolution of the filter group delay for different values of applied external voltage.

A group delay variation (GDV) about 0.5 ns is obtained at the passband. Since 1 ns is considered a reasonably good value for the GDV [5.18], it can be inferred that the achieved value for the GDV in this filter is quite good.

On the other hand, as expected, since negative group delays are related to zero transmissions, as it was mentioned in Chapter 4, it is observed that the minimum values of the filter group delay (it means where the group delay is negative) appear at the same frequency as the zero transmissions of the frequency response.

5.4.c. Band-pass ripple and roll off factor

The band-pass ripple is defined as the variation of the S_{21} parameter within the passband. It means the difference between the higher and the lower value of S_{21} within the passband. The evolution of the S_{21} parameter within the passband for several values of external applied voltage is shown in Fig. 5.25. It is observed that the band-pass ripple is about 2 dB. In microwave filters, a band-pass ripple of less than 0.5 dB is considered a good value, so the achieved value is too much high. The poor value obtained for the filter return loss may be a reason that explains the high band-pass rippled of the measured filter [5.19].

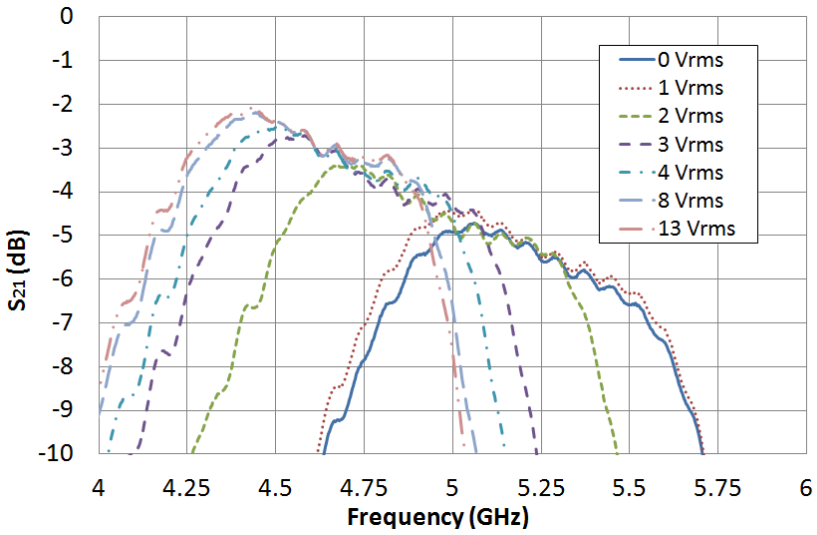

Figure 5.25. Evolution of the S_{21} parameter within the passband for several values of external applied voltage.

Directly related to features within the passband, roll off factor is a fundamental characteristic. Applied to insertion loss of a filter, it measures the steepness of the transition between the passband and the stopband. In simple first order filter, roll off factor is equal to 6 dB per octave. That value would translate to about 0.8 dB as frequency increases 1.1 times assuming that frequencies were much higher than the cutoff frequency. This transformation is

mandatory within the narrow range of measurement with frequency for the LC band-pass filter response of Figure 5.21 a). By measuring roll off factor for the curve of 3 V_{rms} from 5 GHz to 5.5 GHz, it is equal to 35 dB, that is, more than 40 times greater than that of a first-order filter. It is a sharp roll off factor, so it could serve in applications to prevent the crosstalk between adjacent channels.

5.4.d. Filter power linearity

A linear behavior of a device ensures that every device output is a representation of every device input. This is a key aspect in electronics, since a non-linear behavior may cause distortions.

It is assumed that a device is linear if the ratio P_{in}/P_{out} is constant when P_{in} is changed. Usually, it is considered acceptable a device which presents a linear behavior in a determined range of input power [5.20].

In order to characterize the power linearity of a device, the input power of the microwave signal is swept in a range of values and S_{21} parameter is tested. For the LC conventional dual-mode band-pass filter, the same procedure has been applied; microwave signal has been changed from -15 dBm to 5 dBm, which is the maximum power range allowed by the network analyzer of the experimental set-up. It is observed that profile of S_{21} parameter does not change for any value of external voltage applied to the LC, which means that the ratio P_{in}/P_{out} remains constant in that power range. Therefore, it can be concluded that the filter behavior is linear for an input power range of 20 dBm.

5.5. Improved performance in liquid crystal dual-mode band-pass filters

As mentioned previously, the structure used in the band-pass filter was reshaped (Figure 5.26). The values of the patch dimensions of both filters are the same and the geometrical modification included only consisted in making a square cut of side length k etched on the patch. The theoretical study of this geometry was detailed in section 5.1.b. This new microstrip patch is expected to improve pass-band return loss and to narrow filter bandwidth. Properties of the dielectric substrates and tunable LCs used for the filters were summarized in Table 5.3.

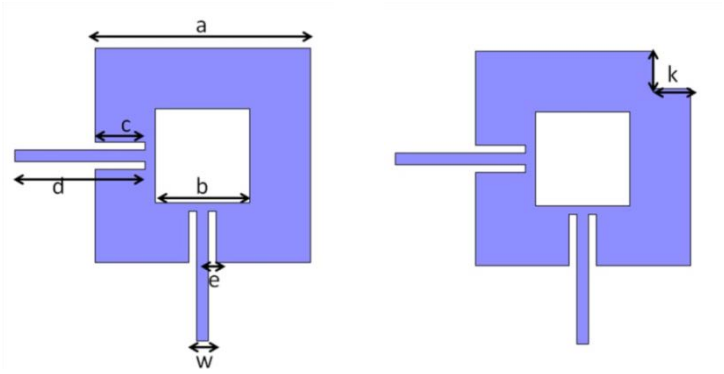

a) Conventional LC dual-mode band-pass LC filter with square notch. (Experimental nematic LC mixture 1631E).

b) Improved LC dual-mode band-pass filter with square notch. (Commercial nematic LC MDA-98-1602).

MICROSTRIP DIMENSIONS	
Dimension	***Value (mm)***
a	11.6
b	5
c	2.8
d	10
e	0.5
w	0.65
k	2

Figure 5.26. Comparison between conventional and improved geometries of microstrip dual-mode square patch resonators.

5.5.a. Validation of the structure

Before the fabrication of the device and the filling with the LC, several electromagnetic simulations by using the software Ansoft HFSS were run for optimizing the filter dimensions. Initially, the LC cavity was considered to be empty in the simulations, that is, $\varepsilon_r = 1$. Once the dimensions have been fixed, a square cut with side k is made in the conventional microstrip square patch in the opposite corner to the feed lines. The value k = 2 mm was chosen from simulations because a significant pass-band return loss improvement is achieved. Figure 5.27 shows a comparison between the frequency response obtained in simulation for the filter with new dual-mode patch and for the filter with the conventional one. Table 5.5 summarizes the performance of both structures.

	Central frequency (f_c)	***Bandwidth (BW)***	***Return loss (RL)***
With a conventional patch	7.69 GHz	1320 MHz	4.3 dB
With a new patch	7.665 GHz	1050 MHz	5.8 dB

Table 5.5. Comparison between the performances of both dual-mode empty filters.

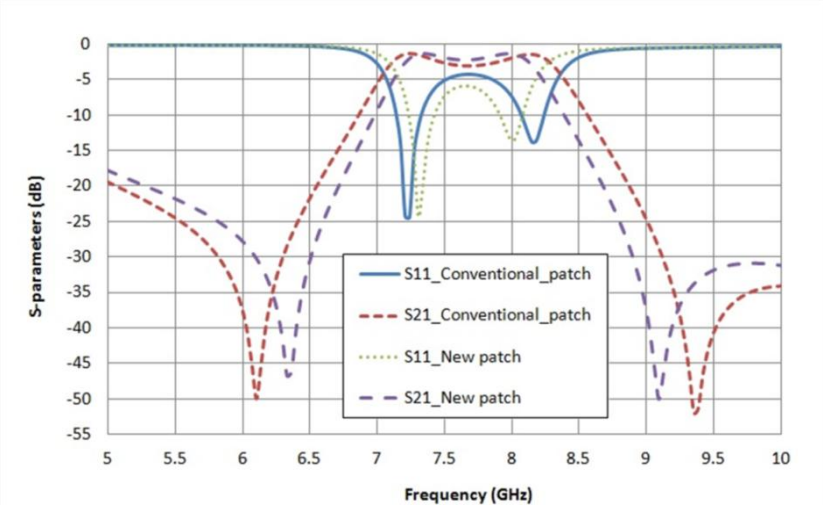

Figure 5.27. S-parameters obtained in simulation for two empty filters: one filter with a conventional dual-mode patch and the other with the new dual-mode patch with a square cut.

The results for the empty filters suggest that the patch with the new shape improves the pass-band return loss (RL) and narrows the filter bandwidth. A filter bandwidth reduction of 20.5% is achieved, which leads to obtain a pass-band return loss increase of 1.5 dB. Despite this value seems not to be so significant, relative increment, 35%, is notable.

5.5.b. Improved parameters

Once the new structure was validated in simulation, the device with the new patch structure and the dimensions given in Fig. 5.26 was manufactured, as described in section 5.3.a. The manufactured filter is shown in Fig. 5.28 Next step was to fill the band-pass filter with a LC material. The filter was filled with MDA-98-1602 nematic LC from Merck. LC permittivities of that material are unknown at microwave frequencies, so the extreme values ($\varepsilon_{r\perp}$ and $\varepsilon_{r||}$) have been estimated and some results have extracted for simulations. The details of LC permittivity estimations are given in section 5.6. The improvement of the filter parameters has been characterized in terms of frequency response and the tuning capability of the central frequency. Nevertheless, other important parameters of the filter have been studied, such as the group delay, the band-pass ripple, the roll off factor or the filter power linearity.

The same experimental set-up showed in section 5.4 was assembled for this study. Once again, a sinusoidal AC signal of 1 kHz was used as the voltage for switching the LC. In order to superimpose the LC driving voltage with the microwave signal, a bias-T device was connected between the port 1 of the analyzer and the filter input.

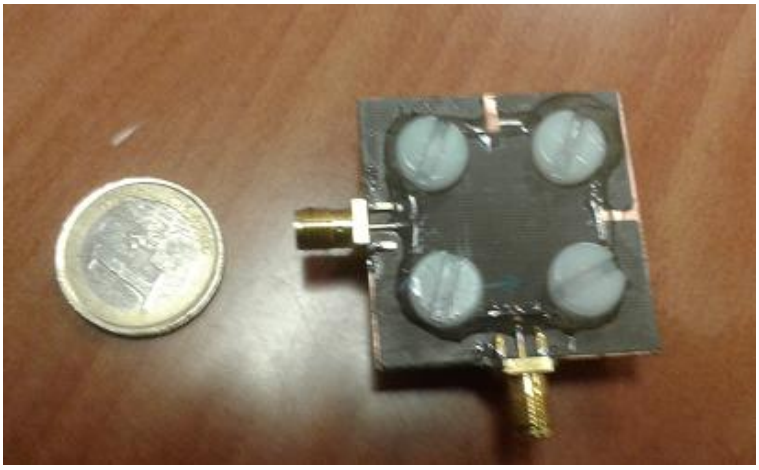

Figure 5.28. Manufactured filter with conventional patch structure filled with MDA-98-1602

i) Frequency response

The filter was measured for several values of external LC driving voltage between 0 V_{rms} and 15 V_{rms}. Figures 5.29 and 5.30 graph the frequency dependence of S_{21} and S_{11} parameters, respectively, for different values of applied voltage. In absence of applied voltage, the filter central frequency reaches its maximum value, 5.098 GHz. As it was expected, this value is clearly below the obtained in simulation when the LC cavity was considered to be empty (7.665 GHz), because LC permittivity is supposed to be greater than 1. As an increasing voltage is applied, the LC permittivity increases, so the filter central frequency decreases. When the LC driving voltage reaches the saturation value (15 V_{rms}), the filter central frequency is minimum, 4.775 GHz, because of the fact that the LC permittivity is maximum, ε_l. The tunability of the filter central frequency as a function of the LC driving voltage is shown in Fig 5.31.

A filter central frequency tuning range of 323 MHz is achieved, which means a tuning relative range of 6.5%. The obtained value is slightly higher than the achieved in other filter designs using commercial nematic LC, for example K15 from Merck, where a relative tuning range of 4.8% around 5 GHz was obtained [5.21]. However, higher tuning ranges, about 10%, can be achieved by using experimental LC of high dielectric anisotropy [5.22].

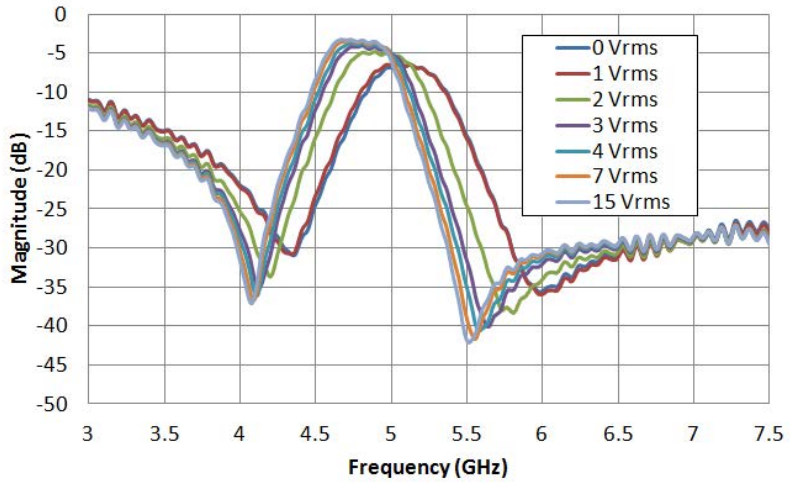

Figure 5.29. LC driving voltage dependence of the S_{21} parameter for an improved LC dual-mode band-pass filter with square notch.

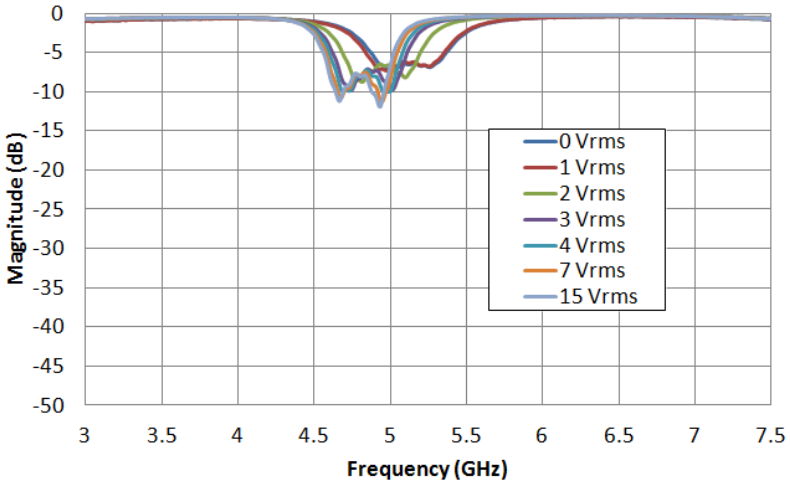

Figure 5.30. LC driving voltage dependence of the S_{11} parameter for an improved LC dual-mode band-pass filter with square notch.

The filter bandwidth gets narrower as an increasing voltage is applied, while the relative bandwidth, defined as the ratio between the bandwidth and the central frequency, remains constant. The pass-band return loss of the filter slightly gets worse as an increasing voltage is applied. Table 5.6 shows a summary of the measurements.

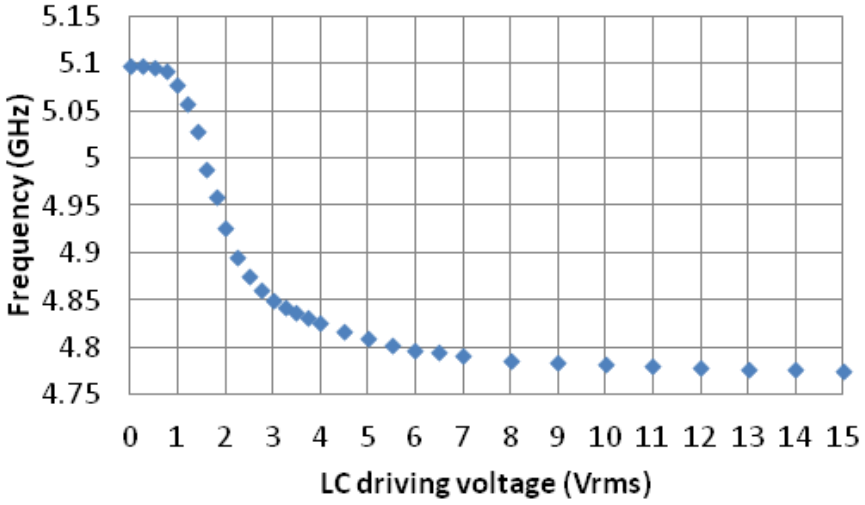

Figure 5.31. Tunability of the filter central frequency as a function of the LC driving voltage for an improved LC dual-mode band-pass filter with square notch.

LC drive voltage	*LC dielectric constant*	*Central frequency (f_c)*	*Bandwidth (BW)*	*Relative bandwidth (BW/f_c)*
0 V_{rms}	$\varepsilon_{r\perp}$	5.098 GHz	484 MHz	0.095
15 V_{rms}	$\varepsilon_{r\parallel}$	4.775 GHz	461 MHz	0.096

Table 5.6. Summary of the relevant experimental results for performance of the improved dual-mode band-pass filter.

For obtaining a complete characterization of the filter, the device has been also measured in a broad spectrum of frequencies from 1 GHz to 20 GHz. By measuring the filter in this spectrum, the existence of nearby spurious frequencies, which could affect the filter frequency response in the pass-band, can be noticed.

Fig. 5.32 and Fig 5.33 show the frequency response between 1 GHz and 20 GHz considering 0 V_{rms} and 15 V_{rms}, respectively. The first spurious band appears around 9 GHz, far enough from the filter pass-band, so it can be concluded that this spurious frequency does not affect the filter performance.

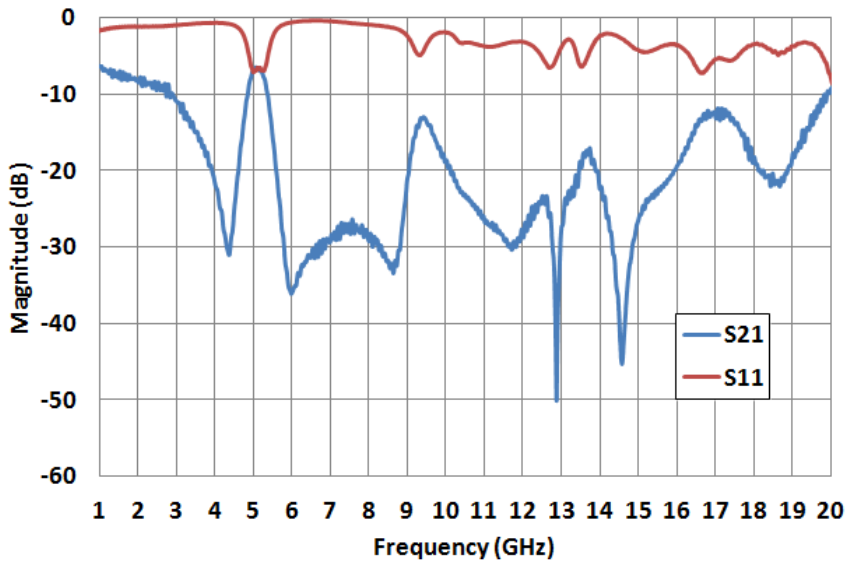

Figure 5.32. Frequency evolution of parameters S_{21} and S_{11} in the range 1 GHz - 20 GHz. No voltage is applied to LC filter.

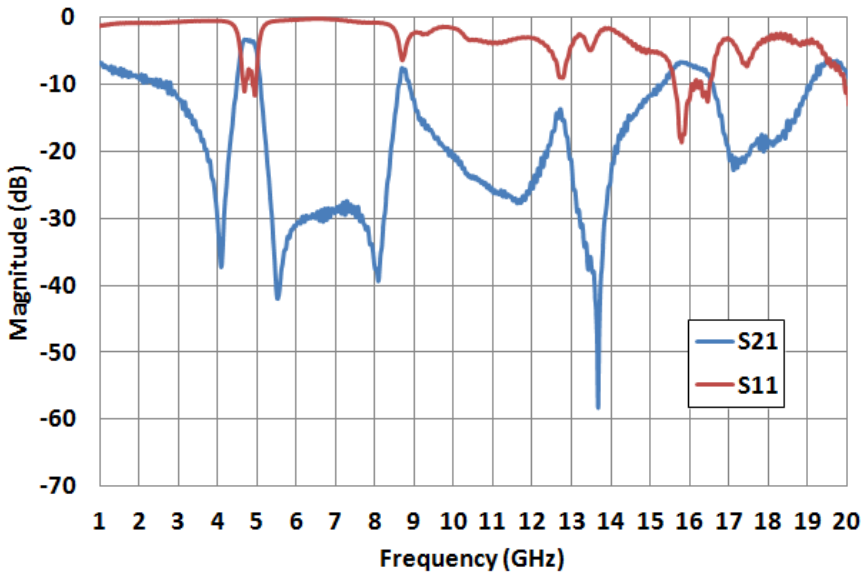

Figure 5.33. Frequency evolution of parameters S_{21} and S_{11} in the range 1 GHz - 20 GHz. The saturation voltage value (15 V_{rms}) is applied to LC filter.

ii) Group delay

Fig. 5.34 shows the evolution of the filter group delay variation (GDV) with the frequency for different values of external applied voltage.

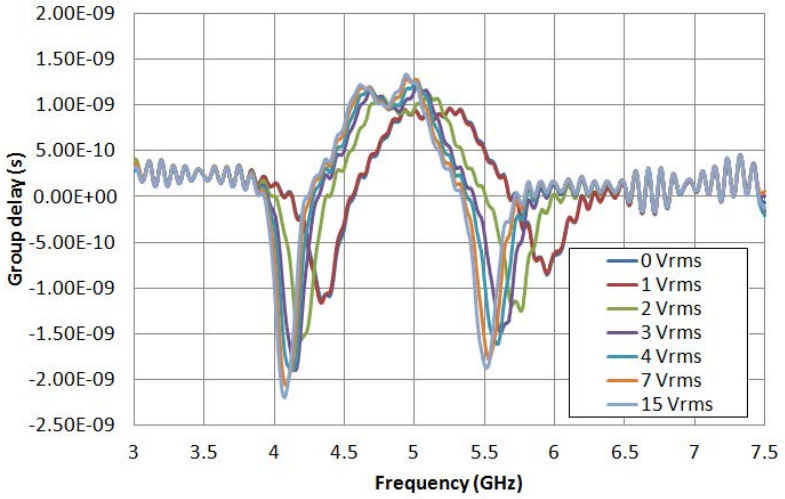

Figure 5.34. Evolution of the filter group delay for different values of applied external voltage.

As observed, the filter group delay variation in the filter pass-band does not exceed 0.5 ns for any value of applied voltage, so the filter GDV is considered to be quite good. On the other hand, as happened in previous designs, the negative group delay appears in the frequencies where transmission zeros are located.

iii) Band pass ripple and roll-off factor

The evolution of the S_{21} parameter within the pass-band for several values of external applied voltage is shown in Fig. 5.35. The band pass ripple observed is lower than 1.5 dB. Although this value is not considered to be optimum (0.5 dB is considered for microwave filters), improves the obtained in the previous design related in section 5.4. This improved can be involved by the increase of the filter return loss.

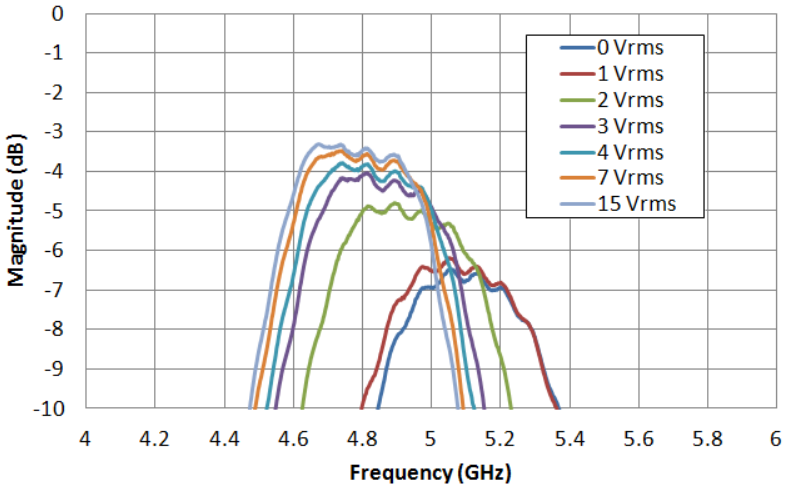

Figure 5.35. Evolution of the S_{21} parameter within the passband for several values of external applied voltage.

On the other hand, a roll-off factor of about 35 dB is measured for the curve of 3 V_{rms}, which means 40 times greater than a first order filter. Due to this high value, it can be considered that the filter presents a quite good selectivity.

iv) Filter power linnearity

The input power of the microwave signal was swept in a range of values from -15 dBm to 5 dBm, the maximum power range permitted by the analyzer. Since no changes are observed in the filter S_{21} parameter for any value of applied voltage, it is concluded that the filter has a linear behavior for the input power range from -15 dBm to 5 dBm.

5.5.c. Comparison with the conventional patch structure

In order to compare the performance of the filter with the new patch performance, a filter with conventional structure and filled with the LC MDA-98-1602 from Merck is also manufactured and measured. The filter patch dimensions are the detailed in Fig. 5.26 (a). The filter is manufactured as it was described in section 5.3.a and is filled with the mentioned LC. The manufactured device is shown in Fig. 5.36. For making the comparison, the frequency response of this new device is characterized and compared with the filter frequency response of the filter with the new patch performance.

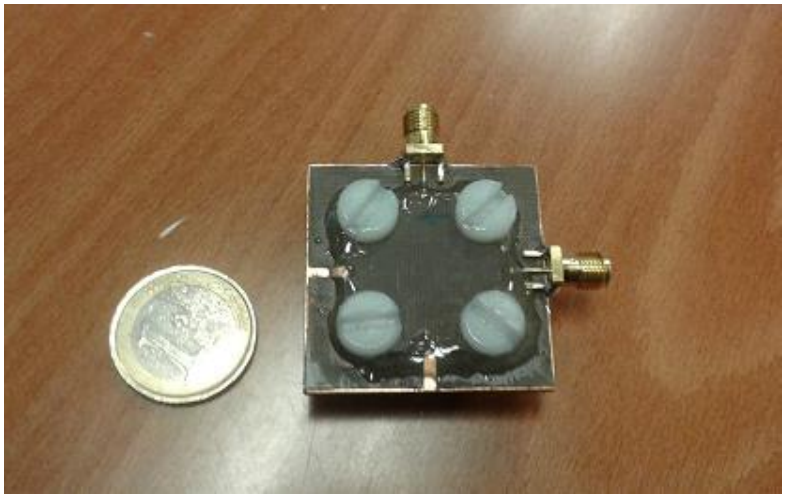

Figure 5.36. Manufactured filter with conventional patch structure filled with MDA-98-1602

The new dual-mode filter with conventional structure was measured for several different values of external LC driving voltage from 0 V_{rms} to 15 V_{rms}. Fig. 5.37 and Fig. 5.38 show the obtained frequency response (S_{21} and S_{11} parameters) when different values of external vltage are applied. When no voltage is applied, the filter central frequency, as expected,

reaches its maximum value, 5.114 GHz. As the LC permittivity increases, when an increasing external voltage is applied, the filter central frequency gets lower and when the LC saturation voltage value (15 V_{rms}) is reached, the filter central frequency is minimum, 4.802 GHz. The evolution of the filter central frequency as a function of the LC driving voltage is shown in Fig 5.39.

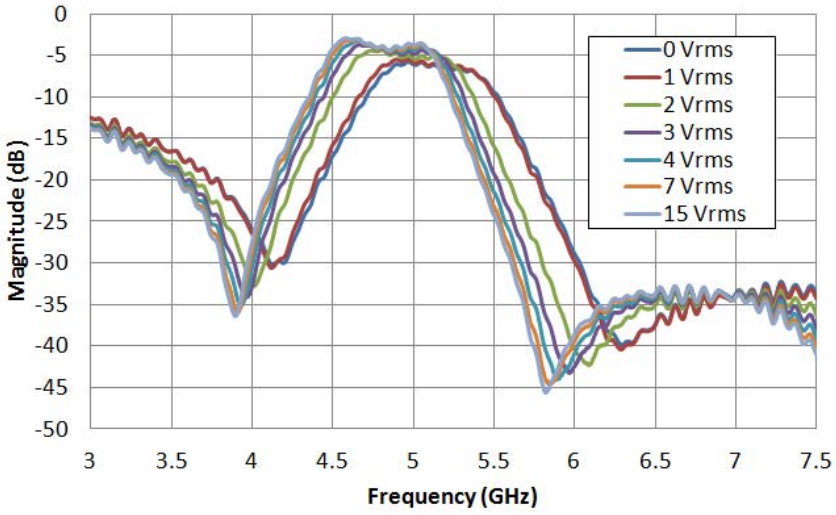

Figure 5.37. LC driving voltage dependence of the S_{21} parameter for an improved LC dual-mode band-pass filter with square notch.

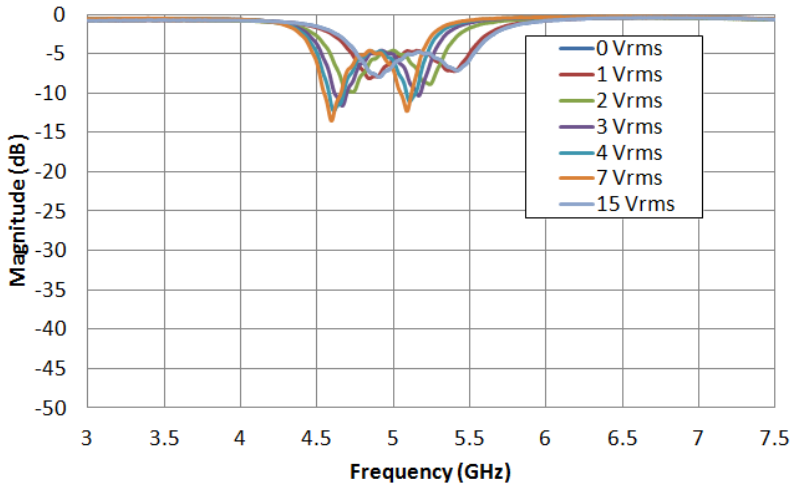

Figure 5.38. LC driving voltage dependence of the S_{11} parameter for an improved LC dual-mode band-pass filter with square notch.

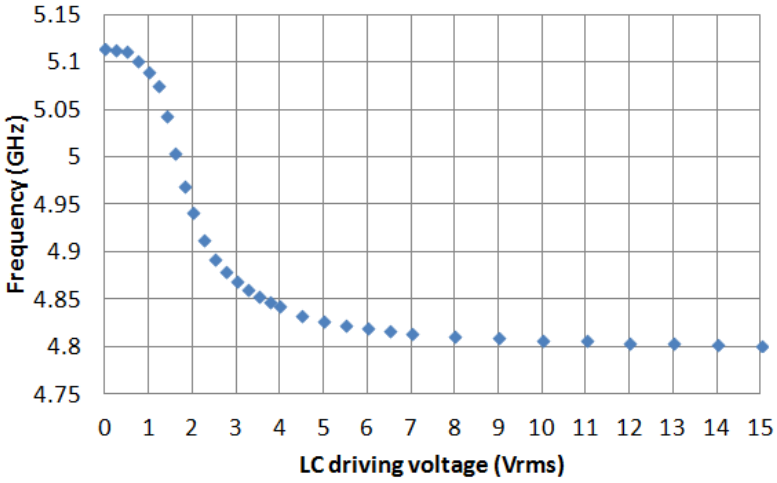

Figure 5.39. Tunability of the filter central frequency as a function of the LC driving voltage for an improved LC dual-mode band-pass filter with square notch.

In this case, a filter central frequency tuning range of 312 MHz is obtained, which means a tuning relative range of 6.3%. As happened in previous designs, as an increasing voltage is applied, the filter bandwidth gets narrower, while the relative filter bandwidth, remains constant. Table 5.7 shows a summary of the measurements.

LC drive voltage	***LC dielectric constant***	***Central frequency (f_o)***	***Bandwidth (BW)***	***Relative bandwidth (BW/f_o)***
0 V_{rms}	$\varepsilon_{r\perp}$	5.114 GHz	720 MHz	0.141
15 V_{rms}	$\varepsilon_{r\parallel}$	4.802 GHz	686 MHz	0.142

Table 5.7. Summary of the relevant experimental results for performance of the improved dual-mode band-pass filter.

With these measurements, a comparison between the microstrip conventional square patch and the new patch, can be obtained. Fig. 5.40 and Fig 5.41 show a comparison between the frequency response of both structures considering 0 V_{rms} and 15 V_{rms}, respectively. In Table 5.8, the performances of the new square patch structure and the conventional one are summarized. A filter bandwidth narrowing of 32.7% has been achieved by using the new patch structure. Besides, a pass-band return loss increase of 1.8 dB, which means an increase of 39.1%, has been obtained for the new structure when no voltage is applied, while a RL increase of 3 dB (63.8%) is managed by applying the saturation voltage value.

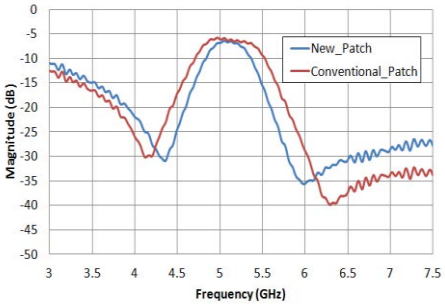

a) S_{21} parameter measured for both structures when no voltage is applied

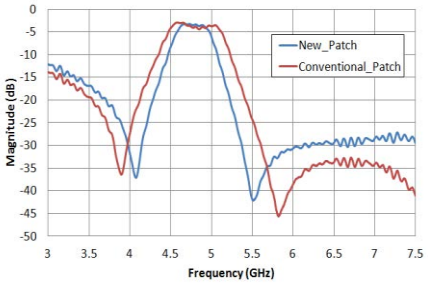

b) S_{21} parameter measured for both structures by applying 15 V_{rms}.

Figure 5.40. S_{21} parameter comparison for both structures

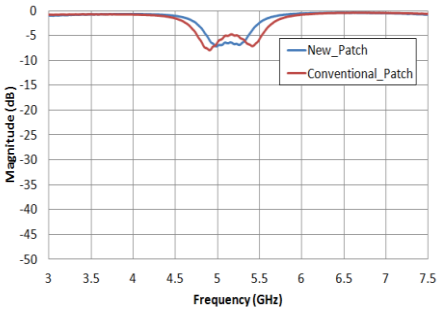

a) S_{11} parameter measured for both structures when no voltage is applied.

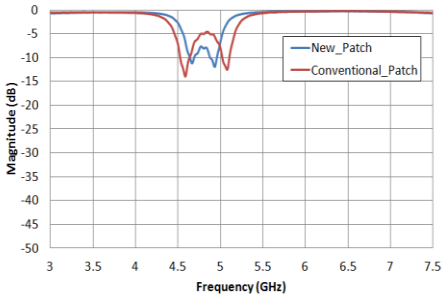

b) S_{11} parameter measured for both structures by applying 15 V_{rms}

Figure 5.41. S_{11} parameter comparison for both structures.

LC drive voltage	Filter	*Central frequency (f_c)*	*Bandwidth (BW)*	*Return loss (RL)*
0 V_{rms}	***Conventional patch***	5.114GHz	720 MHz	4.6 dB
	New patch	5.098 GHz	484 MHz	6.4 dB
15 V_{rms}	***Conventional patch***	4.775 GHz	686 MHz	4.7 dB
	New patch	4.802 GHz	461 MHz	7.7 dB

Table 5.8. Comparison between the performance of both dual-mode filters

5.6. Estimation of LC permittivity by a dual-mode band-pass filter

A complementary analysis of the spectral response performance, comparing the simulations and the measurements, has been carried out this time for both filters filled with the LC Merck MDA-98-1602, the one with the new patch and the one with the conventional patch. Due to the LC Merck MDA-98-1602 features are initially unknown at microwave frequencies, an iterative process is programmed for fitting both experimental and simulated responses. The routine considers several values for LC permittivity and loss tangent, and keeps the devices dimensions invariant. As a result, the software protocol gives rise to a preliminary estimation of the dielectric properties of the LC. So, the extreme values of permittivities, $\varepsilon_{r\perp}$ and $\varepsilon_{r\parallel}$, and LC loss tangent, $tan\ \delta_{\perp}$ and $tan\ \delta_{\parallel}$, are inferred. As it is shown in Fig. 5.42 (a) and Fig. 5.43 (a), a fairly good agreement between the measured filters frequency response (when no voltage is applied) and the simulated responses (with $\varepsilon_r = 2.6$ and $tan\ \delta = 0.05$) is achieved. In the same way, the measured frequency responses by applying the saturation voltage value (15 V_{rms}) and the simulation responses, considering $\varepsilon_r = 3$ and $tan\ \delta = 0.02$, are also in reasonable agreement (Fig. 5.42 (b) and Fig. 43 (b)).

Therefore, in a preliminary estimation, it can be inferred that the dielectric properties for the used LC at 5 GHz are the shown in Table 5.8.

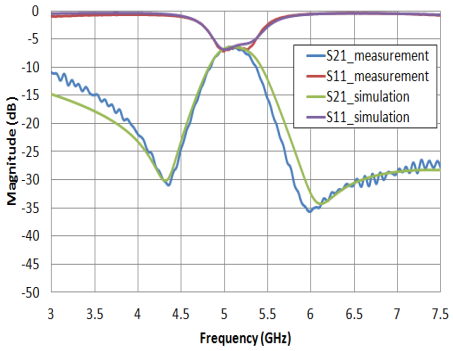

a) When no voltage is applied and ε_r = 2.6 , tan δ = 0.05 in simulation

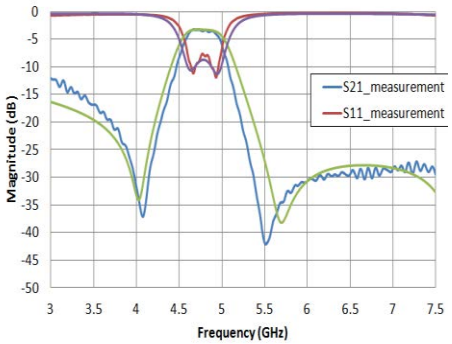

b) When 15 Vrms are applied and ε_r = 3, tan δ = 0.02, in simulation.

Figure 5.42. Comparison between simulated and measured S_{21} and S_{11} parameters in a filter with a new dual-mode patch with a square cut.

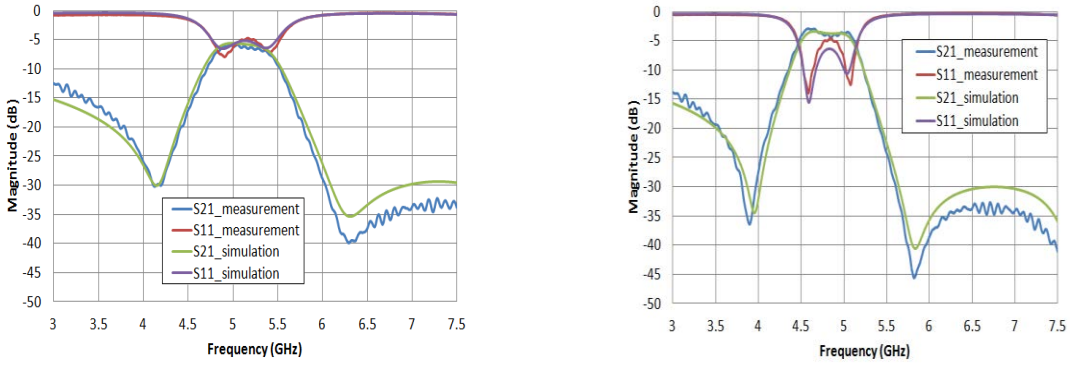

a) When no voltage is applied and ε_r = 2.62 , tan δ = 0.05 in simulation.

b) When 15 Vrms are applied and ε_r = 3.06, tan δ = 0.02, in simulation.

Figure 5.43. Comparison between simulated and measured S_{21} and S_{11} parameters in a filter with a new dual-mode patch with a square cut.

LC dielectric constant (Ɛ)	LC loss tangent (*tan δ*)
$\varepsilon_{r\perp} = 2.6$	$tan\ \delta_{\perp} = 0.05$
$\varepsilon_{r\parallel} = 3$	$tan\ \delta_{\parallel} = 0.02$

Table 5.9. Preliminary estimation of the dielectric properties extreme values for the LC Merck MDA-98-1602.

Let us note that LC loss tangent estimated values are high. This may be the reason why the filter exhibits high pass-band insertion loss, as it is shown in Fig. 5.28.

In the same way, a new estimation of the LC 1631E permittivity can be done parting from the experimental results of the dual-mode filter with conventional structure. In spite of the fact that this parameter was already estimated in the previous chapter, it is convenient to make a new calculation and compare the results with the obtained in chapter 4.

The process is the same as the previously used for the LC Merck MDA-98-1602. Fig. 5.44 (a) shows a good agreement between the measured filter frequency response (in absence of voltage) and the simulated response (with ε_r = 2.36 and *tan δ* = 0.044) is obtained. On the other hand, the measured frequency response by applying the saturation voltage value (in this case, 13 V_{rms}) and the simulation response, considering ε_r = 3.15 and *tan δ* = 0.018, are also in agreement (Fig. 5.44 (b)). The new inferred results are shown in Table 5.9.

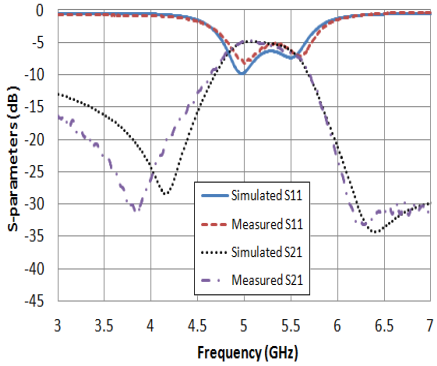

a) When no voltage is applied and Ɛr = 2.36 , tan δ = 0.044 in simulation.

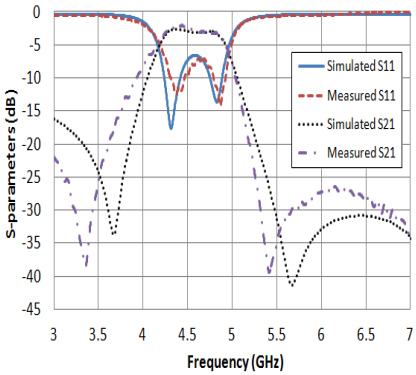

b) When 13 Vrms are applied and Ɛr = 3.15, tan δ = 0.018, in simulation.

Figure 5.44. Comparison between simulated and measured S_{21} and S_{11} parameters in a filter with a conventional patch.

LC dielectric constant (Ɛ)	LC loss tangent (*tan δ*)
$\varepsilon_{r\perp} = 2.36$	$tan\ \delta_{\perp} = 0.044$
$\varepsilon_{r\parallel} = 3.15$	$tan\ \delta_{\parallel} = 0.018$

Table 5.10. Estimation of the dielectric properties extreme values for the LC 1631E

The obtained results are very similar to the obtained in the previous chapter (see Table 5.1), so a good agreement is considered to have been achieved.

5.7. Conclusions

In this chapter, tunable band-pass filters based on LC with dual-mode structure have been studied.

The generation of a band-pass filter with tunable central frequency has been demonstrated in a band-pass filter based on liquid crystal technology. This result has been achieved by a band-pass filter with a dual-mode structure by using a conventional patch. This compact resonator, that makes a 2-degree filter possible, involves an important size reduction. Frequency response of the filter has been designed, simulated, and the filter manufactured and characterized. Because of the anisotropy of the LC molecules, the filter central frequency has been tuned from 4.54 GHz to 5.19 GHz by applying an external LC drive voltage. It means that a tuning range relative to the central frequency of 13.4% has been achieved. This high tuning range is obtained due to the use of a high dielectric anisotropy LC, the LC 1631E developed by Military University of Warsaw.

In order to improve the return loss of the first characterized prototype, a reshaping of a square patch dual-mode geometry has been proposed as the microstrip filter. This new structure is expected to achieve a significant pass-band return loss improvement by reducing the filter bandwidth. The new device is manufactured and filled with the LC MDA-98-1602 from Merck, whose dielectric parameters, which were initially unknown at 5 GHz, have been estimated to be $\varepsilon_{r\perp} = 2.6$ and $\varepsilon_{r\parallel} = 3$ for the LC permittivity and $\tan \delta_{\perp} = 0.05$ and $\tan \delta_{\parallel} = 0.02$ for the loss tangent.

A filter central frequency variation from 4.775 GHz to 5.098 GHz is experimentally obtained for the new patch structure, which means a relative tuning range of 6.5%. A filter with a conventional patch has been also manufactured and filled with the LC MDA-98-1602 from Merck. The comparison between the measurements of both devices has suggested that a significant bandwidth reduction, which leads to an important return loss increase, is achieved by using the new patch structure.

Finally, the work carried out in this chapter has involved two JCR Journal publications [5.23], [5.24] and two conference communications [5.25], [5.26].

5.8. References

[5.1] I. Wolff, "Microstrip bandpass filter using degenerate modes of a microstrip ring resonator", Electronic Letters, Vol. 8, p. 302–303, Jun. 1972.

[5.2] S. Luo, L. Zhu and S. Sun, "A dual-band ring-resonator bandpass filter based on two pairs of degenerate modes", IEEE Transactions on Microwave Theory and Techniques, Vol. 58, p. 3427-3432, 2010.

[5.3] X. D. Huang and C. H. Cheng, "A novel coplanar-waveguide bandpass filter using a dual-mode square-ring resonator", IEEE Microwave and Wireless Components Letters., Vol. 16, No. 1, p. 13-15, 2006.

[5.4] R. Zhang, L. Zhu and S. Luo, "Dual-mode dual-band bandpass filters withadjustable frequency ratiousing an annular ring resonator", IEEE Microwave and Wireless Components Letters., Vol. 23, No. 1, p. 13-15, 2013.

[5.5] R. Mao and X. Tang, "Novel dual-mode bandpass filters using hexagonal loop resonators", IEEE Transactions on Microwave Theory and Techniques, Vol. 54, p. 3526-3533, 2006.

[5.6] L. Athukorala and D. Budimir "Compact Dual-Mode Open Loop Microstrip Resonators and Filters", IEEE Microwave and Wireless Components Letters., Vol. 19, No 11, p. 698-700, 2009.

[5.7] J. S. Hong, H. Shaman and Y. H. Chun, “Dual-Mode Microstrip Open-Loop Resonators and Filters”, IEEE Transactions on Microwave Theory and Techniques, Vol. 55, No. 8, p. 1764-1770, 2007.

[5.8] L. Zhu, B. C. Tan and S. J. Kuek, “Miniaturized dual-mode bandpass filter using inductively loaded cross-slotted patch resonator”, IEEE Microwave and Wireless Components Letters., Vol. 15, p. 22-24, 2005.

[5.9] S. Li, H. Cai, W. Wu, Y. Li and Z. Wang, “New dual-mode microstrip bandpass filter with a square notch”, IEEE ICCT, pp. 656-658, 2010.

[5.10] R. J. Cameron, C. M. Kudsia, R. R. Mansour, “Microwave filters for communications systems. Fundamentals, Design and Applications”, Wiley Interscience, 1st ed., pp. 485 – 499, 2007.

[5.11] P. K. Singhal, S. Mathur, R. N. Baral, “Compact Narrow Band Non-Degenerate Dual-Mode Microstrip Filter with Etched Square Lattices”, J. Electromagnetic Analysis & Applications, Vol. 2, pp. 98-103, 2010.

[5.12] A. H. Reja, S. N. Ahmad, D. A. Mahmood, “Study the Effect of Adding New Components on Conventional Microstrip LPF Design”, International Conference on Computing for Sustainable Global Development, New Dehli (India), pp. 42 – 47, 2014.

[5.13] J. Torrecilla, E. Ávila, C. Marcos, V. Urruchi, J. M. Sánchez-Pena, J. Arias, M. M. Sánchez-López, “Dielectric permittivity estimation of liquid crystals at microwave frequencies based on the characterization of a spiral spurline notch filter”, XXVIII Simposiun Nacional Unión Científica Internacional de Radio (URSI), Santiago (Spain), 2013.

[5.14] V. Urruchi, C. Marcos, J. Torrecilla, J.M. Sánchez-Pena, R. Dąbrowski, "Tunable notch filter based on liquid crystal for microwave applications", Rev. Sci. Instrum, vol. 84, 026102, 2013.

[5.15] J. Torrecilla, E. Ávila, C. Marcos, V. Urruchi, J. M. Sánchez-Pena, J. Arias, M. M. Sánchez-López, "Microwave tunable notch filter based on liquid crystal using spiral spurline technology", Microwave Opt. Technol. Lett. vol. 55, no. 10, pp. 2420 – 2423 2013.

[5.16] R. Dickie, R. Cahill, H. Gamble, Y. Ismail, V. Fusco, D. Linton, N. Grant, S. Rea, “Liquid Crystal Tunable mm Wave Frequency Selective Surface”, IEEE Microwave and Wireless Components Letters, Vol. 17, No. 9, p. 3717-3719, 2007.

[5.17] A. R. Eskandari, L. Mohammadi, “Group delay variations in wideband transmission lines: analysis and improvement”, International Journal of Soft Computing and Engineering, Vol. 1, No. 4, pp. 122 – 128, 2011.

[5.18] J. Torrecilla, “Diseño y ajuste de filtros en banda Ka construidos con resonadores dieléctricos”, Proyecto Fin de Carrera, ETSIT-UPM, 2008.

[5.19] Z. Zacaria, M. Mutalib, M. Isa, M. Saat, M. Ismail, N. Zainuddin, "Design of Generalized Chebyshev Microwave bandpass filter based on suspended stripline structure", Advanced Science Letters, Vol. 20, No. 2, 2014.

[5.20] O. Tornblad, G. Ma, R. W. Dutton, "Device analysis of linearity in rf power devices by harmonic balance device simulation", IEEE MMT-S International Microwave Symposium Digest, pp. 868 – 871, San Francisco, USA, 2006.

[5.21] J. F. Bergineaud, N. Martin, P. Laurent, C. Quendo, G. Tanne, B. Della, F. Huret, P. Gelin, "Liquid crystal tunable filter based on DBR topology", Proceedings of the 36th European Microwave Conference, Manchester, United Kingdom, 2006.

[5.22] F. Goelden, A. Gaebler, O. Karabey, M. Goebel, A. Manabe, R. Jakoby, "Tunable Band-Pass Filter Based on Liquid Crystal", V German Microwave Conference, pp. 979-982, Berlin, 2010.

[5.23] J. Torrecilla, V. Urruchi, J. M. Sánchez-Pena, N. Bennis, A. García, D. Segovia, "Improving the pass-band return loss in liquid crystal dual-mode bandpass filters by microstrip patch reshaping", Materials, 7 (6), pp. 4524-4535, 2014.

[5.24] J. Torrecilla, C. Marcos, V. Urruchi, J. M. Sánchez-Pena, O. Chojnowska, "Liquid crystal dual-mode band-pass filter with improved performance", *Opto-Electron. Rev.* vol. 23, No. 2, 2015.

[5.25] J. Torrecilla, C. Marcos, V. Urruchi, J.M. Sánchez-Pena, O. Chojnowska, "Liquid crystal dual-mode band-pass filter with improved performance", XX Conference on Liquid Crystals. Chemistry, Physics and Applications, CLC 2013, Milkolajki, Poland, 2013.

[5.26] J. Torrecilla, C. Marcos, V. Urruchi, J.M. Sánchez-Pena, "Tunable dual-mode bandpass filter based on liquid crystal technology", XLIII European Microwave Conference, European Microwave Conference 2013, Nüremberg, Germany, 2013.

CHAPTER 6. CONCLUSIONS AND FUTURE RESEARCH LINES

In spite of the fact that previous chapters had a specific section for conclusions, there are some common aspects which have to be remarked. In this way, this chapter is dedicated to the main general conclusions related to the implementation of tunable LC devices. Finally, in the last section of this chapter, the most important future research lines are suggested.

6.1. General conclusions

The main goal of this work was the demonstration of the feasibility of spectral filtering using LC technology in advanced passive devices. The research has reinforced the use of this technology to tune the parameters of the filters at GHz frequencies in a similar way to other technologies that are already on the market. Specifically, the work was focused on the design of tunable filters by using microstrip technology. Two kinds of filters have been explored in depth: Notch and band-pass filters. An extensive research about the design, fabrication and characterization of the devices has been carried out in all cases.

Two different types of notch filters were fabricated and measured, using two variants of the spurline structure: the conventional structure and the spiral structure. In both devices relative tuning ranges of the rejection frequency nearby 10% were obtained due to the implementation of these filters with experimental LC´s of high dielectric anisotropy. This value is higher than the obtained in other LC-based filters which employed commercial LC´s [6.1], [6.2].

Additionally, an important effort was dedicated to the design and characterization of another kind of filters: the band-pass filters. Concretely, dual-mode technology was used for the implementation of the filters because of the advantages that this technology offers in terms of size. A first prototype of a dual-mode band-pass filter was filled with an experimental LC and a tuning range of 13.4% for the filter central frequency was reached, which is also higher than the managed with commercial LC´s..

In order to improve the performance of this dual-mode filter, a reshape of the microstrip layout was made. Two new filters were designed and characterized, using the new structure and the previous structure, respectively. A significant improvement of the filter return loss and an important reduction of the filter bandwidth were also achieved by using this new structure.

Another important aim of this work was the characterization of the LC dielectric properties, that is the LC permittivity, at microwave frequencies, since the LC properties are usually unknown at those frequencies. LC permittivity has been estimated, for both experimental (1631E, 1631F) and commercial (MDA-98-1602 from Merck) nematic LC mixtures. Additionally, a new estimation of the dielectric permittivity of the LC 1631E, carried out in collaboration with University College London (UCL), is shown in the final appendix.

6.2. Future research lines

Firstly, one of the key points in the future research is the study of the improvements in the prototypes already designed and characterized. Specifically, the study of better approaches in dual-mode band-pass filters is one of the goals in order to improve the device performance in terms of the selectivity of the filters. Cascade-connected filters can be conceived as new solutions for improve that feature.

Regarding the mixtures, the structures and configurations proposed in this work devised for working at GHz frequencies, can be considered as new tools for characterizing the electrical properties of new promising LC mixtures, specially synthesized for working at those frequencies.

An interesting subject that continues the research line of this work is the study of tunable SIW (substrate integrated waveguide) filters based on LC technology. A preliminary collaborative work with Universidad Politécnica de Valencia, who has a wide experience in the design of SIW filters at microwave frequencies [6.3 – 6.6], has started. The use of LCs as a substrate in the structure of SIW filters allows these devices to be voltage-controlled. In this case it involves technology on waveguides instead of microstrip technology, which imply to explore a new line of work.

On the other hand, there is a great interest in the study of other tunable devices different from the filters studied. Specifically, the development of LC tunable antennas is another important challenge to face. As it was mentioned in Chapter 1, there have been some reported studies about LC antennas in the bibliography. Since antennas are essential devices for transmitting or receiving the electromagnetic wave, in telecommunication systems, one of our main future aims is the development of new and innovative antenna designs based on LC technology. There is an initial agreement to collaborate with Grupo de Teoría de la Señal of Universidad Carlos III de Madrid for the design of such LC antennas.

Additionally, due to the interest in reflectarray antennas, also described in chapter 1, other interesting and open research line is the design and characterization of LC cells for this kind of antennas as part of a new collaboration with Universidad Politécnica de Madrid.

In terms of characterization of new LC mixtures, it is expected to maintain the collaboration with Military University of Warsaw in order to study new high anisotropic LCs

which are synthesized in that University. Morover, it would be interesting to keep or even increase the collaboration with the university we have worked with, that is, Universidad Miguel Hernández of Elche and University College London.

6.3. References

[6.1] R. Dickie, R. Cahill, H. Gamble, Y. Ismail, V. Fusco, D. Linton, N. Grant, S. Rea, "Liquid Crystal Tunable mm Wave Frequency Selective Surface", IEEE Microwave and Wireless Components Letters, Vol. 17, No. 9, p. 3717-3719, 2007.

[6.2] M. Yazdanpanahi, P. Deo, D. Mirshekar-Syahkal, "Tunable liquid-crystal millimeter-wave bandpass filter using periodical structure", IEEE Radio and Wireless Symposium (RWS), New Port Beach (USA), 2014.

[6.3] E. Díaz, H. Esteban, A. Belenguer, V. Boria, "Método híbrido para el diseño eficiente de filtros en guía de ondas integrada en sustrato", XXVI Simposiun Nacional Unión Científica Internacional de Radio (URSI), Leganés, Spain, 2011.

[6.4] C. Bachiller, H. Esteban, J. V. Morro, V. Boria, "Hybrid mode matching method for the efficient analysis of rods in waveguided structures", Mathematical and Computer Modelling, Vol. 57, pp. 1832 – 1839, 2013.

[6.5] A. Belenguer, H. Esteban, E. Díaz, C. Bachiller, J. Cascón, V. Boria, "Hybrid technique plus fast frequency sweep for the efficient and accurate analysis of substrate integrated waveguide devices", IEEE Transactions on Microwave Theory and Techniques, Vol. 59, no. 3, pp. 552 – 560, 2011.

[6.6] E. Miralles, H. Esteban, C. Bachiller, A. Belenguer, V. Boria, "Improvement for the Design Equations for Tapered Microstrip-to-Substrate Integrated Waveguide Transitions", International Conference on Electromagnetics in Advanced Applications, pp. 652 – 655, Torino, Italy, 2011.

APPENDIX I: KNOWLEDGE DISSEMINATION

This Thesis work has involved the following journal publications and conference communications.

I.1. JCR Journal Publications

- V. Urruchi, C. Marcos, J. Torrecilla, J.M. Sánchez-Pena, R. Dąbrowski, "**Tunable notch filter based on liquid crystal for microwave applications**", Rev. Sci. Instrum, vol. 84, 026102, (2013).

- J. Torrecilla, E. Ávila, C. Marcos, V. Urruchi, J. M. Sánchez-Pena, J. Arias, M. M. Sánchez-López, "**Microwave tunable notch filter based on liquid crystal using spiral spurline technology**", Microwave Opt. Technol. Lett. vol. 55, no. 10, pp. 2420 – 2423 (2013).

- J. Torrecilla, V. Urruchi, J. M. Sánchez-Pena, N. Bennis, A. García, D. Segovia, "**Improving the pass-band return loss in liquid crystal dual-mode bandpass filters by microstrip patch reshaping**", Materials, 7 (6), pp. 4524-4535, (2014).

- J. Torrecilla, C. Marcos, V. Urruchi, J. M. Sánchez-Pena, O. Chojnowska, "**Liquid crystal dual-mode band-pass filter with improved performance**", Opto-Electronics Review, *Opto-Electron. Rev.* vol. 23, no. 2, (2015).

I.2. Conference communications

- C. Marcos, J. Torrecilla, V. Urruchi, J. M. Sánchez-Pena, "**Dispositivo de fase sintonizable para microondas basado en cristal líquido**", XXVI Simposiun Nacional Unión Científica Internacional de Radio (URSI), Leganés, Spain, 2011.

- V. Urruchi, C. Marcos, J. Torrecilla, J.M. Sánchez-Pena, R. Dąbrowski, "**Tunable notch filter based on liquid crystal for microwave applications**", XIX Conference on Liquid Crystals. Chemistry, Physics and Applications, CLC 2011, Międzyzdroje, Poland, 2011.

- J. Torrecilla, E. Ávila, C. Marcos, V. Urruchi, J. M. Sánchez-Pena, J. Arias, M. M. Sánchez-López, "**Resonador microstrip spurline en espiral para filtros**

sintonizables con tecnología cristal líquido", XXVII Simposiun Nacional Unión Científica Internacional de Radio (URSI), Elche, Spain, 2012.

- J. Torrecilla, E. Ávila, C. Marcos, V. Urruchi, J. M. Sánchez-Pena, J. Arias, M. M. Sánchez-López, "**Dielectric permittivity estimation of liquid crystals at microwave frequencies based on the characterization of a spiral spurline notch filter**", XXVIII Simposiun Nacional Unión Científica Internacional de Radio (URSI), Santiago de Compostela, Spain, 2013.

- J. Torrecilla, C. Marcos, V. Urruchi, J.M. Sánchez-Pena, O. Chojnowska, "**Liquid crystal dual-mode band-pass filter with improved performance**", XX Conference on Liquid Crystals. Chemistry, Physics and Applications, CLC 2013, Milkolajki, Poland, 2013.

- J. Torrecilla, C. Marcos, V. Urruchi, J.M. Sánchez-Pena, "**Tunable dual-mode bandpass filter based on liquid crystal technology**", XLIII European Microwave Conference, European Microwave Conference 2013, Nüremberg, Germany, 2013.

- **J. Torrecilla**, V. Urruchi, J. M. Sánchez-Pena, "Microstrip dual-mode patch resonators for tuning the spectral response of liquid crystal band-pass filters filters", *XVI Optics of Liquid Crystals (OLC) Conference*, Sopot, Poland, 2015.

APPENDIX II. MICROWAVE FREQUENCY BANDS

Microwave frequency band (300 MHz – 300 GHz), as previously mentioned, is widely used in telecommunication systems because of its advantages in terms of bandwidth and low level of interferences, which allows the electromagnetic waves to propagate across the atmosphere with less difficulty than waves of a smaller wavelength. Therefore, this band is very suitable for broadcasting communications, so it is widely employed in satellite communications, RADAR or mobile communications.

Microwave frequency band is divided into sub-bands as it is shown in Table I.1.

Band	Frequency range (GHz)
L	0.5 – 1.5
S	2 – 4
C	4 – 8
X	8 – 12
Ku	12 – 18
K	18 – 26
Ka	26 – 40
V	40 – 75
W	75 - 111

Table II.1. Microwave frequency bands.

APPENDIX III. A NEW METHOD FOR THE ESTIMATION OF THE LIQUID CRYSTAL PERMITTIVITY AT MICROWAVE FREQUENCIES

In this appendix, a new method for the characterization of the LC´s dielectric properties at microwave frequencies is presented. This method has been developed by University College London, where the author was working during three months, in collaboration with Essex University.

Concretely, the characterized LC is the experimental mixture 1631E. The dielectric permittivity and loss tangent of this LC were already estimated in Chapters 4 and 5. Therefore, it is also important to compare the obtained results by using this new method with the results previously achieved.

Firstly, it is important to take account that the developed method estimates the LC properties between 15 GHz and 60 GHz, which means that the frequency is higher than the one in which we have worked previously. Nevertheless, it seems that there are not relevant changes in the GHz frequency region.

The method for the estimation of the LC permittivity consists of two steps: the experimental measurement of the S-parameters of a device filled with LC and the calculation of the LC permittivity by using a specific software parting from the experimental results.

The experimental measurement of the LC is carried out in Essex University. A resonant microstrip structure is designed and manufactured in order to characterize the LC. The phase of the S_{21} parameter of this structure is measured by a network analyzer twice between 15 GHz and 60 GHz: the first time without LC, and then, LC is filled and the response is measured for several values of external voltage. The microstrip structure is shown in Fig. III.1.

Parting from the measurements from Essex, UCL estimates the LC dielectric permittivity by using a specific software programmed by Matlab. In a preliminary estimation, the extreme values of the dielectric permittivity of the experimental LC 1631E between 15 GHz and 60 GHz are about $\varepsilon_{\perp} = 2.4$ and $\varepsilon_{\parallel} = 3.2$. These values are in good agreement with the obtained in estimations shown in Chapters 4 and 5 of this Thesis work. The values of the LC permittivity as a function of the frequency are shown in Figure III.2.

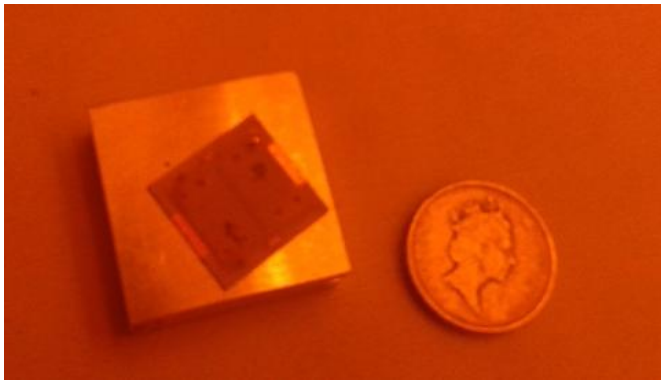

Figure III.1. Microstrip device for the measurement of the LC permittivity.

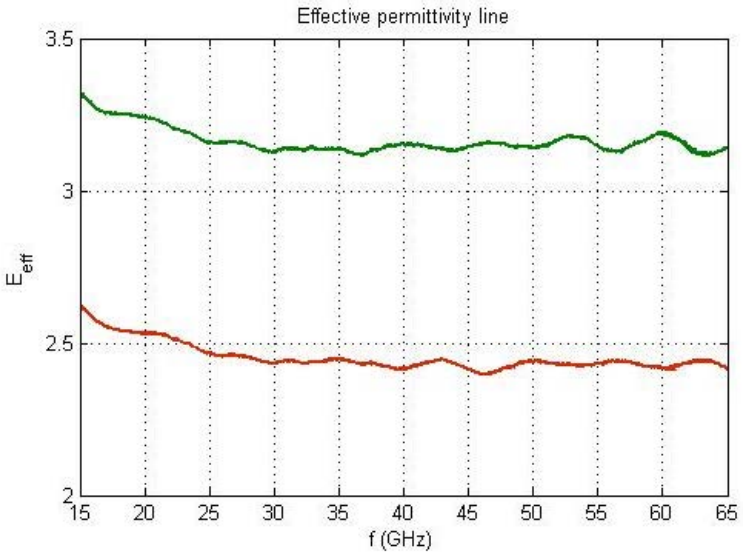

Figure III.2. Evolution of the LC permittivity between 15 GHz and 60 GHz.